AUTOPILOT AND GUIDANCE FOR ANTI-TANK IMAGING INFRARED GUIDED MISSILES

A THESIS SUBMITTED TO
THE GRADUATE SCHOOL OF NATURAL AND APPLIED SCIENCES
OF
MIDDLE EAST TECHNICAL UNIVERSITY

BY

ALİ ERDEM ÖZCAN

IN PARTIAL FULFILLMENT OF THE REQUIREMENTS
FOR
THE DEGREE OF MASTER OF SCIENCE
IN
ELECTRICAL AND ELECTRONICS ENGINEERING

OCTOBER 2008

Approval of the thesis:

AUTOPILOT AND GUIDANCE FOR ANTI-TANK IMAGING INFRARED GUIDED MISSILES

submitted by **ALİ ERDEM ÖZCAN** in partial fulfillment of the requirements for the degree of **Master of Science in Electrical and Electronics Engineering Department, Middle East Technical University** by,

Prof. Dr. Canan Özgen ___________
Dean, Graduate School of **Natural and Applied Sciences**

Prof. Dr. İsmet Erkmen ___________
Head of Department, **Electrical and Electronics Engineering**

Prof. Dr. Kemal Leblebicioğlu ___________
Supervisor, **Electrical and Electronics Engineering Dept., METU**

Examining Committee Members:

Prof. Dr. Mübeccel Demirekler _____________
Electrical and Electronics Engineering Dept., METU

Prof. Dr. Kemal Leblebicioğlu _____________
Electrical and Electronics Engineering Dept., METU

Prof. Dr. Gözde Bozdağı Akar _____________
Electrical and Electronics Engineering Dept., METU

Assoc. Prof. Dr. Aydın Alatan _____________
Electrical and Electronics Engineering Dept., METU

M. Sc. Emre Turgay _____________
Image Processing Dept., ASELSAN

Date: _____________

I hereby declare that all information in this document has been obtained and presented in accordance with academic rules and ethical conduct. I also declare that, as required by these rules and conduct, I have fully cited and referenced all material and results that are not original to this work.

Name, Last name: Ali Erdem Özcan

Signature :

ABSTRACT

AUTOPILOT AND GUIDANCE FOR ANTI-TANK IMAGING INFRARED GUIDED MISSILES

Özcan, Ali Erdem
M.S., Department of Electrical and Electronics Engineering
Supervisor: Prof. Dr. Kemal Leblebicioğlu

October 2008, 113 Pages

An anti-tank guided missile is a weapon system primarily designed to hit and destroy armored tanks and other armored vehicles. Developed first-generation command-guided and second-generation semi-automatic command guided missiles had many disadvantages and lower hit rates. For that reason, third generation imaging infrared fire-and-forget missile concept is very popular nowadays.

In this thesis, mainly, a mathematical model for a fire-and-forget anti-tank missile is developed and a flight control autopilot design is presented using PID and LQR techniques. For target tracking purposes, “correlation”, “centroid” and “active contour” algorithms are studied and these algorithms are tested over some scenarios for maximizing hit rate. Different target scenarios and counter-measures are discussed in an artificially created virtual environment.

Keywords: Anti-tank Missile, Autopilot, Imaging Infrared, Tracking

ÖZ

KIZILÖTESİ GÖRÜNTÜLEME GÜDÜMLÜ ANTİ-TANK FÜZELER İÇİN OTOPİLOT VE GÜDÜM GELİŞTİRİLMESİ

Özcan, Ali Erdem
Yüksek Lisans., Elektrik ve Elektronik Mühendisliği Bölümü
Tez Yöneticisi: Prof. Dr. Kemal Leblebicioğlu

Ekim 2008, 113 Sayfa

Anti-tank güdümlü füzeler öncelikle yüksek zırh etkinliği bulunan tankları ve diğer zırhlı araçları vurmak ve yok etmek için geliştirilen silah sistemlerdir. Geliştirilen birinci ve ikinci nesil komut-güdümlü ve yarı-otomatik komut-güdümlü füzeler birçok dezavantajı beraberinde getirmiş ve düşük vuruş yüzdeleri elde etmiştir. Bu sebeple, son yıllarda üçüncü nesil kızılötesi görüntüleme güdümlü at-unut füzeler gündeme gelmiştir.

Bu tezde temel olarak, at-unut anti-tank bir füze için matematiksel model belirlenmiş ve uçuş kontrol otopilotu PID ve LQR teknikleri kullanılarak yaratılmıştır. Kızılötesi görüntü üzerinden hedef takibi yapabilmek için “alan izleme”, “nokta izleme” ve “aktif çerçeve” teknikleri ortaya konmuş ve bu algoritmalar vasıtasıyla füzenin hedefi yüksek vuruş yüzdesi ile vurması için önerilen algoritma anlatılmıştır. Oluşturulan sanal dünya üzerinde farklı hedef senaryoları ve karşı-tedbir önlemleri tartışılmıştır.

Anahtar Kelimeler: Anti-tank Füze, Otopilot, Kızılötesi Görüntüleme, Hedef Takip

Bana izlemekte olduğum yolu gösteren annem ve babama;
O yolu birlikte kat ettiğim eşime;
Ve yolları henüz kendilerini bekleyen çocuklarıma.

ACKNOWLEDGMENTS

I would like to express my appreciation to my supervisor Prof. Dr. Kemal LEBLEBİCİOĞLU for his guidance, support and suggestions throughout the research.

I wish to thank Dr. Özgür ATEŞOĞLU and Hamza Ergezer for their valuable advices and encouragements during the preparation of this thesis.

I would like to acknowledge the manager of Thermal Systems Design Department in ASELSAN INC, Baki ŞENSOY and all of my colleagues for their support.

Last, but definitely not the least, I would like to thank to my parents, Seydi ÖZCAN, Çetin SARAÇOĞLU, Nurten ÖZCAN, Nimet SARAÇOĞLU, Mert ÖZCAN, Orkun SARAÇOĞLU and Buket SARAÇOĞLU URAL for their love and support in my entire life. I wish to express my deepest special thanks to my endless love, Merve ÖZCAN for her help, patience and motivation. I would not be here without her.

TABLE OF CONTENTS

CHAPTERS

APPENDICES

LIST OF TABLES

TABLES

LIST OF FIGURES

FIGURES

LIST OF SYMBOLS

f_E	Normal-Earth fixed frame
f_B	Body frame
x_E, y_E, z_E	Normal-Earth fixed frame axes
x_B, y_B, z_B	Body frame axes
G	Missile (body) center of mass
ψ	Yaw angle
θ	Pitch angle
Φ	Roll angle
T_{EB}	Transformation matrix that represents a transformation from f_E to f_B
u, v, w	Components of missile velocity vector in Body frame
p, q, r	Components of missile angular velocity vector in Body frame
F_x, F_y, F_z	Components of total force acting on the missile in Body frame
$\vec{F}$	Sum of all externally applied forces acting on the missile in Body frame
L, M, N	Components of total moment acting on the missile in Body frame
$\vec{M}$	Total moment acting on the missile in Body frame
I_{xy}, I_{xz}, I_{yz}	Cross inertia elements
I_{xx}, I_{yy}, I_{zz}	Components of inertia matrix
m	Missile mass
V_T	Total missile velocity

$\vec{a}$	Total missile acceleration
$\hat{i}, \hat{j}, \hat{k}$	Unit vectors
$\vec{\Omega}$	Angular velocity in Body frame
h_B	Inertia dyadic
q_i	Dynamic pressure
ρ	Air density
α	Angle of attack
h	Altitude
β	Sideslip angle
V_s	Speed of sound
$\delta_1, \delta_2, \delta_3, \delta_4$	First, second, third and fourth control fin angles
δ_a	Aileron fin deflection
δ_e	Elevator fin deflection
δ_r	Rudder fin deflection
S	Cross-sectional Area of the Missile
C_X	Axial force coefficient
C_Y	Side force coefficient
C_Z	Normal force coefficient
P_X, P_Y, P_Z	Components of proportional force
C_L	Rolling moment coefficient
C_M	Pitching moment coefficient
C_N	Yawing moment coefficient
d_M	Missile diameter
M	Mach number
K_P, K_I, K_D	PID gains
Q, R	LQR weight matrices
J	LQR cost function
H	Hamiltonian
K	Feedback gain

r, g, b	RGB color components
h, s, v	HSV color components
θ_g	Gimbal angle
ε	Error angle
θ_L	Look angle
θ_b	Body attitude
γ	Centroid algorithm update rate
i	Pixel intensity
T	Number of target pixels
Y	Number of pixels enclosed in the background gate
c_X, c_Y	Centroid coordinates
x_j	X projection of the jth row
y_n	Y projection of the nth column
k_X, k_Y	Centroid algorithm enlarge/shrink size
g_2	Centroid algorithm changing rate
g_1	Centroid algorithm enclosing rate
C_{ab}	Correlation of a and b signature

CHAPTER 1

INTRODUCTION

1.1 General Information

Since their development in the early 1900's, missiles have become an increasingly critical element in military warfare. Today, missile systems are developed for a large variety of purposes [1]. In general, missile systems can be categorized into four classes:

- Air-to-Air Missiles,
- Air-to-Surface Missiles,
- Surface-to-Surface Missiles,
- Surface-to-Air Missiles.

Surface-to-Surface missiles and Air-to-Surface missiles are operated from an air or land platform toward a surface target. Anti-tank missiles have one of the most important technological advances among these two categories. The anti-tank guided missile is a weapon system primarily designed to destroy armored tanks and other armored vehicles.

During the 1973, Yom Kippur War between Israel and Egypt, the Russian 9M14-Malyutka man-portable anti-tank missile proved efficient against Israeli tanks. Since that time, anti-tank missiles have been manufactured and used in great demand.

Anti-tank guided missiles range in size from shoulder-launched weapons to vehicle or platform integrated missile systems.

Regarding the modern anti-tank missiles, the components and structure can be summarized in Figure-1 below:

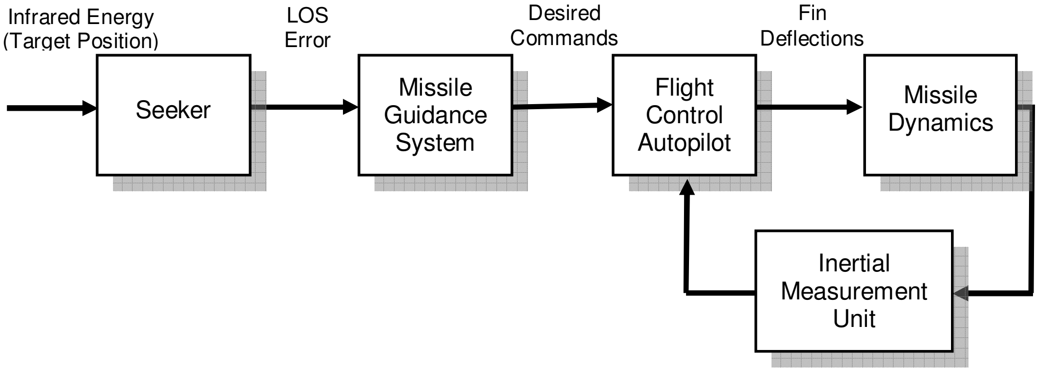

Figure 1 General Structure of an Anti-tank Missile

The seeker part is responsible for the estimation of target’s position. A typical seeker consists of three major components: (1) An imaging system, (2) a gimbal, and (3) a processor [2]. Modern anti-tank missile systems have become increasingly dependent upon passive imaging infrared sensor technology [1]. Imaging infrared sensors use detection of thermal energy to create the scene picture. The gimbal is designed to maintain the orientation of the imaging sensor without regard to any particular target or boresight position [3]. The processor closes the loop by computing the target position used to drive the gimbal and guidance section.

The missile guidance system provides the desired flight path information in order to achieve the mission requirements by using the seeker’s output. There are different kinds of guidance algorithms for anti-tank missiles such as MCLOS, SACLOS, fire-and-forget, etc.

The flight control autopilot stabilizes the missile with respect to the desired commands and generates fin deflection commands for controlling missile properly.

When designing the flight control autopilot, knowledge of the missile dynamics and airframe are critical. Generic missiles are composed of 12 nonlinear equations.

1.2 Scope of the Thesis

The thesis is organized in the following manner:

In Chapter 2, the mathematical model of the missile is constructed. It models the aerodynamic forces and moments acting on the missile. These come up to be 12 nonlinear equations (6 kinematics and 6 dynamics). These equations are primarily functions of aerodynamic coefficients. They are found using Missile DATCOM software. Nonlinear equations are linearized in order to represent them in state-space.

In Chapter 3, two different flight control autopilot designs are studied. They are based on PID (proportional integral derivative) and LQR (linear quadratic regulator) techniques. Their performances are compared according to the simulation results.

In Chapter 4, an imaging infrared seeker model is given. Seeker subcomponents are presented one by one. The gimbal structure is modeled and target detection and tracking schemes are applied. Centroid, correlation and active contour (snake) tracking algorithms are presented in detail and proposed tracking algorithm, which combines positive sides of these methods, is developed. Guidance design is presented for providing the proper flight path according to the target state.

In Chapter 5, different simulations related with target contrast, clutter, noise, field-of-view and countermeasures are discussed. Advantages of proposed algorithm instead of using centroid, correlation and active contour methods alone are presented.

In Chapter 6, overall study is concluded and recommendations for future works are presented.

CHAPTER 2

MATHEMATICAL MODEL OF A GENERIC MISSILE

During the design of the flight control autopilot, missile mathematical modeling is one of the most important stages. In this chapter, missile mathematical model will be constructed using 12 nonlinear equations (6 kinematics and 6 dynamics) for a 6 DOF (degree-of-freedom) representation. Kinematics equations are the consequences of transformation matrix applications that relates the reference axis systems through the Euler Angles and dynamic equations are derived by Newton's second law of motion, which relates the summation of the external forces and moments to the linear and angular accelerations of the body [5]. Since several coordinate systems are used, frame definitions of missile will be described. Finally, linearization of 12 nonlinear equations based on several assumptions will be presented.

2.1 Frame Definitions

Two coordinate frames can be defined in order to describe the motion of the missile: Normal Earth-fixed frame F_E and Body frame F_B. Both of them are three-dimensional, orthogonal and right-handed [6].

2.1.1 Normal Earth-Fixed Frame

The origin of the frame is linked to a fixed point O on the Earth and its axes are x_E,y_E,z_E. The x-axis is directed towards the geographical North, the z-axis is directed towards the descending direction of gravitational attraction and the y-axis is the complementing axis.

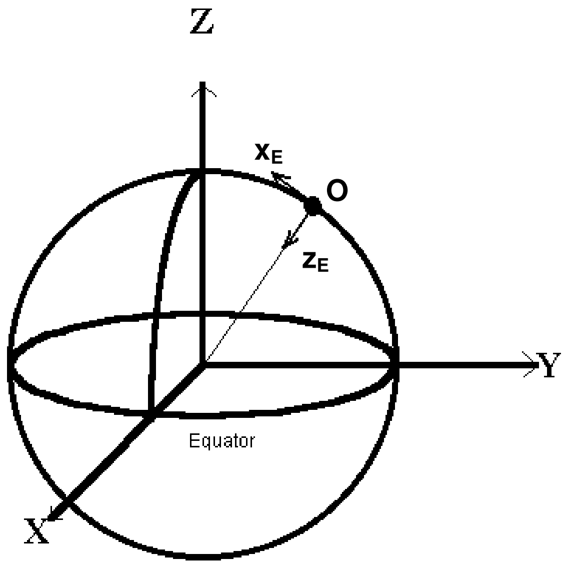

Figure 2 Normal Earth-Fixed Coordinate System

2.1.2 Body Frame

The origin of the body frame is linked to the missile body and the center of mass. Its axes are x_B,y_B,z_B. The x-axis, called the roll axis, points towards the front belonging the symmetrical plane; the y-axis, called the pitch axis, is directed towards the lateral side of the missile; and the z-axis, called the yaw axis, is the complementing axis. G point is the center of mass.

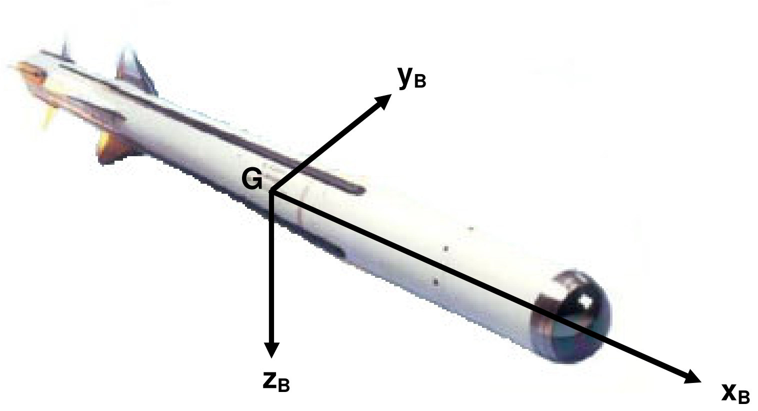

Figure 3 Body Coordinate System

2.1.3 Transformation from the Normal Earth-Fixed Frame to Body Frame

After two frames have been established, next it is useful to define their relations by means of angles. There are three angles in each coordinate system, which allow the transformation from the Normal Earth Fixed Frame (F_E) to the Body Frame (F_B) [6].

1st rotation	ψ yaw angle	about axis z_E
2nd rotation	θ pitch angle	about axis y_E
3rd rotation	Φ roll angle	about axis x_E

Yaw, pitch and roll angles are called Euler angles. These three transformations are associated with the transformations below:

$$F^E = (T_\psi T_\theta T_\phi) \cdot F^B = T_{EB} \cdot F^B \qquad (2.1)$$

$$T_\varphi = \begin{pmatrix} \cos\psi & -\sin\psi & 0 \\ \sin\psi & \cos\psi & 0 \\ 0 & 0 & 1 \end{pmatrix}, \; T_\theta = \begin{pmatrix} \cos\theta & 0 & \sin\theta \\ 0 & 1 & 0 \\ -\sin\theta & 0 & \cos\theta \end{pmatrix}, \; T_\phi = \begin{pmatrix} 1 & 0 & 0 \\ 0 & \cos\Phi & -\sin\Phi \\ 0 & \sin\Phi & \cos\Phi \end{pmatrix}$$

$$T_{EB} = \begin{pmatrix} \cos\psi & -\sin\psi & 0 \\ \sin\psi & \cos\psi & 0 \\ 0 & 0 & 1 \end{pmatrix} \cdot \begin{pmatrix} \cos\theta & 0 & \sin\theta \\ 0 & 1 & 0 \\ -\sin\theta & 0 & \cos\theta \end{pmatrix} \cdot \begin{pmatrix} 1 & 0 & 0 \\ 0 & \cos\Phi & -\sin\Phi \\ 0 & \sin\Phi & \cos\Phi \end{pmatrix}$$

$$= \begin{pmatrix} \cos\theta\cos\psi & \sin\theta\sin\Phi\cos\psi - \sin\psi\cos\Phi & \cos\psi\sin\theta\cos\Phi + \sin\Phi\sin\psi \\ \sin\psi\cos\theta & \sin\theta\sin\Phi\sin\psi + \cos\psi\cos\Phi & \sin\theta\cos\Phi\sin\psi - \sin\Phi\cos\psi \\ -\sin\theta & \cos\theta\sin\Phi & \cos\theta\cos\Phi \end{pmatrix}$$

(2.2)

T_{EB} representation describes the transformation from the Normal Earth Fixed Frame to the Body Frame.

2.2 General Equations of Motion

The related parameters acting on the missile are defined in Table 1 below:

	x	**y**	**z**
Angle	Φ (roll)	Θ (pitch)	Ψ (yaw)
Velocity	u	v	w
Position	x_B	y_B	z_B
Angular Rate	p	q	r
Force	F_x	F_y	F_z
Moment	L	M	N
Inertia	I_{xx}	I_{yy}	I_{zz}
Product of Inertia	I_{yz}	I_{xz}	I_{xy}

Table 1 Missile Parameters

The principal assumptions, which are used to derive the equations of missile motion, are given below as

A.1: The missile is a rigid body, elastic deformations are not considered.

A.2: Mass is constant.

Using the above assumptions dynamics and kinematics equations are derived as follows.

2.2.1 Dynamic Model

Using the Newton's law, the force equation is obtained as [7]

$$F = m \cdot \vec{a} = m \cdot \dot{\vec{V}}_T \tag{2.3}$$

where F is the sum of all externally applied forces acting on the missile, m is the mass, a is the acceleration of the center of mass relative to the body frame and V_T is the velocity of center of mass relative to body frame. Formula 2.3 is defined in the normal earth-fixed frame. The linear velocity V_T is stated as,

$$\vec{V}_T = u\hat{i} + v\hat{j} + w\hat{k} \tag{2.4}$$

In the body frame, the acceleration of the center of mass is expressed as,

$$\left\{\dot{V}_T\right\}_B = \dot{V}_T + \left\{\vec{\Omega}\right\}_B \cdot V_T \tag{2.5}$$

where $\{\}_B$ indicates that the coordinate is defined in body frame. Moreover, Newton's force equation is defined in body frame as,

$$\left\{\vec{F}\right\}_B = m \cdot \left[\dot{V}_T + \{\Omega\}_B \cdot V_T\right] \tag{2.6}$$

where Ω is the angular velocity of body frame defined as (found in the kinematic model),

$$\{\vec{\Omega}\}_B = \begin{bmatrix} 0 & -r & q \\ r & 0 & -p \\ -q & p & 0 \end{bmatrix} \tag{2.7}$$

And finally, the force is derived using 2.6 and 2.7 as,

$$\vec{F} = \begin{bmatrix} F_x \\ F_y \\ F_z \end{bmatrix} = \begin{bmatrix} m\dot{u} + m(qw - rv) \\ m\dot{v} + m(ru - pw) \\ m\dot{w} + m(pv - qu) \end{bmatrix} \tag{2.8}$$

After deriving the force equations, the moment equations of the missile are derived as follows. In the body frame, relationship between angular momentum and moment is stated as follows,

$$\{\vec{M}\}_B = \left\{\dot{h}_B\right\}_B + \{\Omega\}_B \cdot h_B \tag{2.9}$$

where h_B is written as

$$h_B = \begin{bmatrix} I_{xx} & -I_{xy} & -I_{xz} \\ -I_{xy} & I_{yy} & -I_{yz} \\ -I_{xz} & -I_{yz} & I_{zz} \end{bmatrix} \tag{2.10}$$

The missile is, in general, symmetrical about planes XZ and YZ and consequently, inertia product terms I_{xy} and I_{yz} vanish. Then,

$$h_B = \begin{bmatrix} I_{xx} & 0 & -I_{xz} \\ 0 & I_{yy} & 0 \\ -I_{xz} & 0 & I_{zz} \end{bmatrix} \tag{2.11}$$

I_{xx}, I_{yy}, I_{zz} and I_{xz} are the mass moment of inertia and the product of inertia of the missile about body-fixed coordinate frame. Thus, the moment equation is stated as follows,

$$\vec{M} = \begin{bmatrix} L \\ M \\ N \end{bmatrix} = \begin{bmatrix} I_{xx}\dot{p} - I_{xz}\dot{r} \\ I_{yy}\dot{q} \\ I_{zz}\dot{r} - I_{xz}\dot{p} \end{bmatrix} + \begin{bmatrix} 0 & -r & q \\ r & 0 & -p \\ -q & p & 0 \end{bmatrix} \cdot \begin{bmatrix} I_{xx} & 0 & -I_{xz} \\ 0 & I_{yy} & 0 \\ -I_{xz} & 0 & I_{zz} \end{bmatrix}$$

$$= \begin{bmatrix} I_{xx}\dot{p} - I_{xz}\dot{r} + (I_{zz} - I_{yy})qr - I_{xz}pq \\ I_{yy}\dot{q} + (I_{xx} - I_{zz})pr + I_{xz}(p^2 - r^2) \\ I_{zz}\dot{r} - I_{xz}\dot{p} + (I_{yy} - I_{xx})pq + I_{xz}qr \end{bmatrix} \tag{2.12}$$

where L is defined as the roll moment, M is the pitch moment and N is the yaw moment of missile.

2.2.2 Kinematic Model

The nonlinear equations of kinematics, describing the missile, can be divided into two parts: one is governing the translational motion and the other one governing the rotational motion. In the body frame, the kinematic equations can be formulated as described next.

Using equation 2.2, the transformation matrix from the normal earth fixed frame to body fixed frame relates the translational kinematic equations as

$$\begin{bmatrix} \dot{x} \\ \dot{y} \\ \dot{z} \end{bmatrix} =$$

$$\begin{pmatrix} \cos\theta\cos\psi & \sin\theta\sin\Phi\cos\psi - \sin\psi\cos\Phi & \cos\psi\sin\theta\cos\Phi + \sin\Phi\sin\psi \\ \sin\psi\cos\theta & \sin\theta\sin\Phi\sin\psi + \cos\psi\cos\Phi & \sin\theta\cos\Phi\sin\psi - \sin\Phi\cos\psi \\ -\sin\theta & \cos\theta\sin\Phi & \cos\theta\cos\Phi \end{pmatrix} \cdot \begin{bmatrix} u \\ v \\ w \end{bmatrix} \tag{2.13}$$

Secondly, The Euler rates with respect to the body fixed frame construct the rotational kinematic equations as follows:

$$Identity = I = T_{EB} \times (T_{EB})^T \tag{2.14}$$

Taking the derivative of equation 2.14 leads

$$\frac{d}{dt}(I) = \frac{d}{dt}\left(T_{EB} \times (T_{EB})^T\right) = 0 \tag{2.15}$$

$$\frac{d}{dt}(T_{EB}) \cdot (T_{EB})^T + T_{EB} \cdot \frac{d}{dt}(T_{EB})^T = 0 \tag{2.16}$$

$$\frac{d}{dt}(T_{EB}) \cdot (T_{EB})^T = -\left(T_{EB}{}^T \cdot \frac{d}{dt}(T_{EB})\right)^T \tag{2.17}$$

Definition 2.1 (Skew-Symmetric of a Matrix) [7]

A matrix S is said to be skew-symmetric if:

$$S = -S^T \tag{2.18}$$

This implies that the off-diagonal matrix elements of S satisfy $s_{ij} = -s_{ji}$ for $i \neq j$ while the matrix diagonal consists of zero elements.

Using the definition 2.1, $\frac{d}{dt}(T_{EB}) \cdot (T_{EB})^T$ is a skew-symmetric matrix and consequently there exists a skew-symmetric matrix such that

$$\tilde{\Omega} = \left(\frac{d}{dt}(T_{EB}) \cdot (T_{EB})^T\right) \cdot \begin{bmatrix} p \\ q \\ r \end{bmatrix} \tag{2.19}$$

Then, the skew-symmetric matrix is found as equation 2.7. Solving equation 2.19 and 2.7 leads following equation,

$$\dot{\Phi} = p + \tan(\theta) \cdot \left(q \sin(\Phi) + r \cos(\Phi) \right)$$
$$\dot{\theta} = q \cos(\Phi) - r \sin(\Phi) \tag{2.20}$$
$$\dot{\psi} = \frac{r \cos(\Phi) + q \sin(\Phi)}{\cos(\theta)}$$

where ψ is yaw angle, θ is pitch angle and Φ is roll angle of the missile. Because of the tangent term, equation 2.20 has singularity points at θ = 90° and θ = 270°. So a below assumption is made:

> **A.3:** 90° and 270° pitch angles are never occurred during the missile flight.

2.2.3 Aerodynamic Model

During the flight of the missile, some aerodynamic parameters are appeared to describe the motion and orientation of the missile. Primarily, dynamic pressure, angle of attack, sideslip angle and Mach number are introduced.

Dynamic Pressure: Dynamic pressure shows the aerodynamic pressure experienced by the missile. It is proportional to the square of velocity of the missile and the air density given in the below formula:

$$q_i = \frac{1}{2} \rho v^2 \tag{2.21}$$

where ρ is the air density and calculated as follows:

$$\rho = \begin{cases} 1.223(1 - 0.0000225h)^{4.256}, h \le 10.000m \\ 0.412x10^{-0.000151(h-10.000)}, h > 10.000m \end{cases} \tag{2.22}$$

Angle of Attack: Angle of attack is used to describe the angle between x-axis relative to body frame and direction of airflow wind as seen in Figure 4. It can be described as the angle between where the missile is *pointing* and where it is *going*. It is defined as

$$\alpha = \arctan\left(\frac{w}{u}\right) \tag{2.23}$$

Since w is much smaller than u, the above equation can be written as,

$$\alpha \cong \left(\frac{w}{u}\right) \tag{2.24}$$

Sideslip Angle: Sideslip angle relates to the displacement of the aircraft centerline from the relative wind as seen in the Figure 4. It is defined as,

$$\beta = \arctan\left(\frac{v}{V_T}\right) \tag{2.25}$$

Since v is much smaller than V_T (can be taken as u, so $\dot{u} \cong 0$), the above equation can be written as,

$$\beta \cong \left(\frac{v}{V_T}\right) \cong \left(\frac{v}{u}\right) \tag{2.26}$$

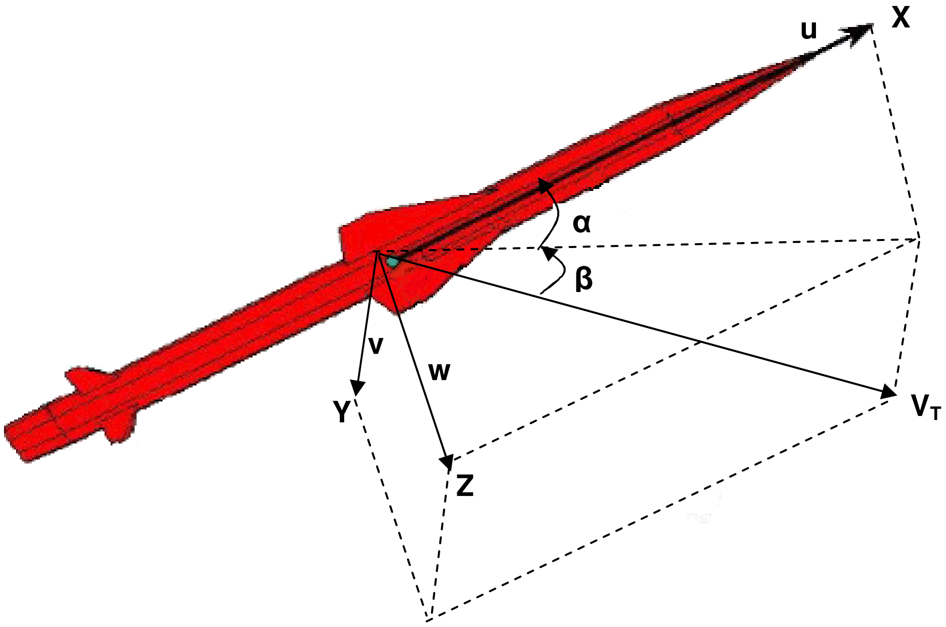

Figure 4 Angle of Attack and Sideslip Angle

Mach Number: Mach number is a dimensionless measure of relative speed, which is defined as speed of the missile divided by the speed of sound in the same medium. It can be expressed as,

$$M = \left(\frac{V_T}{v_s} \right) \qquad (2.27)$$

where v_s is the speed of sound.

In this study, four canard-controlled fins, 90° apart from each other, are applied to control the missile navigation. Control surface deflection angles are taken to be positive in the clockwise direction as in Figure 5 [9].

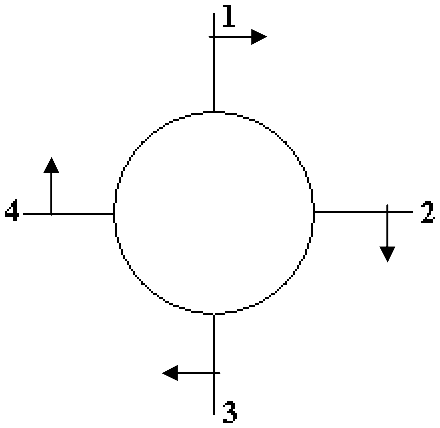

Figure 5 Fin Angles (Rear View) [9]

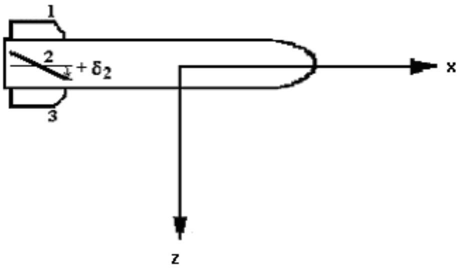

Figure 6 Fin Angles (Side view) [9]

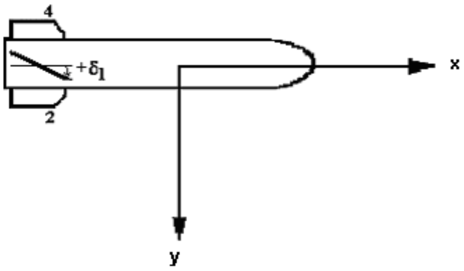

Figure 7 Fin Angles (Top View) [9]

$\delta_1, \delta_2, \delta_3, \delta_4$ angles represent first, second, third and fourth control fin angles, respectively. In the dynamical equations of motion, control surface deflections are categorized in three planes, namely roll, pitch and yaw planes as

δ_a : aileron fin deflections

δ_e : elevator fin deflections

δ_r : rudder fin deflections

These fin deflections are calculated using $\delta_1, \delta_2, \delta_3, \delta_4$ as below:

$$\delta_a = \frac{\delta_1 + \delta_2 + \delta_3 + \delta_4}{4} \tag{2.28}$$

$$\delta_e = \frac{\delta_2 - \delta_4}{2} \tag{2.29}$$

$$\delta_r = \frac{\delta_1 - \delta_3}{2} \tag{2.30}$$

There exist three different forces acting on the missile: (1) Aerodynamic force (2) Gravitational force (3) Propulsion force and two different type of moments acting on the missile (1) Aerodynamic moment (2) Propulsion moment. Therefore, force and moment equations can be separated as follows

$$F = \begin{bmatrix} F_x \\ F_y \\ F_z \end{bmatrix} = \begin{bmatrix} m\dot{u} + m(qw - rv) \\ m\dot{v} + m(ru - pw) \\ m\dot{w} + m(pv - qu) \end{bmatrix} = \begin{bmatrix} q_i S C_x + P_x - mg\sin(\theta) \\ q_i S C_y + P_y + mg\cos(\theta)\sin(\Phi) \\ q_i S C_z + P_z + mg\cos(\theta)\cos(\Phi) \end{bmatrix} \tag{2.31}$$

where q_i is the dynamic pressure; S is the cross-sectional area of the missile; C_x,C_y,C_z are the force coefficients; P_x,P_y,P_z are the propulsion forces.

Further derivations lead following equations:

$$\begin{bmatrix} \dot{u} \\ \dot{v} \\ \dot{w} \end{bmatrix} = \begin{bmatrix} -qw + rv + \dfrac{q_i S C_x + P_x}{m} - g\sin(\theta) \\ -ru + pw + \dfrac{q_i S C_y + P_y}{m} + g\cos(\theta)\sin(\Phi) \\ -pv + qu + \dfrac{q_i S C_z + P_z}{m} + g\cos(\theta)\cos(\Phi) \end{bmatrix} \tag{2.32}$$

Similarly, for the rotational dynamics, the following equations can be derived:

$$M = \begin{bmatrix} I_{xx}\dot{p} - I_{xz}\dot{r} + (I_{zz} - I_{yy})qr - I_{xz}pq \\ I_{yy}\dot{q} + (I_{xx} - I_{zz})pr + I_{xz}(p^2 - r^2) \\ I_{zz}\dot{r} - I_{xz}\dot{p} + (I_{yy} - I_{xx})pq + I_{xz}qr \end{bmatrix} = \begin{bmatrix} L + q_i d_M S C_L \\ M + q_i d_M S C_M \\ N + q_i d_M S C_N \end{bmatrix} \tag{2.33}$$

where q_i is the dynamic pressure; S is the cross-sectional area of the missile; d_M is the missile diameter; C_L,C_M,C_N are the moment coefficients.
Further derivations lead following equations:

$$\begin{bmatrix} \dot{p} \\ \dot{q} \\ \dot{r} \end{bmatrix} = \begin{bmatrix} \dfrac{I_{xz}}{I_{xx}}\dot{r} - \dfrac{(I_{zz} - I_{yy})}{I_{xx}}qr + \dfrac{I_{xz}}{I_{xx}}pq + \dfrac{q_i d_M S C_L}{I_{xx}} \\ -\dfrac{(I_{xx} - I_{zz})}{I_{yy}}pr - \dfrac{I_{xz}}{I_{yy}}(p^2 - r^2) + \dfrac{q_i d_M S C_M}{I_{yy}} \\ \dfrac{I_{xz}}{I_{zz}}\dot{p} - \dfrac{(I_{yy} - I_{xx})}{I_{zz}}pq - \dfrac{I_{xz}}{I_{zz}}qr + \dfrac{q_i d_M S C_N}{I_{zz}} \end{bmatrix} \tag{2.34}$$

The aerodynamic coefficients (C_i) can be defined with respect to flight parameters such as angle of attack, sideslip angle, Mach number, fin deflections and angular rates [8]. These coefficients are nonlinear functions of flight parameters. There exist some experimental methods like wind-tunnel tests or computational fluid dynamics methods in order to calculate the aerodynamic coefficients, but MISSILE DATCOM software will be used alternatively in this thesis. Details of this software are given in Appendix A.

Aerodynamic coefficients can be defined as follows

C_X : Axial force coefficient

C_Y : Side force coefficient

C_Z : Normal force coefficient

C_L : Rolling moment coefficient

C_M : Pitching moment coefficient

C_N : Yawing moment coefficient

Axial, normal force coefficients and pitching moment coefficient will be given for selected missile configuration in Figure 8 and 9.

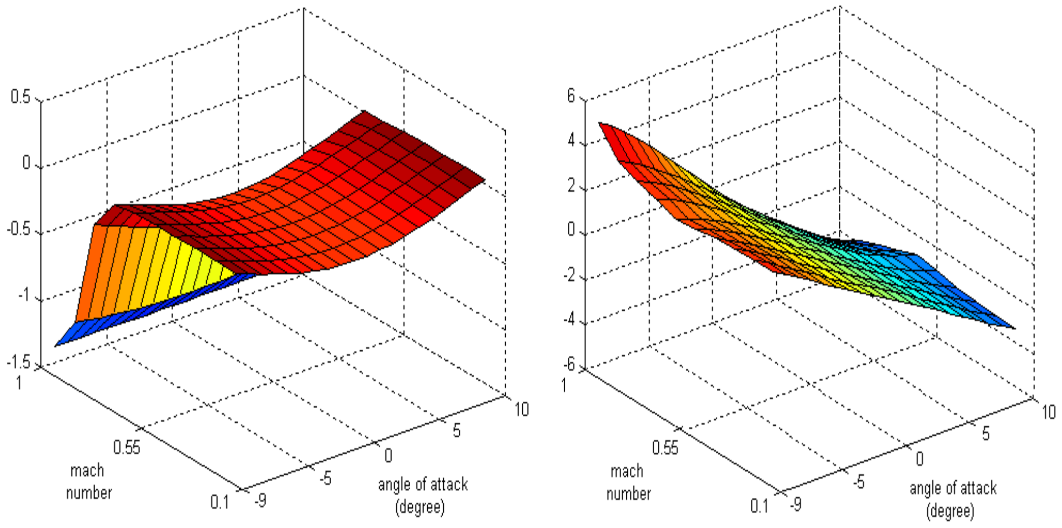

Figure 8 Axial and Normal Force Coefficients

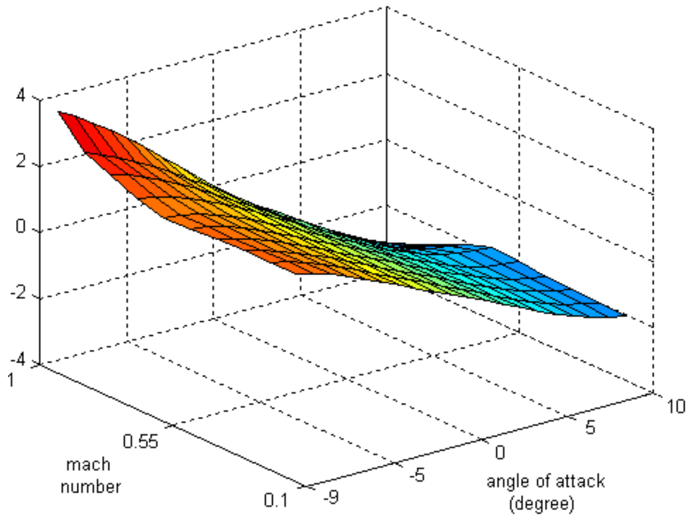

Figure 9 Pitching Moment Coefficient

The aerodynamic coefficients will be linearized by using the Taylor series expansion around the trim points of the flight parameters in order to represent them in flight autopilot design:

$$\begin{aligned}&C_i = C_{i0}(M,\alpha) + C_{i\alpha}(M,\alpha)\cdot\alpha + C_{i\beta}(M,\alpha)\cdot\beta + C_{i\delta_a}(M,\alpha)\cdot\delta_a + \\ &C_{i\delta_e}(M,\alpha)\cdot\delta_e + C_{i\delta_r}(M,\alpha)\cdot\delta_r + C_{ip}(M,\alpha)\cdot p\cdot\frac{d_M}{2\cdot V_T} + \\ &C_{iq}(M,\alpha)\cdot q\cdot\frac{d_M}{2\cdot V_T} + C_{ir}(M,\alpha)\cdot r\cdot\frac{d_M}{2\cdot V_T} + HOT\end{aligned} \tag{2.35}$$

where HOT stands for higher order terms and $\frac{d_M}{2\cdot V_T}$ term is included as a multiplier to the aerodynamic derivatives to make them dimensionless [8].

Aerodynamic derivatives can be written as

$$C_{i\theta_i}(M,\alpha) = \left.\frac{\partial C_i}{\partial \theta_i}\right|_{\theta_i=\theta_{i0}} \tag{2.36}$$

The aerodynamic derivative values are taken at the trim values of the flight parameters and they are kept only as a non-linear function of mach number and angle-of-attack. Since along the flight path of the missile, parameters will be small, so the trim points can be taken as zero. After linearization, the dimensionless aerodynamic coefficients can be written as follows

$$\begin{aligned}
C_x &= C_{x0}(M,\alpha) \\
C_y &= C_{y\beta}(M,\alpha)\cdot\beta + C_{y\delta}(M,\alpha)\cdot\delta_r + C_{yr}(M,\alpha)\cdot r\cdot\frac{d_M}{2\cdot V_T} \\
C_z &= C_{z\alpha}(M,\alpha)\cdot\alpha + C_{z\delta}(M,\alpha)\cdot\delta_e + C_{zq}(M,\alpha)\cdot q\cdot\frac{d_M}{2\cdot V_T} \\
C_l &= C_{l\delta}(M,\alpha)\cdot\delta_a + C_{lp}(M,\alpha)\cdot p\cdot\frac{d_M}{2\cdot V_T} \\
C_m &= C_{m\alpha}(M,\alpha)\cdot\alpha + C_{m\delta}(M,\alpha)\cdot\delta_e + C_{mq}(M,\alpha)\cdot q\cdot\frac{d_M}{2\cdot V_T} \\
C_n &= C_{n\beta}(M,\alpha)\cdot\beta + C_{n\delta}(M,\alpha)\cdot\delta_r + C_{nr}(M,\alpha)\cdot r\cdot\frac{d_M}{2\cdot V_T}
\end{aligned} \tag{2.37}$$

Because of the missile symmetry, aerodynamic coefficients can be taken as follows:

$$\begin{aligned}
C_{z\alpha} &= C_{y\beta} \\
C_{z\delta} &= C_{y\delta} \\
C_{zq} &= -C_{yr} \\
C_{m\alpha} &= -C_{n\beta} \\
C_{m\delta} &= -C_{n\delta} \\
C_{mq} &= C_{nr}
\end{aligned} \tag{2.38}$$

2.2.4 Linearization of Equations

There are several ways to linearize the equations of missile motion. One of them is the specification of flight conditions. By applying the following assumptions, dynamic and kinematic equations of motion can be linearized.

A.4: The velocity of missile, ambient temperature and ambient density are constant.

A.5: Angle of attack, side-slip angle and fin deflections are constant.

A.6: Rolling motion is very small ($p \cong 0$)

A.7: Components of gravitational acceleration are external disturbances.

A.8: The flight after the boost phase is considered so the propulsion forces (P_x,P_y,P_z) and moments (L,M,N) are not included in the equations.

A.9: Coordinate system is located at the center of gravity and XZ plane is axis-symmetric, so that the mass distribution is such that $I_{xz} = I_{yz} = I_{xy} = 0$ and $I_{yy} = I_{zz}$.

By taking into account the assumptions above, the non-linear equations can be reduced as,

$$\begin{bmatrix} \overset{\bullet}{u} \\ \overset{\bullet}{v} \\ \overset{\bullet}{w} \end{bmatrix} = \begin{bmatrix} 0 \\ -ru + \dfrac{q_i S C_y}{m} \\ qu + \dfrac{q_i S C_z + P_z}{m} \end{bmatrix} \tag{2.39}$$

The missile is symmetric, so the lateral inertia moments are taken to be equal and using $p \cong 0$, dynamic equations can be reduced as,

$$\begin{bmatrix} \overset{\bullet}{p} \\ \overset{\bullet}{q} \\ \overset{\bullet}{r} \end{bmatrix} = \begin{bmatrix} \dfrac{q_i d_M S C_L}{I_{xx}} \\ \dfrac{q_i d_M S C_M}{I_{yy}} \\ \dfrac{q_i d_M S C_N}{I_{zz}} \end{bmatrix} \tag{2.40}$$

Assuming the following state:

A.10: Small θ, small ψ and $\Phi = 0$

leads

$$\begin{aligned}
&\sin(\Phi)=0,\cos(\Phi)=1\\
&\sin(\theta)\cong\theta,\cos(\theta)\cong 1\\
&\sin(\psi)\cong\psi,\cos(\psi)\cong 1
\end{aligned}\tag{2.41}$$

Using these facts, the translational kinematic equations become:

$$\begin{aligned}
\begin{bmatrix}\overset{\bullet}{X}\\ \overset{\bullet}{Y}\\ \overset{\bullet}{Z}\end{bmatrix}&=\begin{pmatrix}\cos\theta\cos\psi & \sin\theta\sin\Phi\cos\psi-\sin\psi\cos\Phi & \cos\psi\sin\theta\cos\Phi+\sin\Phi\sin\psi\\ \sin\psi\cos\theta & \sin\theta\sin\Phi\sin\psi+\cos\psi\cos\Phi & \sin\theta\cos\Phi\sin\psi-\sin\Phi\cos\psi\\ -\sin\theta & \cos\theta\sin\Phi & \cos\theta\cos\Phi\end{pmatrix}\\
&\cdot\begin{bmatrix}u\\ v\\ w\end{bmatrix}=\begin{pmatrix}1 & -\psi & \theta\\ \psi & 1 & 0\\ -\theta & 0 & 1\end{pmatrix}\cdot\begin{bmatrix}u\\ v\\ w\end{bmatrix}=\begin{bmatrix}u-v\cdot\psi+w\cdot\theta\\ u\cdot\psi+v\\ -u\cdot\theta+w\end{bmatrix}
\end{aligned}\tag{2.42}$$

Rotational kinematic equations become

$$\begin{aligned}
&\overset{\bullet}{\Phi}=p+\tan(\theta)\cdot\left(q\sin(\Phi)+r\cos(\Phi)\right)=p\\
&\overset{\bullet}{\theta}=q\cos(\Phi)-r\sin(\Phi)=q\\
&\overset{\bullet}{\psi}=\frac{r\cos(\Phi)-r\sin(\Phi)}{\cos(\theta)}=r
\end{aligned}\tag{2.43}$$

In order to simplify the mathematical model, decoupling of the equations of motion is quite suitable whenever possible. This is particularly useful for the analytical study of the equilibrium and the dynamics of the missile [6]. In this direction, decoupling approach suggests two decoupled sub-systems: (1) Longitudinal equations, and (2) Lateral equations. A flight in which the trajectory is contained in the (x, z) plane is called longitudinal and complementary system is called lateral. The linear state equations in longitudinal and lateral planes can be given as shown below.

Longitudinal Plane

When velocity in z-direction (w), angular acceleration about y-axis (q), angle about y-axis (θ) and position in z-direction (z) are taken as states, the longitudinal state equations can be written as:

$$\begin{bmatrix} \overset{\bullet}{w} \\ \overset{\bullet}{q} \\ \overset{\bullet}{\theta} \\ \overset{\bullet}{z} \end{bmatrix} = \begin{bmatrix} \dfrac{q_i S C_{z\alpha}(M,\alpha)}{um} & u + \dfrac{q_i S d_M C_{zq}(M,\alpha)}{2um} & 0 & 0 \\ \dfrac{q_i S d_M C_{m\alpha}(M,\alpha)}{uI_{yy}} & \dfrac{q_i S d_M{}^2 C_{mq}(M,\alpha)}{2uI_{yy}} & 0 & 0 \\ 0 & 1 & 0 & 0 \\ 1 & 0 & -u & 0 \end{bmatrix} \cdot \begin{bmatrix} w \\ q \\ \theta \\ z \end{bmatrix} + \begin{bmatrix} \dfrac{q_i S C_{z\delta}(M,\alpha)}{m} \\ \dfrac{q_i S d_M C_{m\delta}(M,\alpha)}{I_{yy}} \\ 0 \\ 0 \end{bmatrix} \cdot \delta_e \qquad (2.44)$$

$$\begin{bmatrix} \alpha \\ q \\ \theta \\ z \end{bmatrix} = \begin{bmatrix} 1/u & 0 & 0 & 0 \\ 0 & 1 & 0 & 0 \\ 0 & 0 & 1 & 0 \\ 0 & 0 & 0 & 1 \end{bmatrix} \cdot \begin{bmatrix} w \\ q \\ \theta \\ z \end{bmatrix} \qquad (2.45)$$

Lateral Plane

When velocity in y-direction (v), position in y-direction (y), angular acceleration about z-axis (r), angular acceleration about x-axis (p), angle about z-axis (Ψ) and angle about x-axis (Φ) are taken as states, the lateral state equations can be written as:

$$\begin{bmatrix} \dot{v} \\ \dot{r} \\ \dot{p} \\ \dot{\psi} \\ \dot{\Phi} \\ \dot{y} \end{bmatrix} = \begin{bmatrix} \dfrac{q_i S C_{y\beta}(M,\alpha)}{mu} & \dfrac{q_i S d_M C_{yr}(M,\alpha)}{2mu} - u & 0 & 0 & 0 & 0 \\ \dfrac{q_i S d_M C_{n\beta}(M,\alpha)}{uI_{zz}} & \dfrac{q_i S d_M{}^2 C_{nr}(M,\alpha)}{2uI_{zz}} & 0 & 0 & 0 & 0 \\ 0 & 0 & \dfrac{q_i S d_M C_{lp}(M,\alpha)}{2uI_{xx}} & 0 & 0 & 0 \\ 0 & 1 & 0 & 0 & 0 & 0 \\ 0 & 0 & 1 & 0 & 0 & 0 \\ 1 & 0 & 0 & u & 0 & 0 \end{bmatrix}$$

$$\cdot \begin{bmatrix} v \\ r \\ p \\ \psi \\ \Phi \\ y \end{bmatrix} + \begin{bmatrix} \dfrac{q_i S C_{y\delta}(M,\alpha)}{m} & 0 \\ \dfrac{q_i S d_M C_{n\delta}(M,\alpha)}{I_{zz}} & 0 \\ 0 & \dfrac{q_i S d_M C_{l\delta}(M,\alpha)}{I_{xx}} \\ 0 & 0 \\ 0 & 0 \\ 0 & 0 \end{bmatrix} \cdot \begin{bmatrix} \delta_r \\ \delta_a \end{bmatrix} \tag{2.46}$$

$$\begin{bmatrix} \beta \\ r \\ p \\ \psi \\ \Phi \\ y \end{bmatrix} = \begin{bmatrix} 1/u & 0 & 0 & 0 & 0 & 0 \\ 0 & 1 & 0 & 0 & 0 & 0 \\ 0 & 0 & 1 & 0 & 0 & 0 \\ 0 & 0 & 0 & 1 & 0 & 0 \\ 0 & 0 & 0 & 0 & 1 & 0 \\ 0 & 0 & 0 & 0 & 0 & 1 \end{bmatrix} \cdot \begin{bmatrix} v \\ y \\ r \\ p \\ \psi \\ \Phi \end{bmatrix} \tag{2.47}$$

CHAPTER 3

FLIGHT CONTROL AUTOPILOT

Missile flight control autopilots are the control systems, which take reference-desired commands in the longitudinal and lateral planes as input and output the related fin deflections. In this chapter, the autopilot design considering both of the decoupled longitudinal and lateral dynamics will be presented.

3.1 Control Loop

The autopilot loop is shown below:

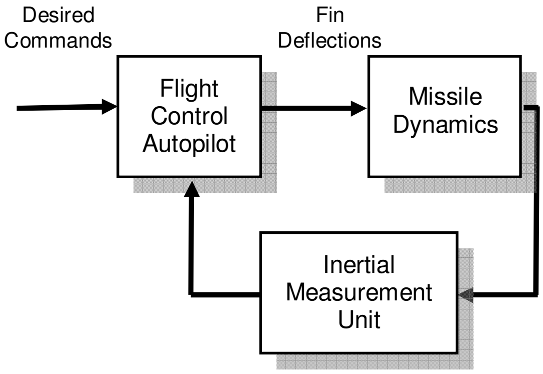

Figure 10 Autopilot Control Loop

Desired commands are provided by the guidance section to achieve the mission objective of the missile. There are different kinds of guidance algorithms and they will be discussed in the following chapter. The autopilot is responsible for the stabilization and outputs the control commands necessary to achieve the commanded signals. Inertial Measurement Unit (IMU) may provide missile position, acceleration or rate parameters and they are compared with the predefined trajectories in autopilot section. Not every parameter is measurable, but acceleration and rate can be measured with a three-axes accelerometer and three-axes gyroscope, respectively. The autopilot closes the loop in this scheme to achieve the required performance criteria.

3.2 Design Requirements

Every design should be based on some requirements, which are related to the performance of the overall system. Following are the design requirements for the autopilot system.

- Rise time should be less than 0.5 seconds,
- Percentage overshot for the step input should be less than 30%,
- Settling time should be less than 1.5 seconds,
- Steady-state error should be less than 5%.

3.3 PID Autopilot Design

While a variety of control methods can be formulated for the autopilot controls, basic PID (proportional-integral-derivative) controller will be implemented in this section. PID controllers are widely used in aerospace applications and they simply attempt to correct the error between measured sensor parameters and the desired values by calculating and outputting a corrective action that can adjust the process accordingly. PID controller has the transfer function:

$$G_C(s) = K_P + \frac{K_I}{s} + K_D \cdot s \tag{3.1}$$

The controller provides a proportional term, an integral term, and a derivative term [11]. The equation for the output in the time-domain is

$$u(t) = K_P e(t) + K_I \int e(t)dt + K_D \frac{de(t)}{dt} \tag{3.2}$$

where K_P is the “proportional gain”, K_I is the “integral gain” and K_D is the “derivative gain”.

The standard PID configuration is shown below:

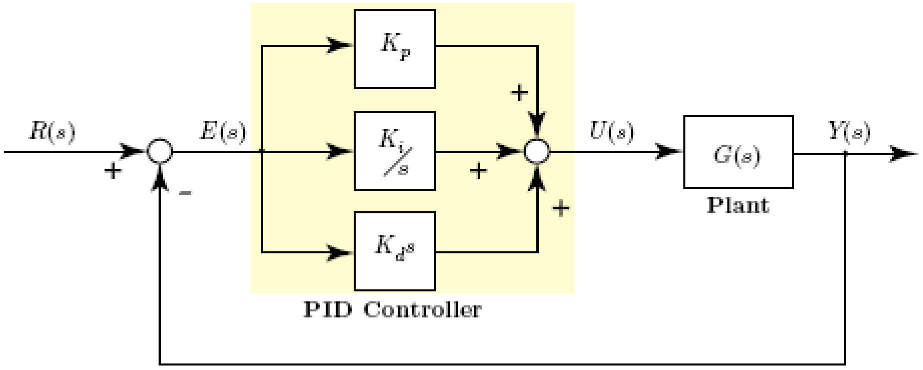

Figure 11 Generic PID scheme [10]

where Y(s) is the output signal, U(s) is the control signal, E(s) is the error signal and R(s) is the reference signal.

Each of the PID components (proportional, integral and derivative) has its advantages and disadvantages. Proportional gain’s obvious advantage is its simplicity; however there may be a steady-state error. The steady-state can be eliminated by integral part. The advantage of the integral controller is that the output is proportional to the accumulated error. The disadvantage of the integral controller is that it makes the system less stable by adding a pole at the origin. The advantage of the derivative controller is that the controller will provide large corrections if the error becomes large; however it will not produce a control output if the error is constant [12]. So by combining each controller into a single PID or a PI controller, one can eliminate most of the disadvantages.

Having obtained plant description and the controller method, the controller parameters should be tuned in order to satisfy the design requirements. Response Optimization of Simulink is used for determining the gain values for the PID controller.

3.3.1 Longitudinal PID Control

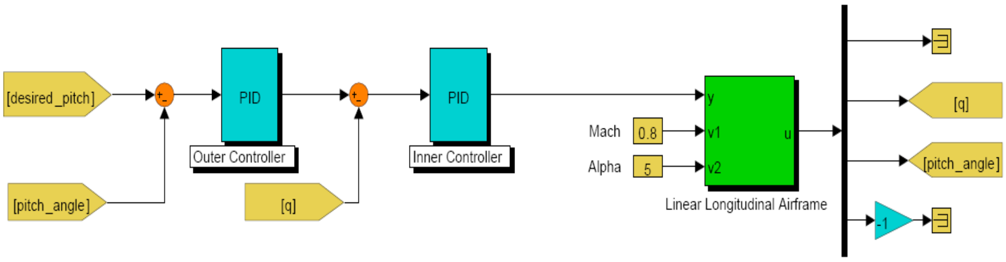

Figure 12 Longitudinal PID Controller

Longitudinal control can be satisfied by using two PID autopilot loops: inner loop stabilizes the fast rotational rate dynamics and the outer loop tracks the desired pitch angle, respectively. Longitudinal airframe implements gain-scheduled state-space representation depending on two scheduling parameters as defined by the following:

$$\begin{aligned} \dot{x} &= A(v_1,v_2)x + B(v_1,v_2)y \\ u &= C(v_1,v_2)x + D(v_1,v_2)y \end{aligned} \qquad (3.3)$$

where v_1 is the mach number and v_2 is the angle of attack over which A, B, C and D state-space matrices are defined. The scheduling assumes that

A.10: The A, B, C and D matrices vary smoothly as a function of v_1 and v_2.

This is a standard assumption especially in missile control applications. If the scheduling parameter inputs to the airframe go out of range, then they are clipped.

The desired and actual pitch angle response for designed system (Mach number = 0.8 and angle of attack = 5) is shown below:

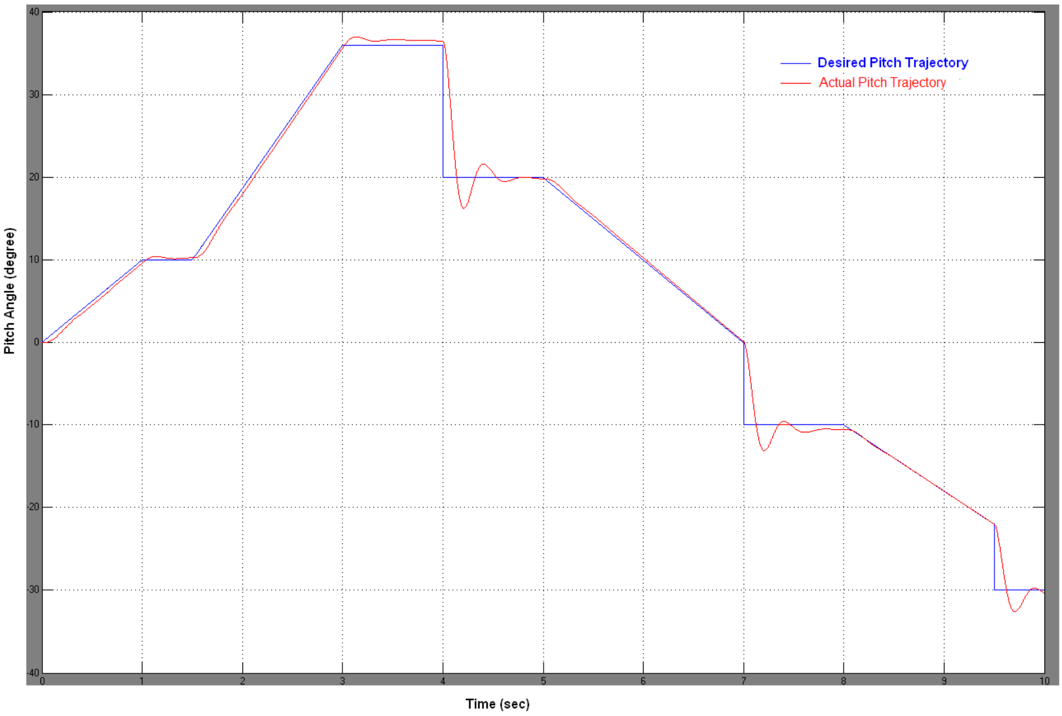

Figure 13 Desired and Actual Pitch Trajectory

The desired and actual pitch angle trajectories are shown above in blue and red lines, respectively. As figured below, all design requirements are satisfied for the system (Mach number = 0.8 and angle of attack = 5).

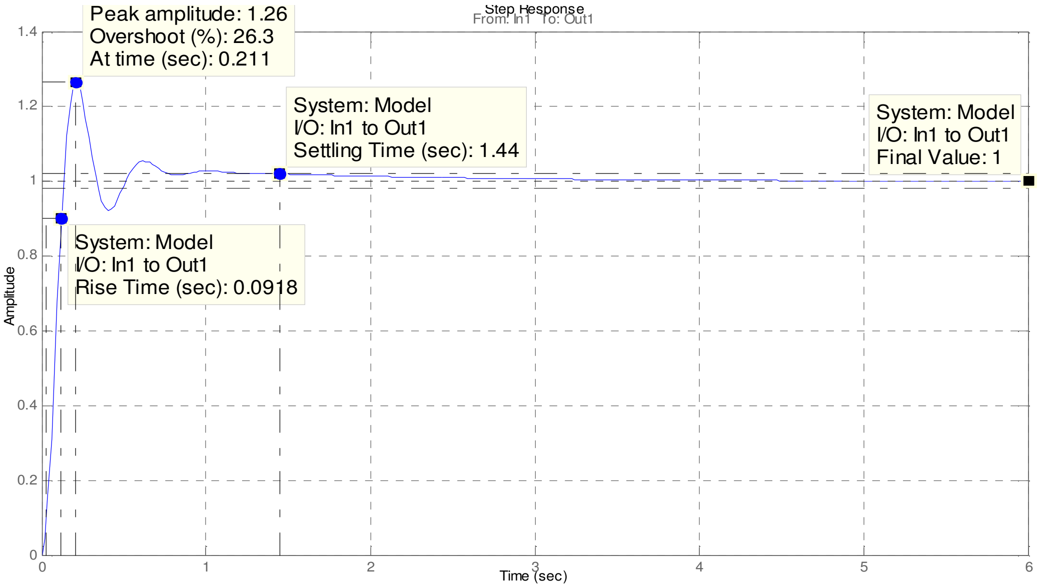

Figure 14 Step Response Graph for Pitch Control

3.3.2 Lateral PID Control

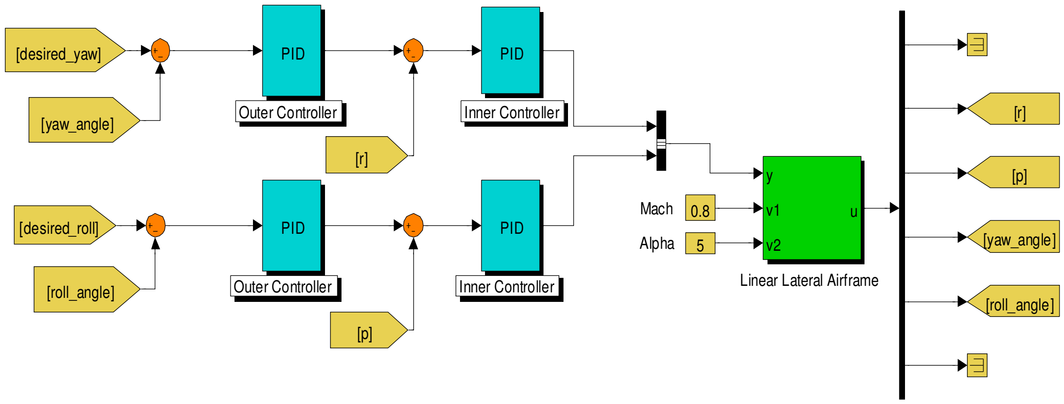

Figure 15 Lateral PID Controller

Lateral control can be satisfied by using two PID autopilot loops: inner loop stabilizes the fast rotational rate dynamics and outer loop tracks the desired yaw and roll angles, respectively. Lateral airframe implements gain-scheduled state-space representation depending on two scheduling parameters as defined by Formula 3.3.

The desired and actual yaw angle response for the system (Mach number = 0.8 and angle of attack = 5) is shown below:

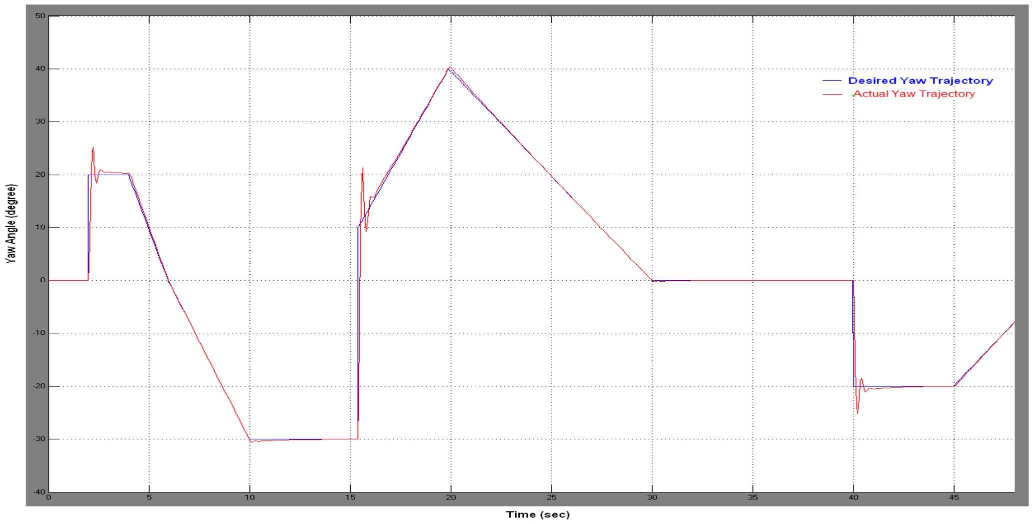

Figure 16 Desired and Actual Yaw Trajectory

The desired and actual yaw angle trajectories are shown above in blue and red lines, respectively. As seen below, all the design requirements are satisfied for the system (Mach number = 0.8 and angle of attack = 5).

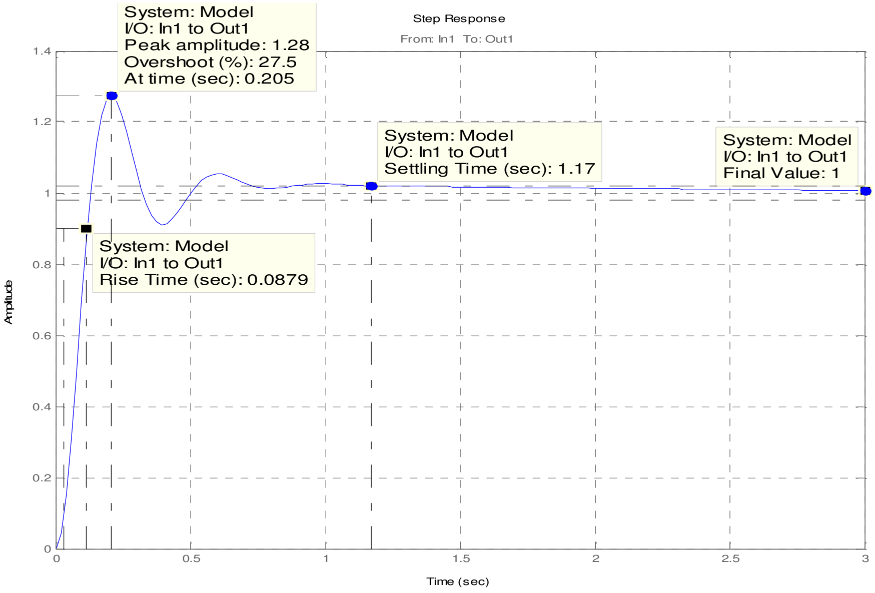

Figure 17 Step Response Graph for Yaw Control

The desired and actual roll angle response for the system (Mach number = 0.8 and angle of attack = 5) is shown below:

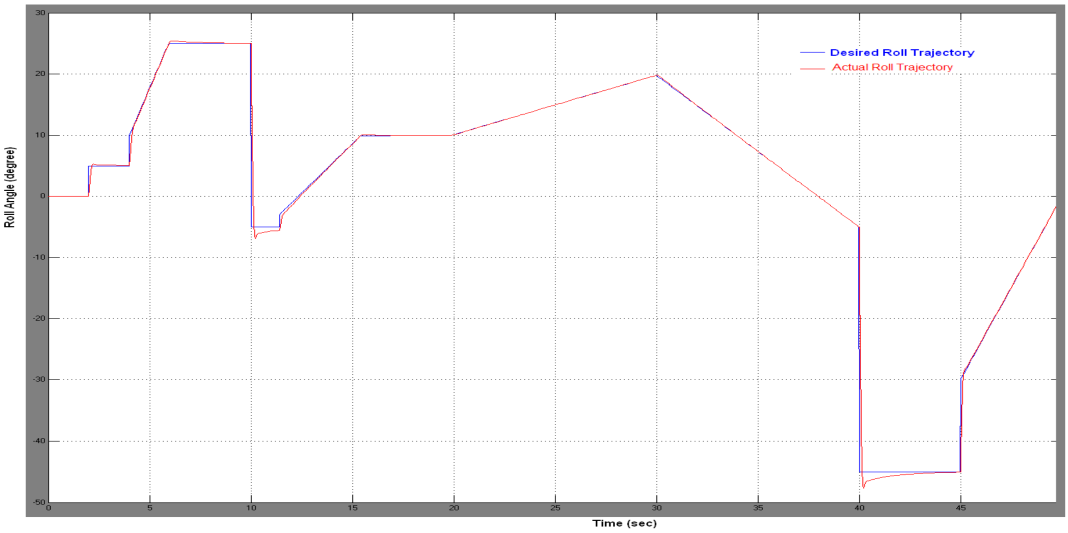

Figure 18 Desired and Actual Roll Trajectory

The desired and actual roll angle trajectories are shown above in blue and red lines, respectively. As seen below, all design requirements are satisfied for the system (Mach number = 0.8 and angle of attack = 5).

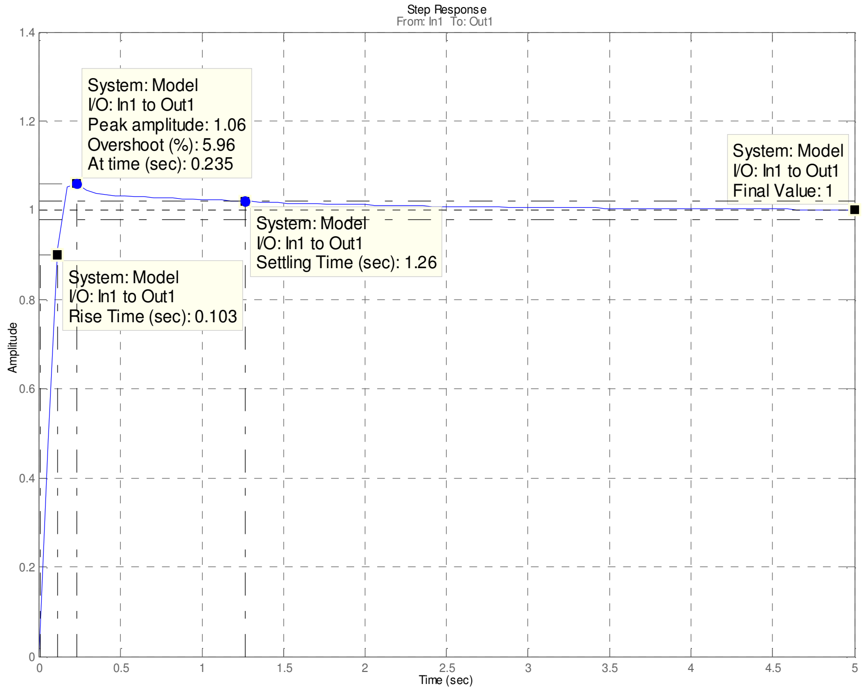

Figure 19 Step Response Graph for Roll Control

3.4 LQR Autopilot Controller

For a continuous linear time-invariant system described by

$$\dot{x} = A\,x + B\;u \qquad (3.4)$$

A LQR control law u = -Kx is determined so that the performance cost function

$$J = \frac{1}{2}\int_0^\infty \left(x^T Q\,x + u^T R\,u\right)dt \qquad (3.5)$$

can be minimized, where $x \in R^{n}$ is the state vector and $u \in R^{r}$ is the control vector. Here, $A \in R^{n \times n}$ and $B \in R^{n \times r}$ are constant matrices, $Q \in R^{n \times n}$ is a positive semi-definite matrix, and $R \in R^{r \times r}$ is a positive definite matrix. The Q and R weighting matrices are determined according to the design requirements.

In order to solve the problem, the dynamic optimization function can be transformed into the static case. Assume that there is a symmetric positive semi-definite matrix P, which satisfies:

$$\frac{d}{dt}\left(x^{T} P x\right) = -x^{T}\left(Q + K^{T} R K\right)x \tag{3.6}$$

Then the performance cost function can be written as,

$$J = \frac{1}{2} x^{T}(0) P x(0) - \frac{1}{2} \lim_{t \to \infty} x^{T}(t) P x(t) \tag{3.7}$$

If we assume that the closed-loop system is asymptotically stable, then cost function becomes:

$$J = \frac{1}{2} x^{T}(0) P x(0) \tag{3.8}$$

For the closed-loop system

$$\dot{x} = (A - BK)x = A_{c} x \tag{3.9}$$

The equation 3.6 becomes

$$-x^{T}\left(Q + K^{T} R K\right)x = \dot{x}^{T} P x + x^{T} P \dot{x} = x^{T}(A_{c}^{T} P + P A_{c})x \tag{3.10}$$

Equivalence stated in equation 3.10 must hold for every initial condition, hence

$$g = A_c^T P + PA_c + K^T RK + Q = 0 \tag{3.11}$$

Thus, the optimization problem is transformed into finding the feedback gains K that minimizes the cost function J. The Lagrange multiplier approach is used to solve the resultant constrained optimization problem. The Lagrangian is

$$H = \frac{1}{2} x^T(0) Px(0) + gS \tag{3.12}$$

where S is a symmetric matrix of Lagrange multipliers. The necessary conditions are:

$$\begin{aligned} 0 &= \frac{\partial H}{\partial S} = g = A_c^T P + PA_c + K^T RK + Q \\ 0 &= \frac{\partial H}{\partial P} = A_c S + SA_c^T + x(0) \\ 0 &= \frac{1}{2}\frac{\partial H}{\partial K} = RKS - BPS \end{aligned} \tag{3.13}$$

If R is positive definite, then the feedback gains (K) can be found as

$$K = R^{-1} B^T P \tag{3.14}$$

So, there is no need to solve the S in order to find feedback gains. This result leads us:

$$0 = A^T P + PA + Q - PBR^{-1} B^T P \tag{3.15}$$

which is called “**Algebraic Riccati Equation**”. Solving equation 3.15 is sufficient to compute feedback gains. During the programming phase, MATLAB’s “lqr” function is used to solve Riccati equations.

3.4.1 Longitudinal LQR Control

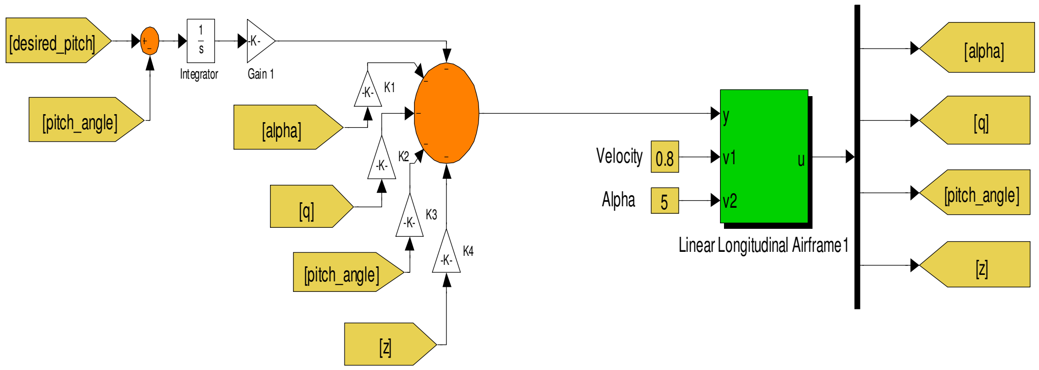

Figure 20 Longitudinal LQR Controller

Longitudinal motion can be controlled using an LQR controller, as well. The feedback gains are found from MATLAB's "lqr" function. Longitudinal airframe implements gain-scheduled state-space representation depending on two scheduling parameters as defined by Formula 3.3.

The desired and actual pitch angle for the system (Mach number = 0.8 and angle of attack = 5) is shown below:

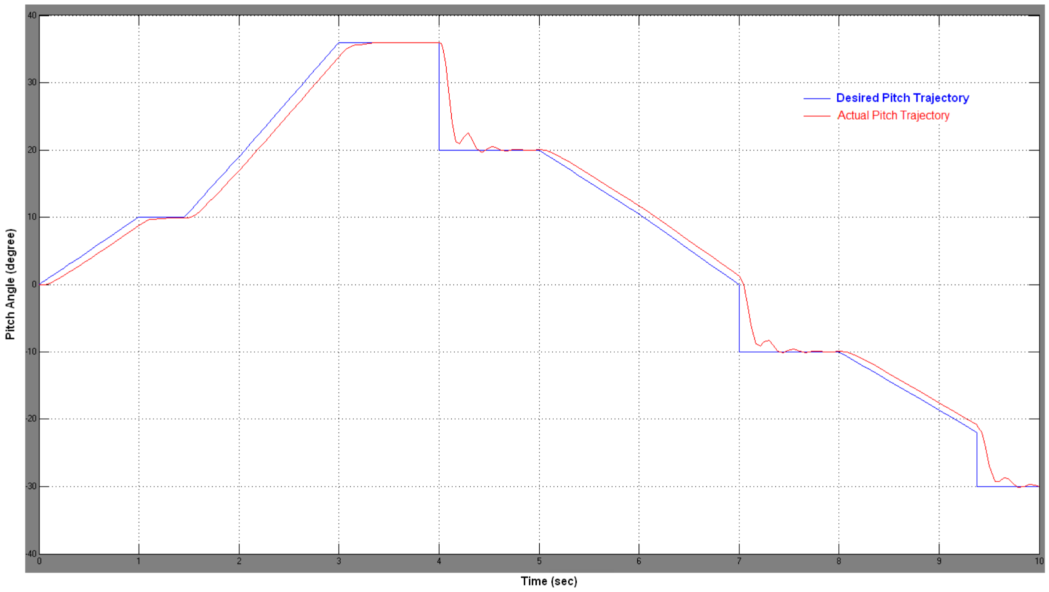

Figure 21 Desired and Actual Pitch Trajectory

The desired and actual pitch angle trajectories are shown above in blue and red lines, respectively. As seen below, the design requirements are satisfied for the system (Mach number = 0.8 and angle of attack = 5).

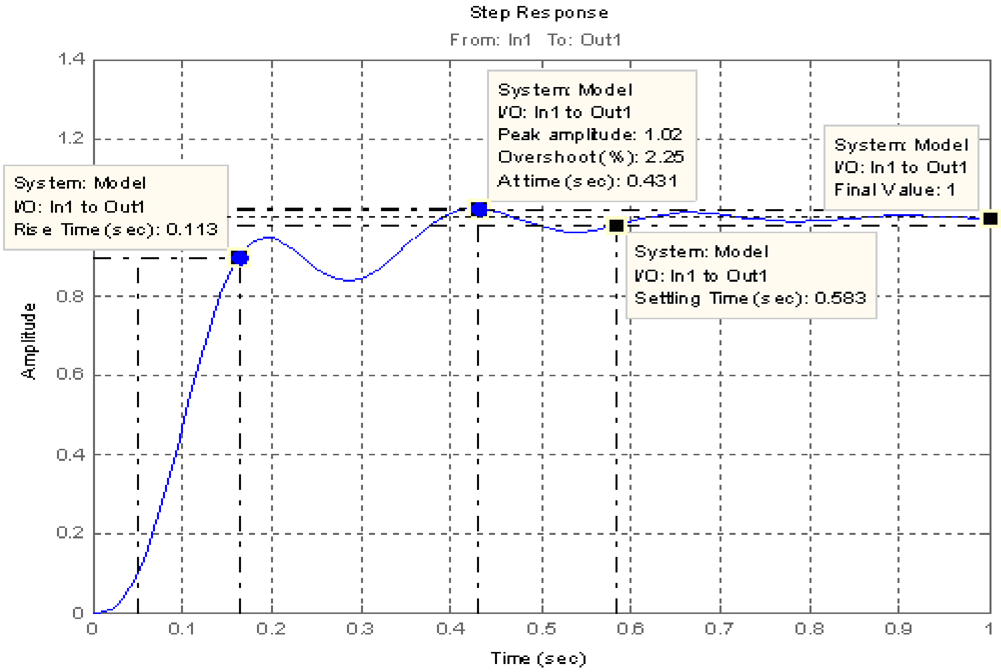

Figure 22 Step Response Graph for Pitch Control

3.4.2 Lateral LQR Control

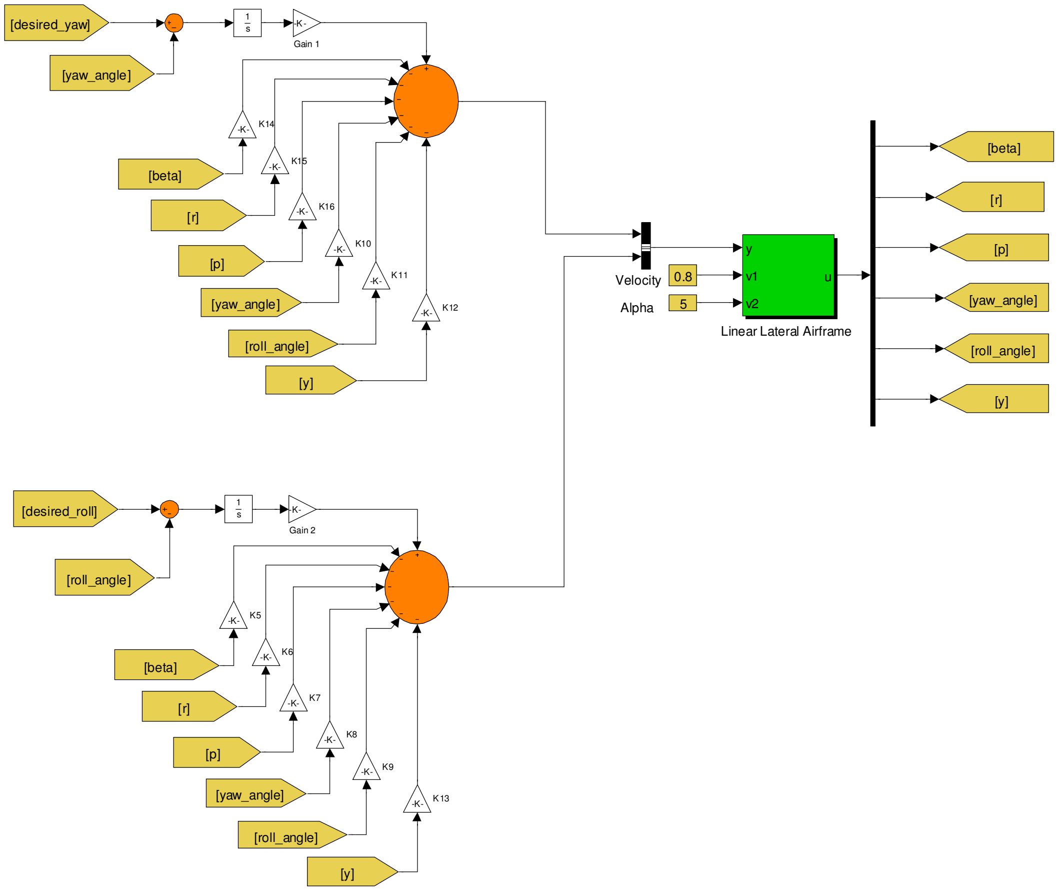

Figure 23 Lateral LQR Controller

Lateral motion can be controlled using an LQR controller, also. The feedback gains are found from MATLAB's "lqr" function. Lateral airframe implements gain-scheduled state-space representation depending on two scheduling parameters as defined by Formula 3.3.

The desired and actual yaw angle for the system (Mach number = 0.8 and angle of attack = 5) is shown below:

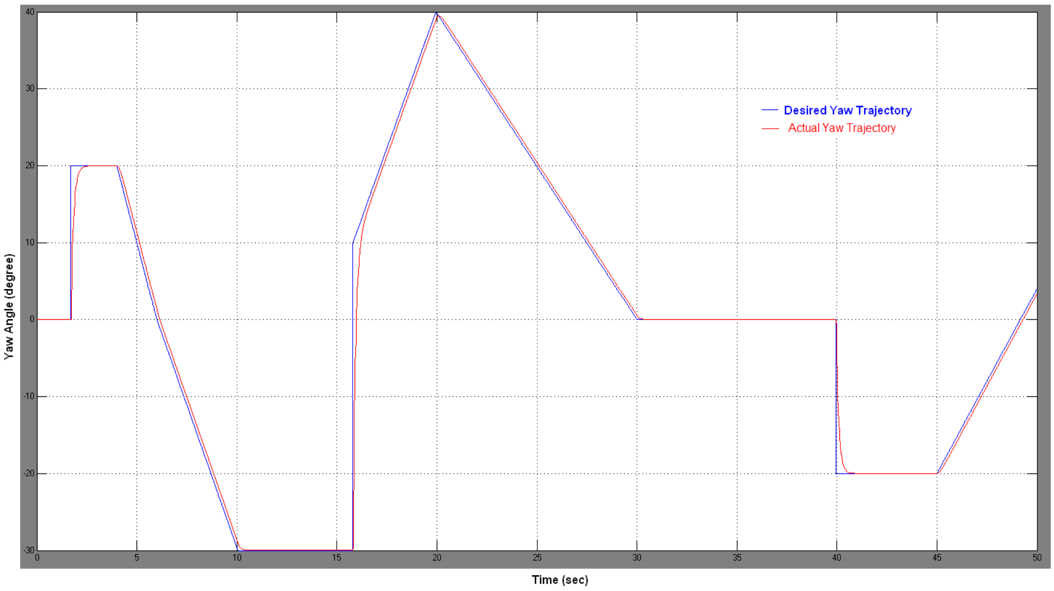

Figure 24 Desired and Actual Yaw Trajectory

The desired and actual pitch angle trajectories are shown above in blue and red lines, respectively. As seen below, the design requirements are satisfied for the system (Mach number = 0.8 and angle of attack = 5).

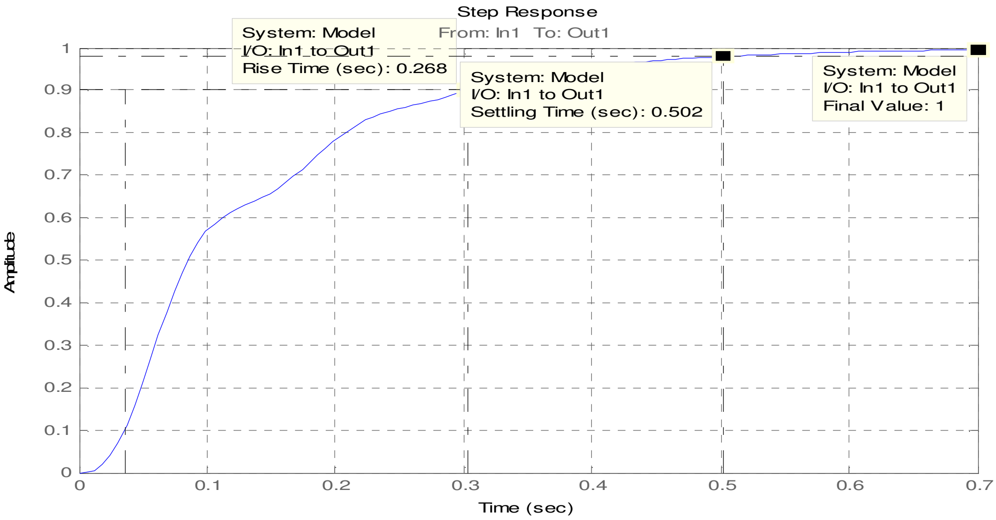

Figure 25 Step Response Graph for Yaw Control

The desired and actual roll angle for the system (Mach number = 0.8 and angle of attack = 5) is shown below:

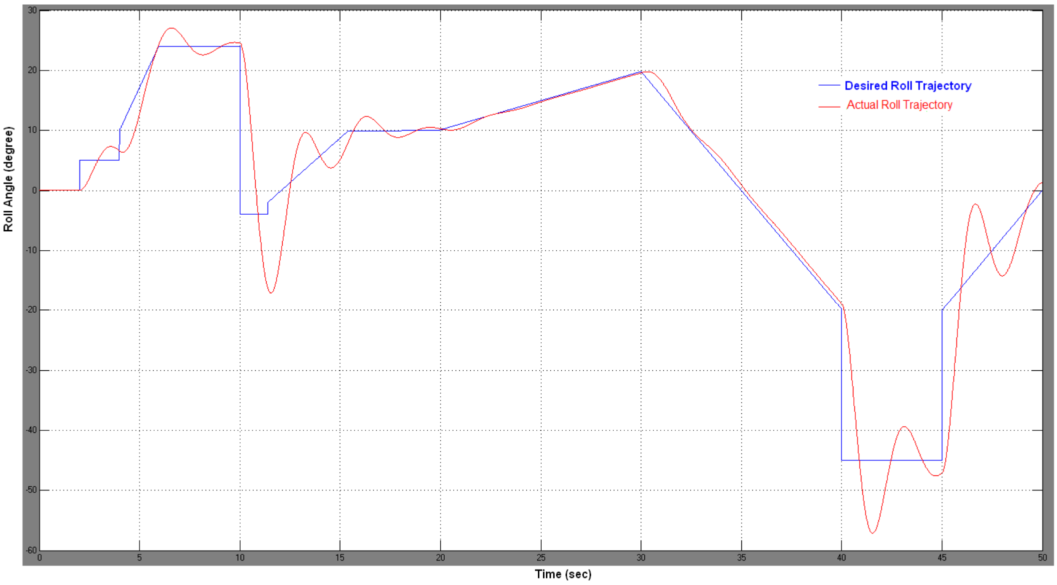

Figure 26 Desired and Actual Roll Trajectory

The desired and actual pitch angle trajectories are shown above in blue and red lines, respectively. As seen below, the design requirements (rise time, settling time and overshoot) are not satisfied for the system (Mach number = 0.8 and angle of attack = 5).

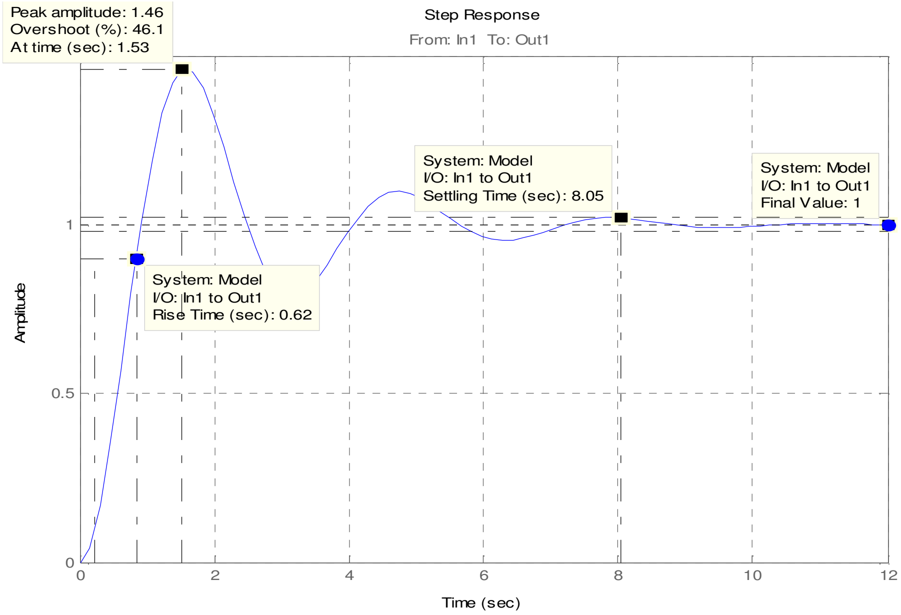

Figure 27 Step Response Graph for Roll Control

PID controller satisfies all of the requirements in both planes; however LQR controller does not satisfy roll control requirements in the lateral plane. Therefore, PID controller is selected as the basic autopilot controller in the following sections.

CHAPTER 4

IMAGING INFRARED GUIDANCE DESIGN

Missile guidance refers to a variety of methods of guiding a missile to its enemy target. It determines the nature of the flight path navigation model. There are various guidance methods for anti-tank missiles by which sensors and a tracking system can be used to deliver the missile to its enemy target.

MCLOS (manual command to line-of-sight) guidance is a *first-generation* method. Typically, the missile is steered with a joystick and the operator must track the missile and the tank simultaneously in order to hit the target. In 1967 Six-day War, in 1972 Vietnam War and in 1973 Yom-Kippur War, MCLOS guided anti-tank missiles were used against enemy tanks. Because MCLOS requires high operator concentration and training, its usage is very limited and average of ~30% hit probability has been achieved [29]. ENTAC, 9K11 Malyutka and SS.11 are popular representatives of MCLOS anti-tank missiles.

SACLOS (semi-automatic command to line-of-sight) guidance is a *second-generation* method. In this guidance technique, the operator has to continuously point a sighting device at the target, while the missile is in flight. MCLOS guided missiles have been mostly replaced by the SACLOS types today. TOW, MILAN, Kornet and Swingfire are popular representatives of SACLOS anti-tank missiles.

Fire-and-forget guidance is a *third-generation* and the most-advanced method, which does not require further guidance after the missile launch. The gunner locks on the automatic target tracker in the missile before launch. Javelin, Spike and AGM-114L Longbow Hellfire are some of the most popular examples of fire-and-forget anti-tank missiles. Some modern fire-and-forget anti-tank missiles include a data link between the missile and the launcher platform, which allows the gunner to watch the video taken by the missile seeker in flight and update the target information as well as fire-and-forget capability. SPIKE family is an example for that concept.

Developed first-generation command-guided and second-generation semi-automatic command guided missiles had many disadvantages and lower hit rates. For that reason, third generation imaging infrared fire-and-forget anti-tank missile concept is very popular nowadays.

In this thesis, the anti-tank missile is considered to be a fire and forget type with update capability. Therefore, the gunner does not need to lock-on the target before launch, but can choose and lock on the target after launch.

In this chapter, major components of fire-and-forget guidance method are developed.

4.1 Imaging Infrared Seeker Model

In order to hit the enemy target, it is vital to get correct information about the target during the missile flight. For imaging infrared fire-and-forget anti-tank missiles, that information is provided by a seeker. A typical seeker consists of three major components: (1) An imaging system, (2) a gimbal, and (3) a processor [2].

4.1.1 Infrared Imaging System

Every object in nature emits radiation, which spread over a frequency spectrum. Due to atmospheric spectral transmittance, there are seven regions in the spectrum as described in Figure 28, which should be considered in the design of an electronic imaging system. The ultraviolet region ranges in wavelength from 0.2 to 0.4 µm. The visible spectrum region ranges in wavelength from 0.4 to 0.7 µm. Televisions, human-eye and most solid state cameras operate in this region. The near infrared imaging spectral region (NIR) spans approximately 0.7 to 1.1

µm. Low light televisions, image intensifiers and night vision goggles operate in this region. The first infrared imaging band is the short wavelength infrared region (SWIR) which covers 1.1 to 2.5 µm. The second infrared band is the mid-wavelength infrared (MWIR) band that covers 2.5 to 7 µm. The third infrared band is the long-wavelength infrared (LWIR) band which covers from 7 to 15 µm. The forth and fifth infrared spectral bands are the far infrared (FIR) and very long wavelength infrared (VLWIR) regions and they extends spectral region beyond 15 µm [14].

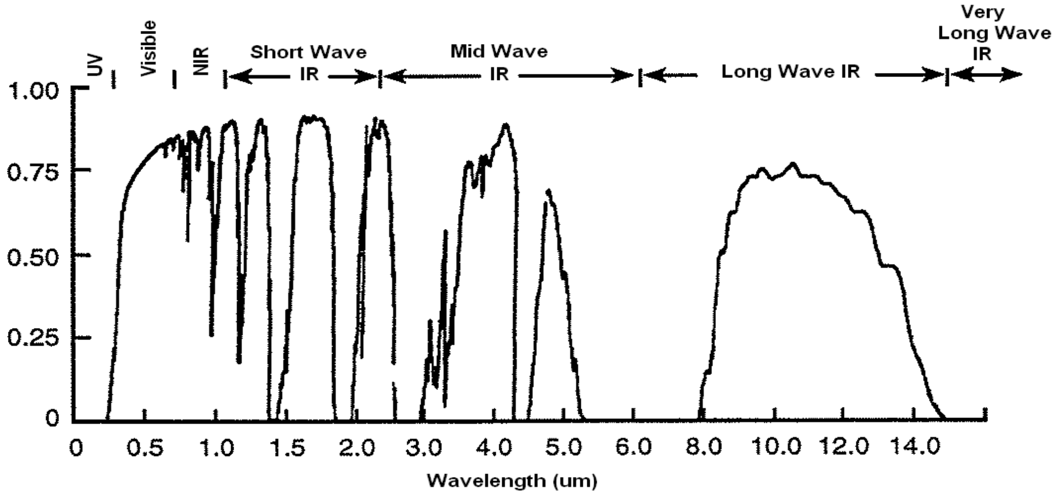

Figure 28 Atmospheric Transmittance [14]

Thermal infrared imaging is generally designed to be in the mid-wavelength infrared or long-wavelength infrared bands. In these spectral regions, thermal or heat sources are sensed rather than visible light [15]. This technology is basically based on sensing and displaying of infrared flux variations. The variations in the displayed image intensity represent apparent temperature variations across the scene [14]. There are many different applications for infrared imaging such as fire control, reconnaissance, target acquisition, border patrol, etc. Anti-tank guided missile is another critical area of infrared imaging and modern anti-tank missile performance strictly depends on the imaging performance. In Figure 29, a reference infrared seeker view of an imaging infrared anti-tank missile is given.

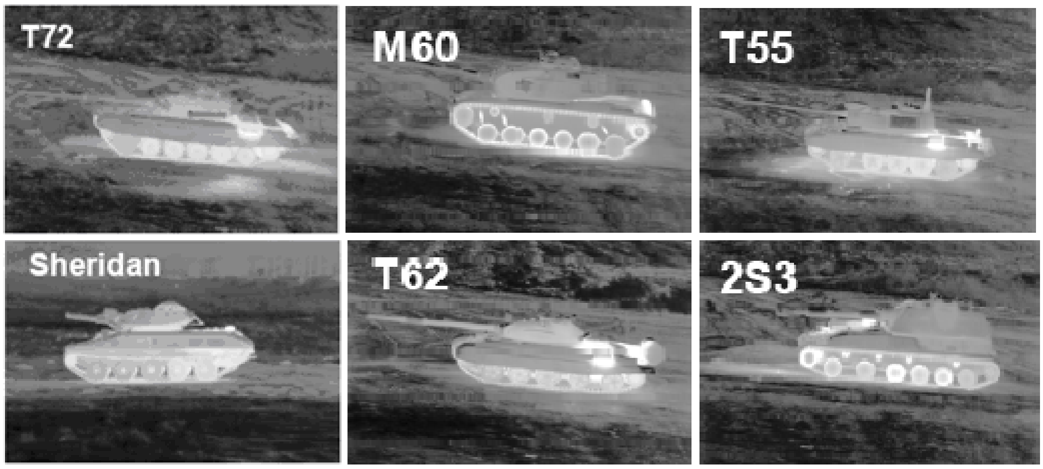

Figure 29 Infrared View of an Anti-Tank Missile [16]

The Infrared imaging system consists of many subsystems. Each of which processes information differently. Figure 30 illustrates the major components: optics and scanner, detector & electronics and digitization & image reconstruction.

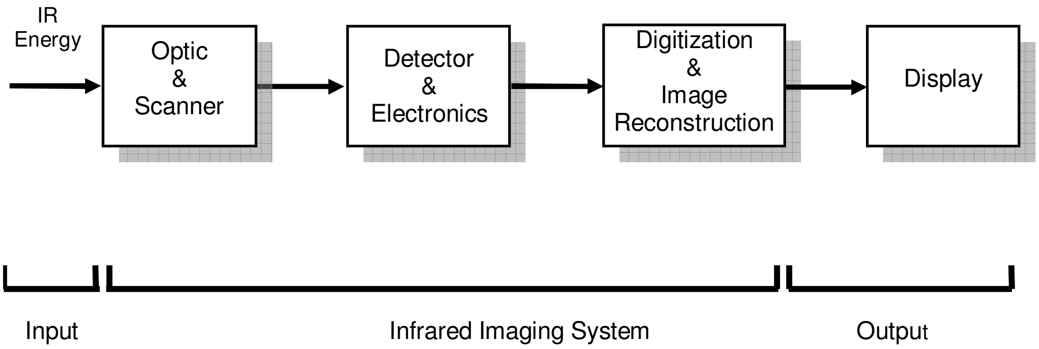

Figure 30 Generic Infrared Imaging System Components

The optics and scanners part take the radiation onto the detector(s) and generally a very limited number of materials (germanium, sapphire, silicon, etc.) are efficiently used in MWIR and LWIR regions. Infrared detectors are costly and difficult to manufacture; for this reason detector arrays are mostly small in extent so the scanners optically move the detector’s instantaneous field-of-view across the desired field-of-view to create a full two-dimensional field-of-view. A detector is the hearth of every optical system because it converts scene radiation into a measurable electrical signal. Amplification and signal processing creates an electronic image in which voltage differences represent scene intensity differences due to the various objects in the field-of-view. Signals are then digitized because of the relative ease to manipulate. Current systems run software such as gain-level normalization, image enhancement and gamma correction algorithms after digitization. Finally, scene image is reconstructed again and displayed on the monitor [14]. For an anti-tank imaging infrared missile, display is on the launcher platform (helicopter or land vehicle), so video is transferred via fiber-optic cable or radio frequency datalink between the missile and the launcher platform. Usually, a human operator views the display and tries to make a decision as to the existence of a target.

Target acquisition performance depends on many parameters such as detector resolution, sensitivity, optics, spectral response, A/D performance, human eye response, display type, etc. In general increasing the range decreases the acquisition performance, since the number of pixels on the target decreases as a function of range. The first task is searching the field-of-view to find a target. It varies on observer training and response characteristics. Operator decides whether suspicious hot spot is a vehicle or a terrain feature on detection level. After detection, attention is focused on a particular area of the scene. As the amount of detail perceived by the observer increases, the class to which the object belongs (tank, tuck, APC, etc.) becomes more clear in the recognition level. Finally, the target is discerned with sufficient clarity to specify the type (M60, T52, etc.) in the identification level as described in Figure 31.

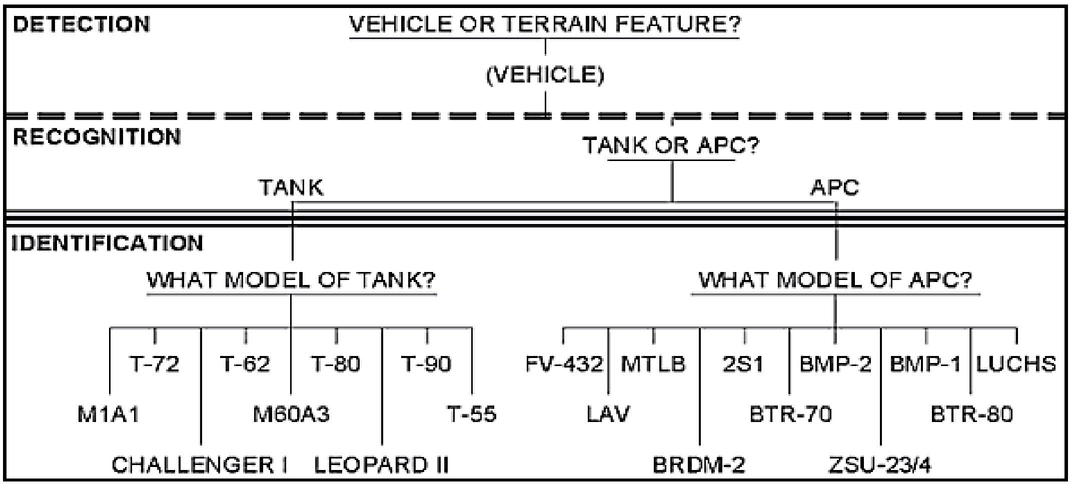

Figure 31 Detection, Recognition and Identification of the Target

Usually, the launcher platform has a high-performance thermal camera contrary to the missile seeker, because the operator needs a high-resolution image to identify a target as friend or foe before launching the missile. The missile seeker’s thermal imager just has to detect the target after the operator has recognized or identified it using the platform camera.

Testing the performance of an anti-tank missile with a real scenario involves firing the missile repeatedly, which maximizes the project cost a lot. Thus, it has become necessary to develop a simulation based performance measure. To validate the simulation results, a limited number of captive flight tests can be made. In the past, imaging infrared scene scenarios were formed by recording the movement of the target using an IR camera. These recordings were played back and performance validations were tested [18]. However, scenarios were very limited in these setups. Therefore, the results obtained from these experiments would not always lead to quantitative conclusions about the system performance.

Nowadays modern simulations are based on low-cost, reliable and realistic computer-based models. While it is necessary to build the imaging infrared views of critical elements in a scene, it is possible to model every detail of the real-world with that type of simulation [17].

In this thesis, Virtual Reality Toolbox in MATLAB® [19] software is used as the simulation environment. The Virtual Reality toolbox is part of the MATLAB® software that is used to create and visualize dynamic systems. It allows user to connect virtual world, defined with VRML (Virtual Reality Modeling Language), to Simulink and MATLAB®. Details of the Virtual Reality Toolbox and VRML language are given in Appendix-2.

In Figure 32, the imaging infrared video generation block is described.

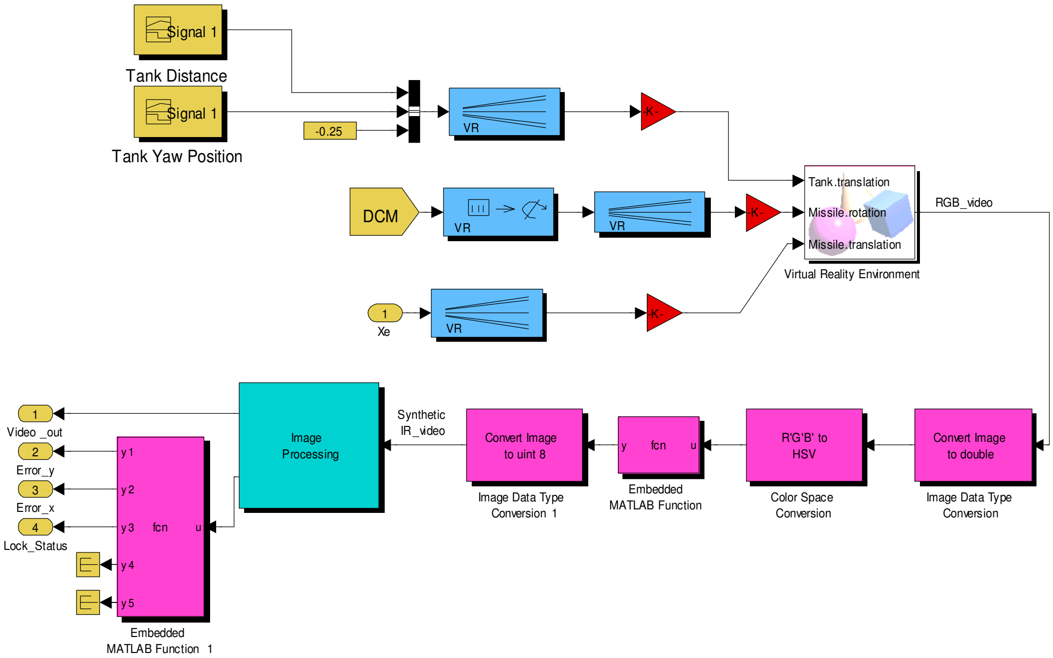

Figure 32 IR Video Generation Block

Because of the difference between MATLAB graphics and VRML coordinate systems as described in Appendix-2, target and missile position and rotation information should be transformed before applying to the Virtual Reality block. Then, Simulink data is written to the virtual world and RGB color video output is generated. This video is directly related with missile seeker field-of-view. For the current version of Virtual Reality Toolbox, there is only a RGB color video output in the related block. Thus, conversion from RGB to infrared video format is necessary for simulation purposes. First method is using commercial infrared scene generators, which directly generates infrared scene representations.

Although, there exist some successful versions of these IR scene generators, it seems not feasible to use them in this thesis, because of the cost. Therefore, an alternative method, transforming RGB to HSV and using saturation channel, is selected. Transformed video is not a real representation of thermal flux variations, but it looks like an infrared scene.

HSV describes colors as points in a cylinder whose central axis ranges from black at the bottom to white at the top with neutral colors between them, where angle around the axis corresponds to “hue”, distance from the axis corresponds to “saturation”, and distance along the axis corresponds to “value” [20]. Conversion from RGB to HSV format is based on the information below:

Let r, g, b $\in$ [0,1] be the red, green, and blue coordinates, respectively, of a color in RGB space and let max be the greatest and min be the least of r, g and b.

hue $\in$ [0, 360] is computed as

$$h = \begin{cases} 0 & \text{if} \quad \max = \min \\ (60^o \times \frac{g-b}{\max - \min}) \bmod 360, & \text{if} \quad \max = r \\ 60^o \times \frac{b-r}{\max - \min} + 120^o, & \text{if} \quad \max = g \\ 60^o \times \frac{r-g}{\max - \min} + 240^o, & \text{if} \quad \max = b \end{cases} \tag{4.1}$$

saturation $\in$ [0,1] is computed as

$$s = \begin{cases} 0, & \text{if} \quad \max = 0 \\ \frac{\max - \min}{m} = 1 - \frac{\min}{\max}, & \text{otherwise} \end{cases} . \tag{4.2}$$

value is computed as

$$v = \max . \tag{4.3}$$

Infrared scene is generated by using Formula 4.4 as

$$IR\_scene = (1-s)\ . \tag{4.4}$$

In Figure 33, a sample RGB image and its HSV versions are presented.

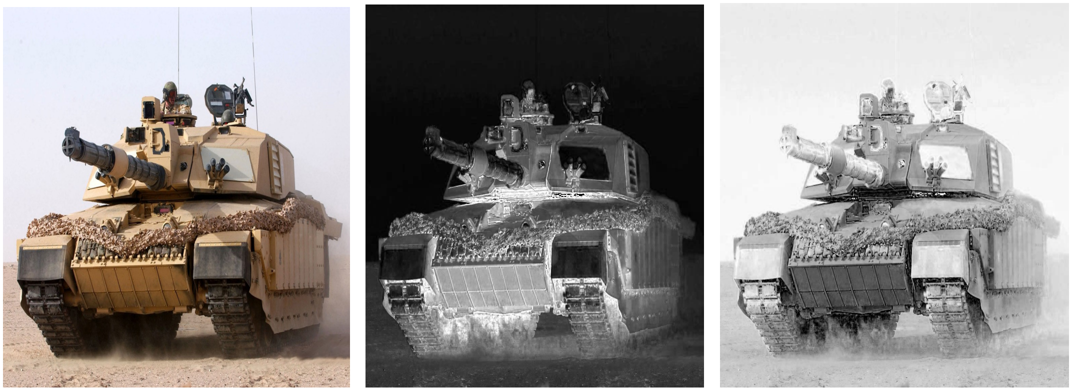

Figure 33 RGB, Saturation and (1-Saturation) Images

4.1.2 Gimbal

The development of stabilization and tracking system technology has been motivated by many applications in which there are a need to stabilize the line-of-sight (aimpoint) [3]. The missile seeker contains two-axis and stabilized gimbal in order to satisfy these needs as described in Figure 34. The gimbal is a pivoted support that allows the rotation of the infrared imaging system about a single axis. The two gimbal angles are the azimuth (ψ) and elevation (θ) angles, which are defined in the same manner as the Euler angles [21]. The x-axis indicates the line-of-sight (LOS) direction.

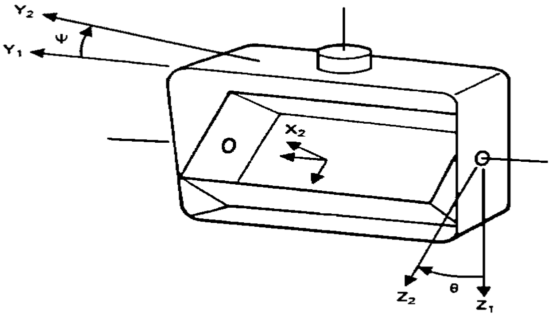

Figure 34 Gimbal [3]

Figure 35 shows a typical missile-target angle representation for a gimbaled seeker. The angle between inertial reference frame and missile body is called body attitude (θ_b). It is the simplest use of the orientation of the missile with respect to the horizon. Gimbal angle (θ_g) is represented by the angle between gimbal axis and the missile body. It is the combination of azimuth (ψ) and elevation (θ) angles defined in Figure 34. If gimbal angle is zero, missile body heads towards the gimbal orientation. The angle between the missile body and missile-target line is called the look angle (θ_L). Above all, the angle between missile-target line and the gimbal axis is the error angle ($\in$), in which the gimbal controller nulls it to hold the target at boresight (in the center of the sensor field-of-view). Gimbal controller performance depends mostly on the error angle size.

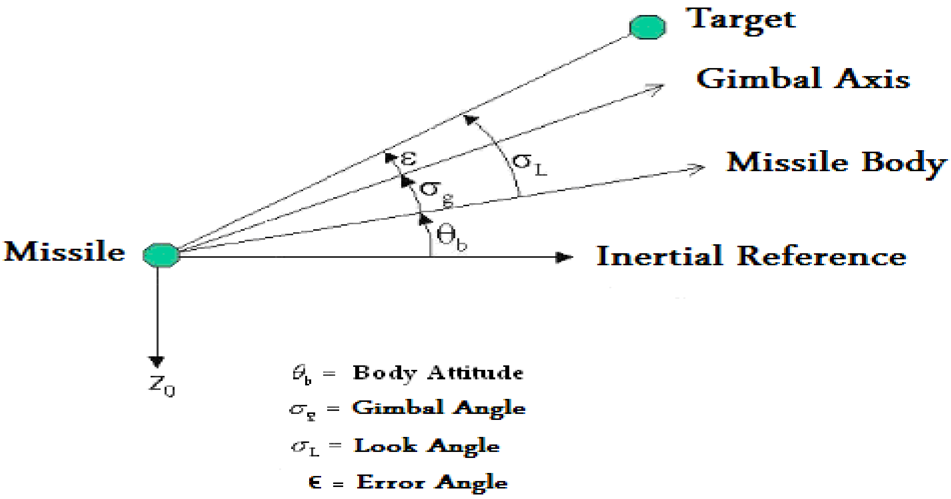

Figure 35 Gimbal and Body Angles

A generic gimbal configuration includes Gimbal dynamics representation, gyro models and a gimbal controller as described in Figure 36. Output pitch_cmd and yaw_cmd signals represent azimuth (ψ) and elevation (θ) gimbal angles. Error angles are produced by the processor section as presented in Chapter 4.1.3.

Gimbal dynamics model is characterized by a second order response as

$$G_{gimbal}(s) = \frac{nf\_gimbal^2}{s^2 + (2 \cdot dr\_gimbal \cdot nf\_gimbal)s + nf\_gimbal^2} \qquad (4.5)$$

where natural frequency of the gimbal (nf_gimbal) is 320Hz and the damping ratio of gimbal (dr_gimbal) is 0.7. Gyro dynamics model is also characterized by a second order response as

$$G_{gyro}(s) = \frac{nf\_gyro^2}{s^2 + (2 \cdot dr\_gyro \cdot nf\_gyro)s + nf\_gyro^2} \tag{4.6}$$

where natural frequency of gyro (nf_gyro) is 620Hz and the damping ratio of gyro (dr_gyro) is 0.7.

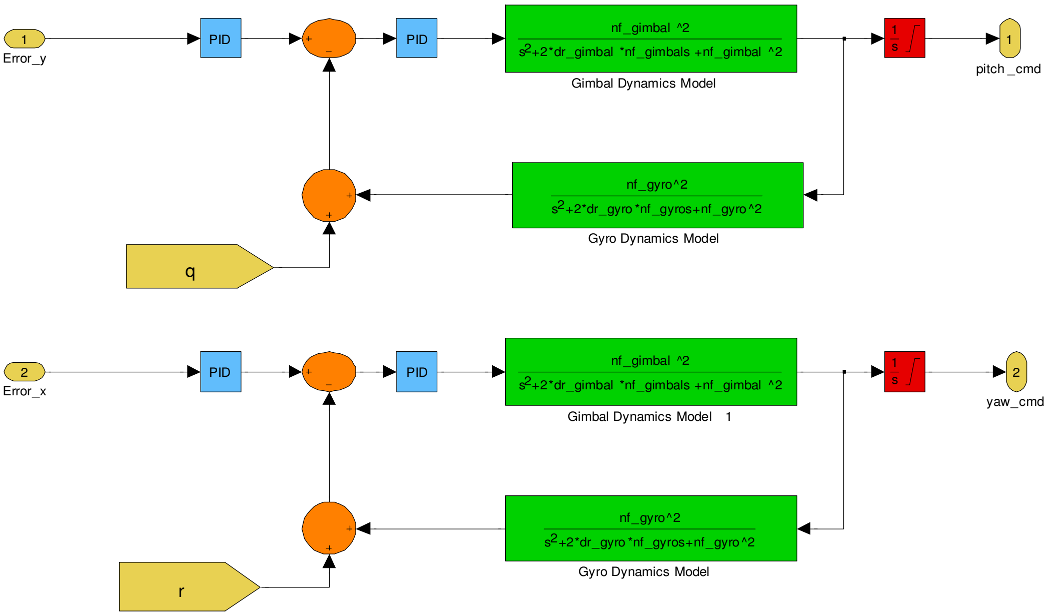

Figure 36 Gimbal Dynamics Representation

Gyro is perhaps the most critical component of the gimbal system. Its dynamic characteristics largely determine the control system bandwidth and system performance that can be achieved [3]. The azimuth gyro has its input axis along the x-axis, and drive the gimbal system about the z-axis, and the elevation gyro has its input axis along the y-axis [21]. For longitudinal orientation, y-axis angular rate (q) is added to the gyro response in order to insert the missile body angular effects to the gimbal dynamics; and for lateral orientation, z-axis angular rate (r) is added to the gyro response in order to insert the missile body angular effects to the gimbal dynamics.

There exist two gimbal controllers for longitudinal and lateral dynamic parts, respectively. First controller (proportional controller) is called the tracking controller; longitudinal part nulls the y-axis error angle (in pixel) and lateral part nulls the x-axis error angle (in pixel). Inner controller is called the stabilization controller, which stabilizes the target in the center of the sensor field-of-view. This inner controller is selected as a PI (proportional integral) controller. Response Optimization of Simulink is used for determining the gain values for P and PI parameters.

4.1.3 Processor

For an anti-tank imaging infrared missile, one of the most critical issues to provide high target kill probability is the tracking performance, running in the processor section. Tracking systems are employed in a wide variety of environments. They are used in numerous applications including fire control, navigation and missile guidance.

In a typical closed loop imaging infrared tracker, the input to the processor subsystem is the infrared video and the output is the angular displacement between the measured target LOS and the gimbal axis [22].

Many different methods of target tracking algorithms have been developed, but fundamental, simple and reliable algorithms, *centroid* and *correlation,* are frequently used in missile applications. Moreover, active contour (snake) method is studied in this thesis, additionally.

4.1.3.1 Centroid Tracker

Centroid tracker is based on target/background classification and target’s centroid computation using target and background histograms. It typically operates by applying a threshold to the image to segment the scene into target and background regions. The threshold is usually updated during missile flight. Once target pixels are estimated, the centroid can be determined as the weighted average of measured intensities [22]. Then the gate position and size are updated according to the centroid coordinates. These steps are presented in Figure 37 and discussed in the following sections.

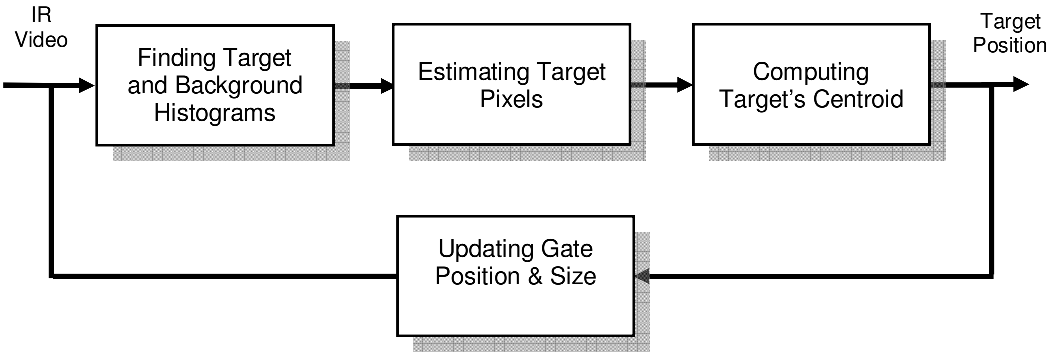
IR Video
Finding Target and Background Histograms
Estimating Target Pixels
Computing Target's Centroid
Target Position
Updating Gate Position & Size

Figure 37 Centroid Algorithm

4.1.3.1.1 Finding Target and Background Histograms

In every frame, centroid tracker estimates new target position and background gates according to the target gate as described in Figure 38. Gating reduces the number of operations that must be performed to determine the target position. In addition to this, effects of noise and clutter on the tracking process are largely suppressed by using target and background gates [2].

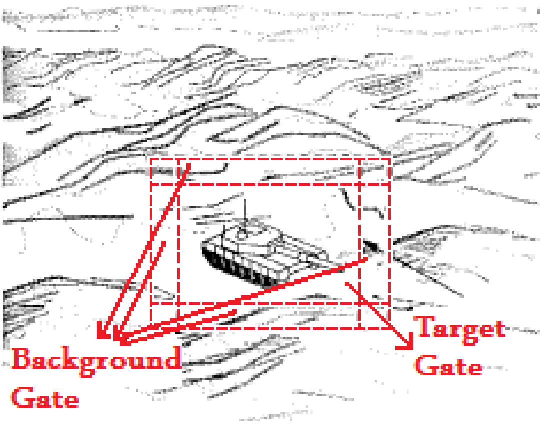

Figure 38 Target and Background Gates

In the implementations in this study, there exist one target gate and four background gates, in which histograms are computed. Histogram shows intensity distribution of gates. Previous and current frame's target and background histograms are correlated using the Formula 4.7, because current histograms can be unreliable in some frames.

$$\begin{aligned}
&Target\_Histogram[i] = \gamma \times Target\_Histogram[i] + \\
&(1-\gamma) \times Previous\_Target\_Histogram[i] \\
&Background\_Histogram[i] = \gamma \times Background\_Histogram[i] + \\
&(1-\gamma) \times Previous\_Background\_Histogram[i]
\end{aligned} \tag{4.7}$$

where 0 < γ < 1 is update rate. While γ increases, histogram update rate increases as well.

4.1.3.1.2 Estimating Target Pixels

After finding target and background histograms, target probability distribution (TPD) is computed by using Formula 4.8 as,

$$TPD[i] = \frac{Target\_Histogram[i]}{Target\_Histogram[i] + Background\_Histogram[i]} \tag{4.8}$$

where i is the intensity and it takes values between 0 and 255 for an 8-bit infrared video density.

TPD becomes 1 only within the target histogram. Example histogram graphs and related target probability distribution are presented in Figure 39.

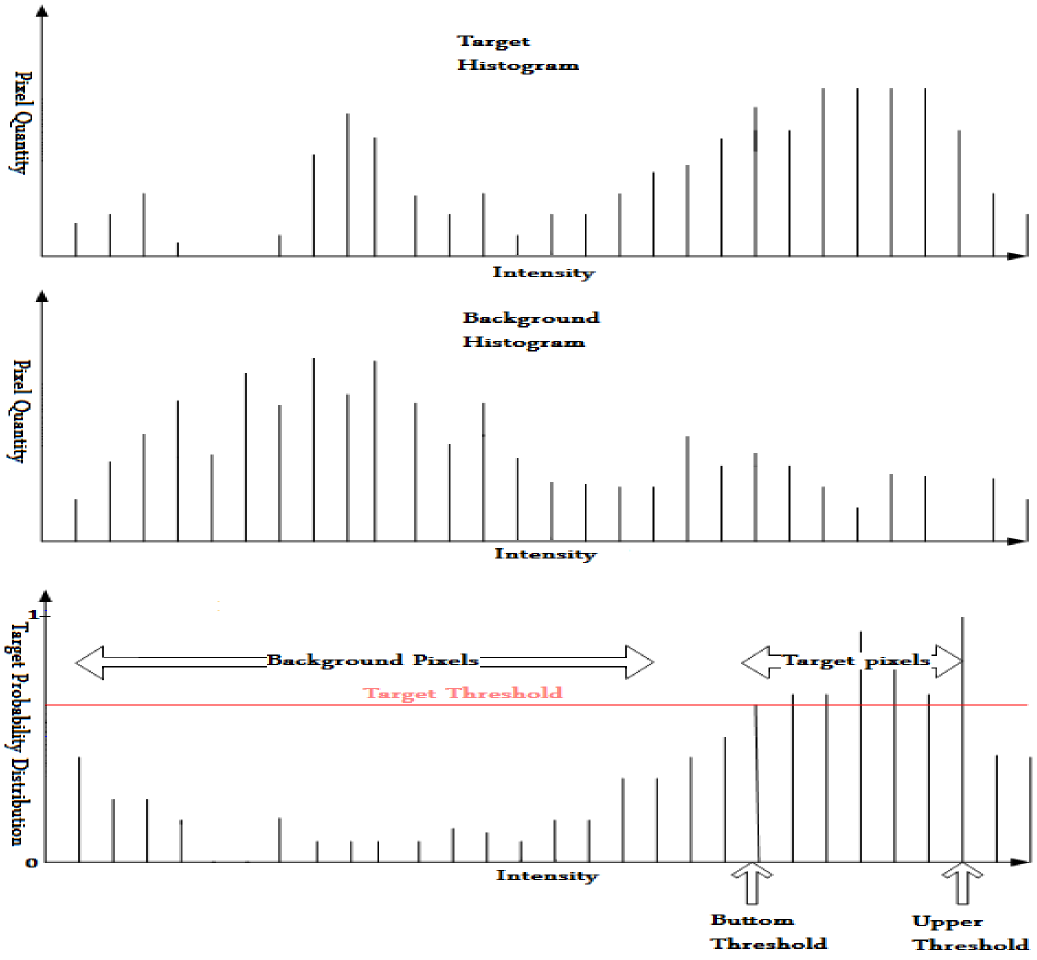

Figure 39 Histogram Analysis

Using target probability distribution, target pixels are found by considering the target threshold. Intensity values bigger than the threshold are considered as target pixels. Thresholding is critical to separate the target from the background, effectively. Therefore, the target threshold should be updated during missile flight in a logical way.

Threshold selection can be based on (1) Histograms Method, (2) Target and Background Gate Method, and (3) Peak and Average Method [23].

In Histogram Method, threshold is found using scene histogram information. This method is applicable if the histogram is bimodal, i.e. two distinct local maxima in the histogram distribution exist. A suitable threshold value can be chosen within these two maxima. However, in general, distributions are not bimodal, so the threshold selection becomes very difficult [23]. Therefore, this method is discarded.

In Target and Background Gate Approach, target and background average intensity levels are computed using Formula 4.9 as

$$\begin{aligned} T\arg et\_Average &= \frac{\sum_{T\arg et\_Pixels} i}{T} \\ Background\_Average &= \frac{\sum_{Background\_Gate} i}{Y} \end{aligned} \tag{4.9}$$

where T is the number of target pixels and Y is the number of pixels enclosed in the background gate. Threshold is between the target and background averages and is usually mean of the two.

In Peak and Average Method, peak and average intensity level of complete scene including target and background are computed. Threshold is fixed in between the average and the peak and is usually mean of the two.

Thresholding is optimized by combining the second and third approaches for the centroid tracker algorithm. Threshold is found using Peak and Average method for the first few frames and later by Target and Background method.

4.1.3.1.3 Computing Target's Centroid

Once target pixels are classified, the centroid can be computed as the weighted average of target intensities.

$$\begin{aligned} c_x &= \sum_{T\arg et\_Gate} \frac{j \times x_j}{T} \\ c_y &= \sum_{T\arg et\_Gate} \frac{n \times y_n}{T} \end{aligned} \tag{4.10}$$

where T is the number of target pixels, j is the column number, n is the row number, x_j is the x projection of j^th column and y_n is the y projection of n^th row.

Target x and y projections are found for computing centroid coordinates c_x and c_y as described in Figure 40, where red point represents the target centroid.

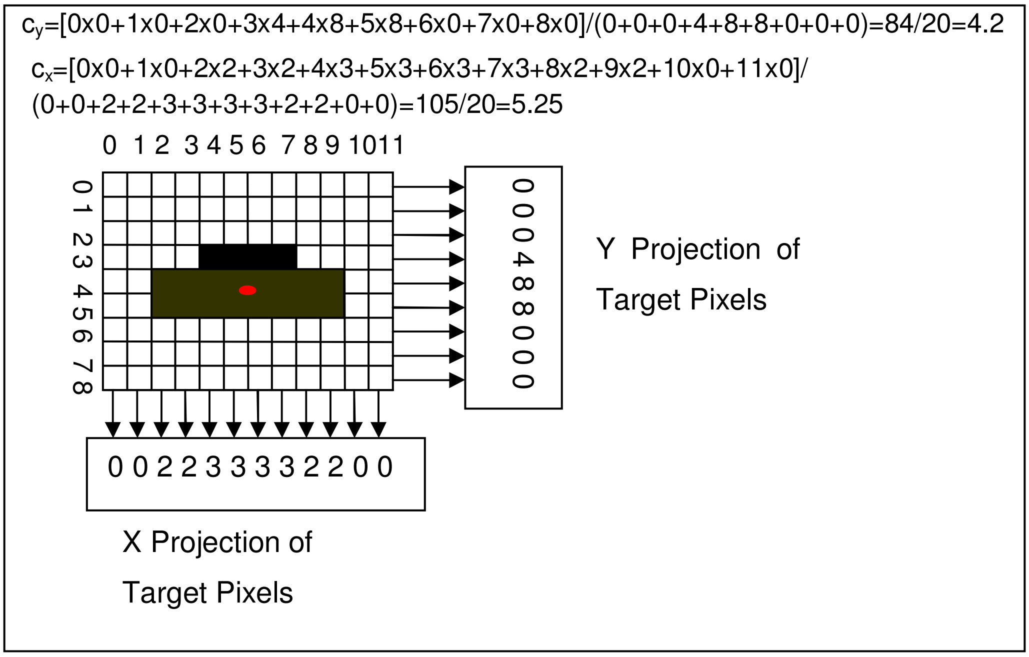

c_y=[0x0+1x0+2x0+3x4+4x8+5x8+6x0+7x0+8x0]/(0+0+0+4+8+8+0+0+0)=84/20=4.2

c_x=[0x0+1x0+2x2+3x2+4x3+5x3+6x3+7x3+8x2+9x2+10x0+11x0]/(0+0+2+2+3+3+3+3+2+2+0+0)=105/20=5.25

Figure 40 Computing Centroid Coordinates

4.1.3.1.4 Updating Gate Position and Size

The placement and sizing of target gate affects the ability of computing target location in the following frame. If the gate is misplaced or is too small, some of the target can be excluded from target position measurement processing. If it is too large, then it will include a quantity of background pixels that may interfere with the computation performance. Therefore, current frame’s characteristics constitute next frame’s target gate position and size. Position is directly related with centroid coordinates.

One of the most advantageous characteristics of the centroid tracker is the adaptation capability of enlarging or shrinking targets according to Formula 4.11 as,

$$
\begin{aligned}
k_x &= \frac{g_2 \times \left(total\_x - g_1 \times (column \cdot search\_right \cdot search\_left)\right)}{(column \cdot search\_right \cdot search\_left)} \\
k_y &= \frac{g_2 \times \left(total\_y - g_1 \times (row \cdot search\_up \cdot search\_buttom)\right)}{(row \cdot search\_up \cdot search\_buttom)}
\end{aligned}
\qquad (4.11)
$$

where g_2 is the changing rate, g_1 is the enclosing rate, column is the total column quantity in gate, row is the total row quantity in gate, search_up is the total number of upper search columns, search_buttom is the total number of buttom search columns, total_x is the total target pixels in search columns, total_y is the total target pixels in search rows, search_right is the total number of right search rows and search_left is the total number of left search rows.

For both x and y axes, if target is enlarging in one direction and target pixels are increasing respectively, then the gate size is adjusted as described with an example in Figure 41 as,

k_y= g2 * [(6+6+10+10) – g1*(12x(2+2))] / (12x(2+2))

= g2 * (26-g1*48)/48 = 5*(26-(1/2)*48)/48=10/48 → 0.208

k_x= g2 * [(0+5+5+0) – g1*(9x(2+2))] / (9x(2+2))

= g2 * (10-g1*36)/36 =5*(10-(1/2)*36)/36=-40/36 → -1.111

round(k_y) = 0 → No change in y direction

round(k_x) = -1→ Reduce 1 pixel in right and left parts in x direction

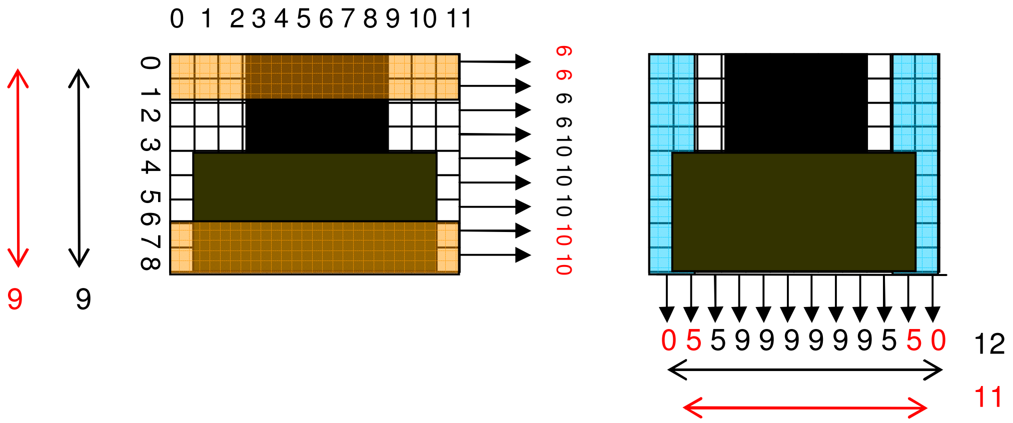

Figure 41 Computing Gate Modify Rate

The sample snapshots of the centroid tracking method are given in Figure 42.

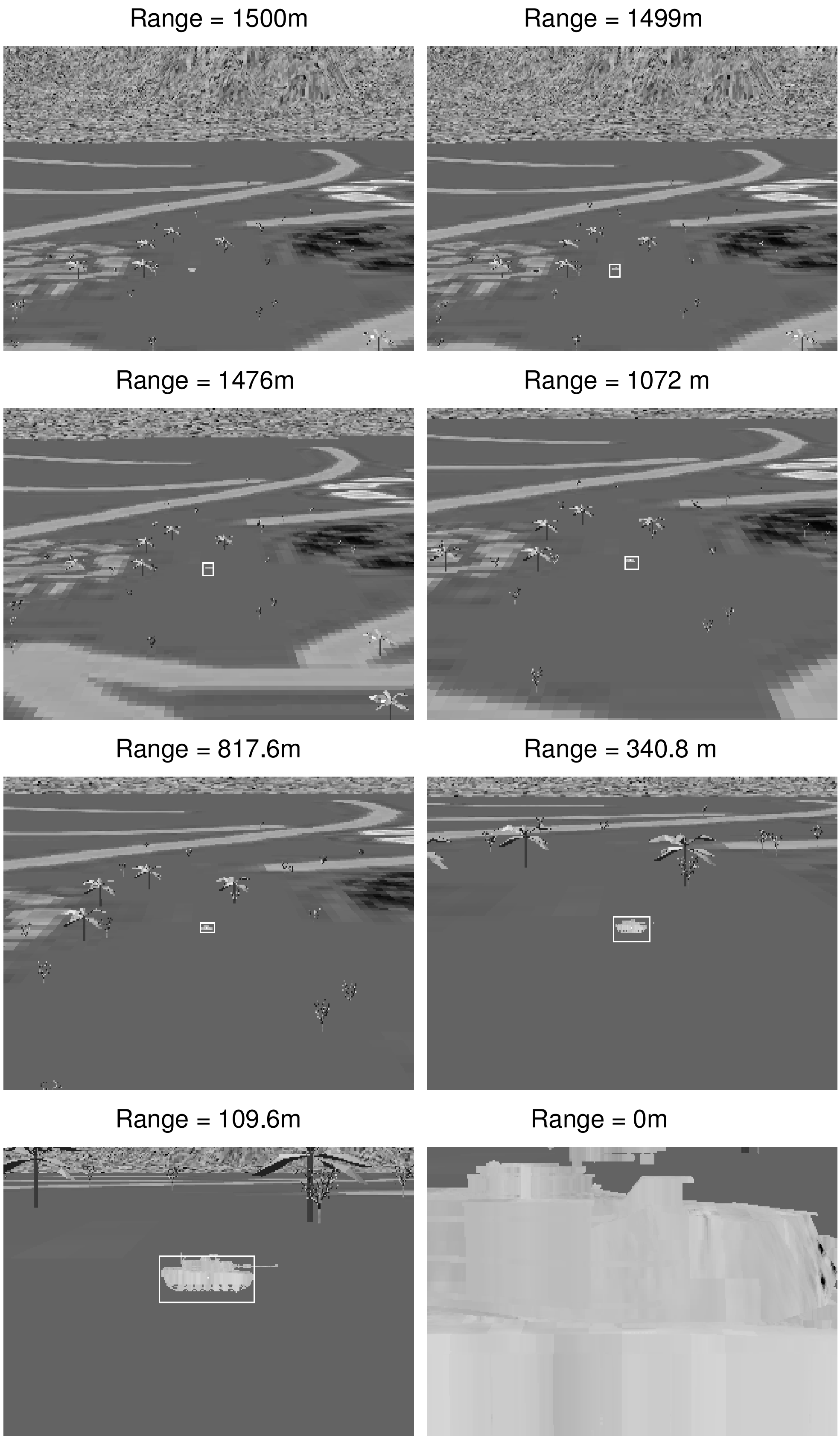

Range = 1500m

Range = 1499m

Range = 1476m

Range = 1072 m

Range = 817.6m

Range = 340.8 m

Range = 109.6m

Range = 0m

Figure 42 Target Hit Using Centroid Method

4.1.3.2 Correlation Tracker

Correlation tracker is based on strength of relationship between two signatures. Once the target has been acquired, a target reference (reference window) is created in the scene. In the following frames, the best correlated signature is found using the reference window in the region of interest (ROI). The best-correlated signature shows the new target position. These steps are presented in Figure 43 and discussed in the following sections.

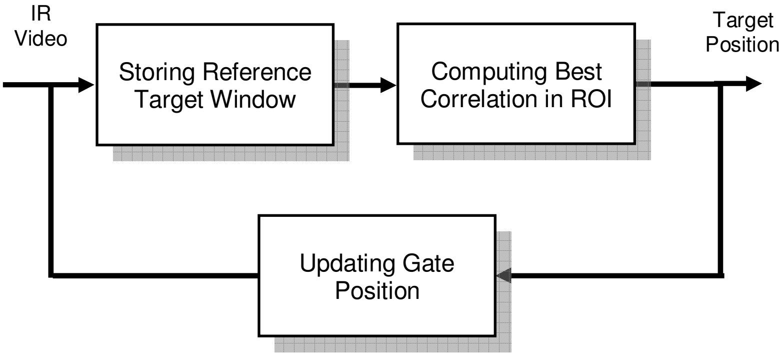
IR Video
Storing Reference Target Window
Computing Best Correlation in ROI
Target Position
Updating Gate Position

Figure 43 Correlation Algorithm

4.1.3.2.1 Storing Reference Target Window

Selected target signature is kept in memory and it is called the reference target window for the following frames. The target reference window can be updated if necessary. However, correlation algorithm is very sensitive to target dynamics and if target is changing its direction or enlarging/shrinking very rapidly, it is very difficult to find the correct target signature by computing the best correlation in the region of interest.

4.1.3.2.2 Estimating Correlation

Once the reference target window is created, a region of interest is developed. Size of the region of interest should be optimized in the algorithm. Correlation is computed by using Formula 4.12 as,

$$C_{ab} = \frac{E[a*b] - (E[a] \times E[b])}{\sqrt{(E[a^2] - E[a]^2) \times (E[b^2] - E[b]^2)}} \tag{4.12}$$

where a and b are the reference and the interested signatures and E[.] is the signature pixel intensity means. Correlation search method is presented in Figure 44.

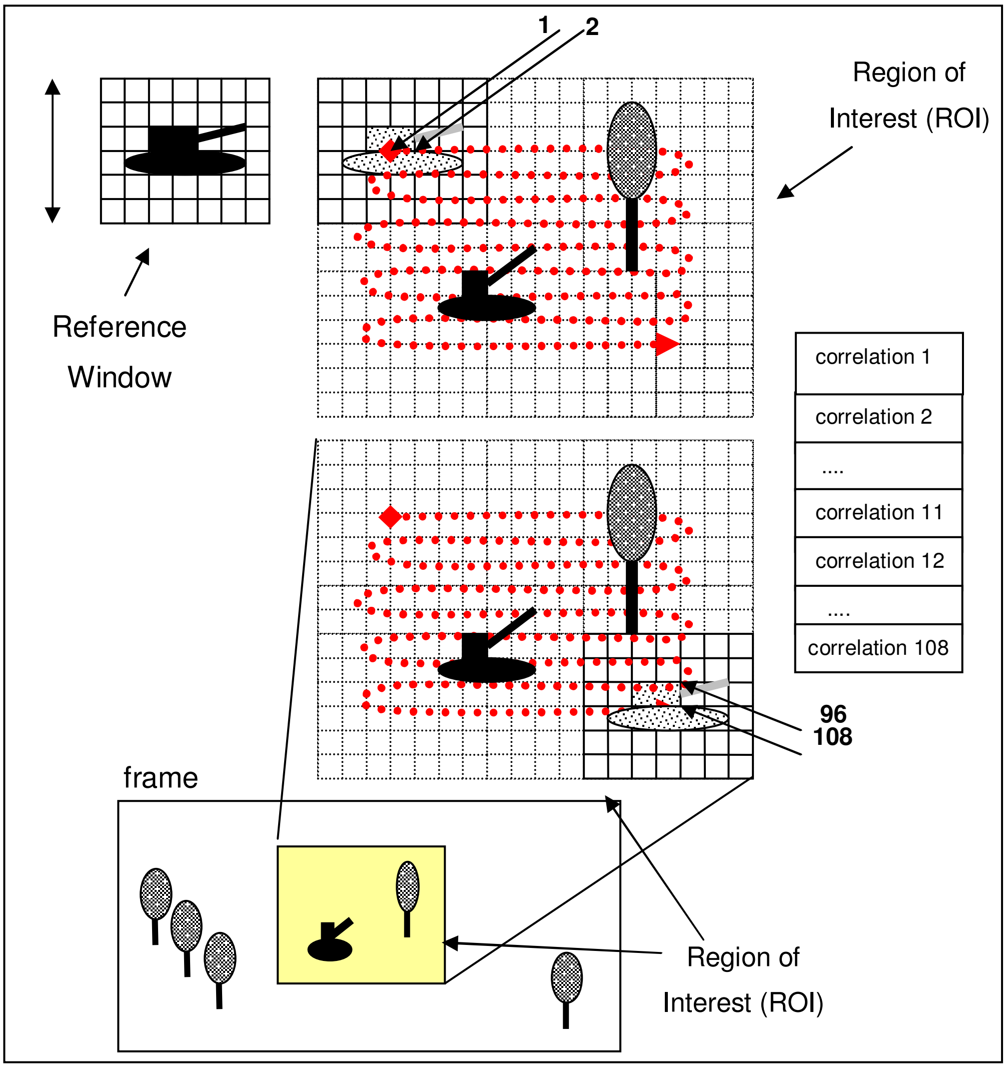

Figure 44 Estimating Correlation

4.1.3.2.3 Updating Gate Position

Best-correlated window in the region of interest shows the new target position. Gate position is adapted according to that.

The sample snapshots of correlation tracking method are given in Figure 45.

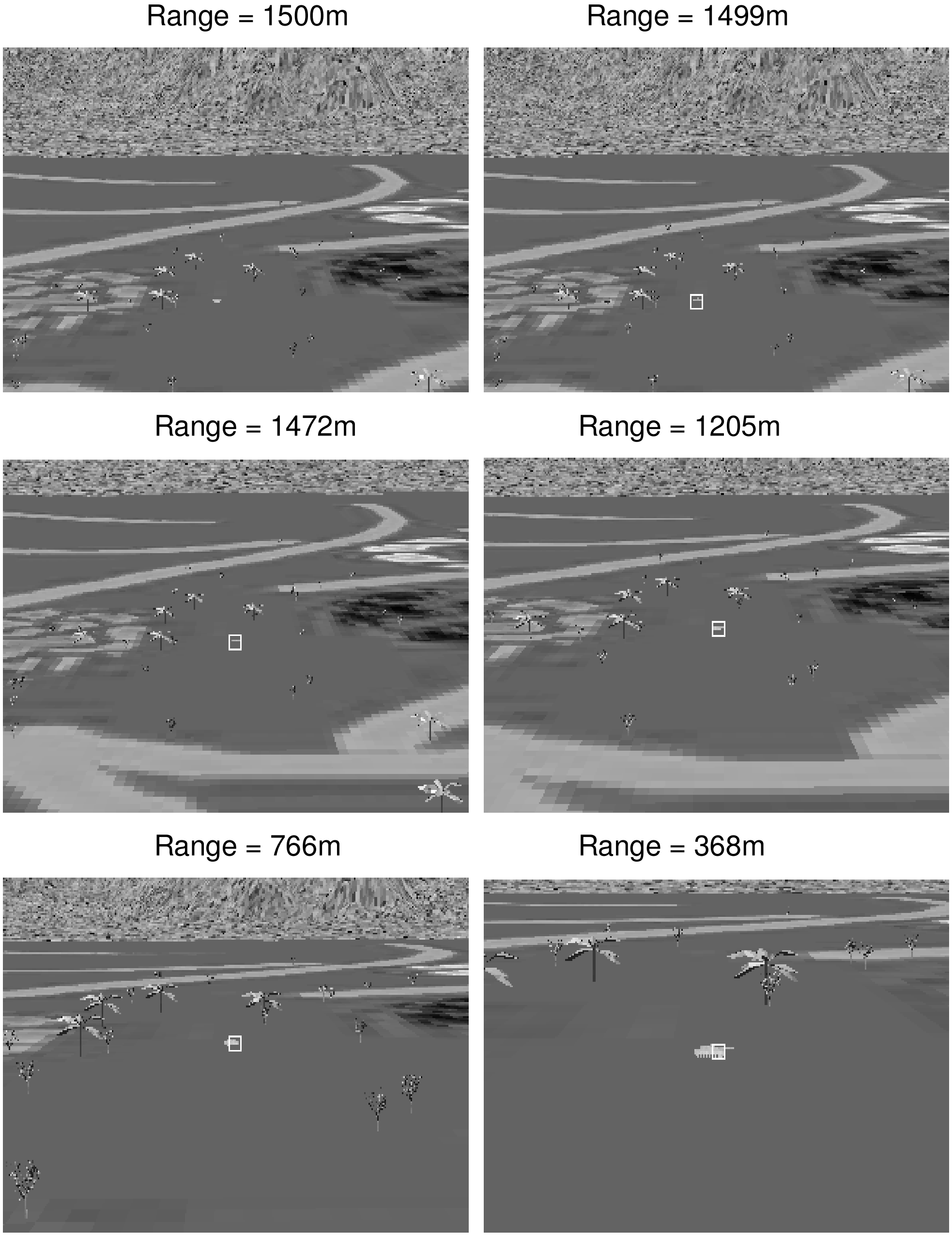

Range = 1500m

Range = 1499m

Range = 1472m

Range = 1205m

Range = 766m

Range = 368m

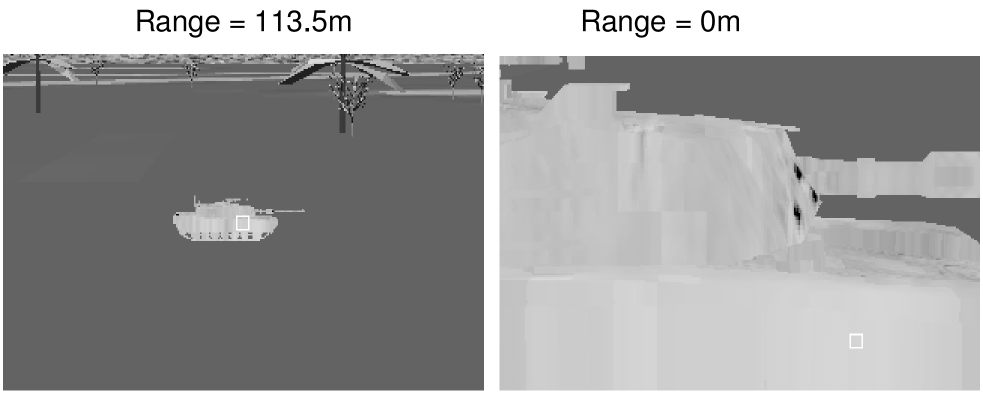

Figure 45 Target Hit Using Correlation Method

4.1.3.3 Active Contour (Snake) Tracker

The active contour (snake) model deforms a contour to lock onto features within an image. Snakes gained large acceptance as a segmentation tool due to the way that it considers the boundary as a single, inherently connected and smooth structure. In short, snakes are energy minimizing parametric contours with smoothness constraints deformed according to image data [31].

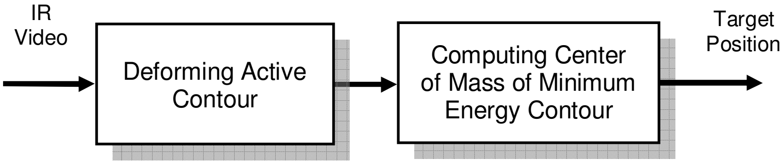

Figure 46 Snake Algorithm

4.1.3.3.1 Deforming Active Contour

A rectangular target gate is initiated on the image by the operator and left to deform in a way that, first, it moves toward features of interest in the image and, secondly, it maintains a certain degree of smoothness in the contour. In order to favor this type of contour deformation, an energy term is associated with the contour and designed to be inversely proportional to the contour's smoothness and to the model fit to desired image features.

An active contour is an ordered collection of n points in the image plane [32]:

$$v = \{v_1, v_2, ..., v_n\}$$
$$v_i = (x_i, y_i), i \in \{1,2,...,n\} \tag{4.13}$$

The points in the contour iteratively approach the boundary of an object through the solution of an energy minimization problem. For each point in the neighborhood of v_i, an energy term is computed:

$$E_i = \alpha \cdot E_{\text{int}}(v_i) + \beta \cdot E_{ext}(v_i) \tag{4.14}$$

where $E_{int}(v_i)$ is an internal energy function dependent of the shape of the contour, $E_{ext}(v_i)$ is an external energy function dependent on the image properties, α and β are constants providing the relative weighting of the energy terms.

The internal energy function is intended to enforce a shape on the deformable contour and to maintain a constant distance between the points in the contour.

$$\alpha \cdot E_{\text{int}}(v_i) = c \cdot E_{con}(v_i) + b \cdot E_{bal}(v_i) \tag{4.15}$$

where $E_{con}(v_i)$ is the continuity energy that enforces the shape of the contour and $E_{bal}(v_i)$ is a balloon force that causes the contour to grow (balloon) or shrink. c and b provide the relative weighting of the energy terms.

The energy term for each element of $E_{con}(v_i)$ is defined as follows [33]:

$$e_{jk}(v_i) = \frac{1}{l(v)} \left\| p_{jk}(v_i) - \gamma(v_{i-1} + v_{i+1}) \right\|^2 \tag{4.16}$$

where $p_{jk}(v_i)$ is the point in the image that corresponds spatially to energy matrix element $e_{jk}(v_i)$, $\gamma = \frac{1}{2 \cdot \cos(\frac{2\Pi}{n})}$ for a closed-contour and the normalization factor

$l(v) = \frac{1}{n}\sum_{i=1}^{n}\left\|v_{i+1} - v_i\right\|^2$ is required to make $E_{con}(v_i)$ independent of size, location and orientation of v.

The energy term for each element of $E_{bal}(v_i)$ is defined as follows:

$$e_{jk}(v_i) = n_i \bullet \left(v_i - p_{jk}(v_i)\right) \tag{4.17}$$

where n_i is the outward unit normal of v at point v_i.

The external energy function attracts the deformable contour towards the interesting features such as object boundaries in the image.

$$\alpha \cdot E_{ext}(v_i) = m \cdot E_{mag}(v_i) + g \cdot E_{grad}(v_i) \tag{4.18}$$

where $E_{mag}(v_i)$ is the expression which attracts the contour to high and low intensity regions and $E_{grad}(v_i)$ is an energy term that moves the contour towards edges. The constants, m and g are provided to adjust the relative weights of the terms.

Each element in the intensity energy matrix $E_{mag}(v_i)$ is assigned the intensity value of the corresponding image point in the neighborhood of v_i which is defined as follows:

$$e_{jk}(v_i) = I\left(p_{jk}(v_i)\right) \tag{4.19}$$

Then, if m is positive, the contour is attracted to regions of low intensity and vice-versa.

The image gradient energy function matrix $E_{grad}(v_i)$ attracts the deformable contour to edges in the image. An energy expression proportional to the gradient magnitude will attract the contour to edge as:

$$e_{jk}(v_i) = -\left|\nabla I\left(p_{jk}(v_i)\right)\right| \tag{4.20}$$

When active contours are used to find object boundaries, an energy expression that discriminates between edges of adjacent objects is desirable. The value of each element in the directional gradient energy matrix $E_{grad}(v_i)$ can therefore be defined by a contour and the image gradient:

$$e_{jk}(v_i) = -n_i \bullet \nabla I\left(p_{jk}(v_i)\right) \tag{4.21}$$

4.1.3.3.2 Computing Center of Mass of Minimum Energy Contour

After finding an active contour with minimum energy, the center of mass of that contour represents the enemy target position. The center of mass is defined as the average of contour points' position in x any y axes.

The sample snapshots of snake tracking method are given in Figure 47.

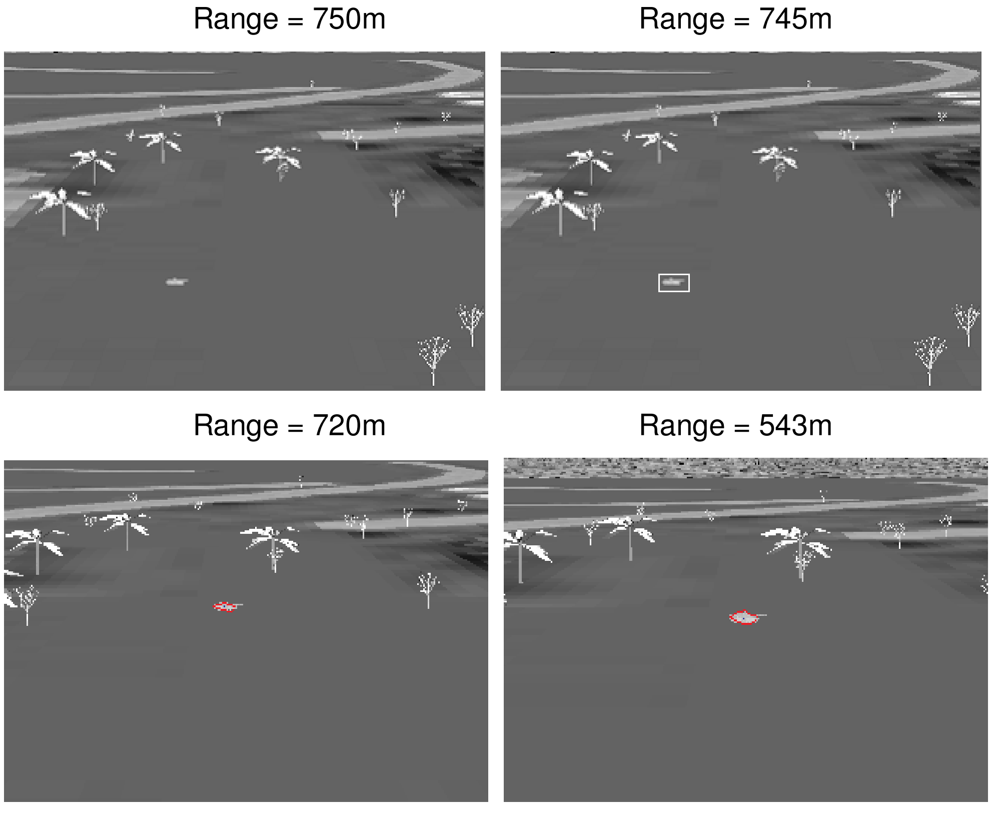

Range = 750m

Range = 745m

Range = 720m

Range = 543m

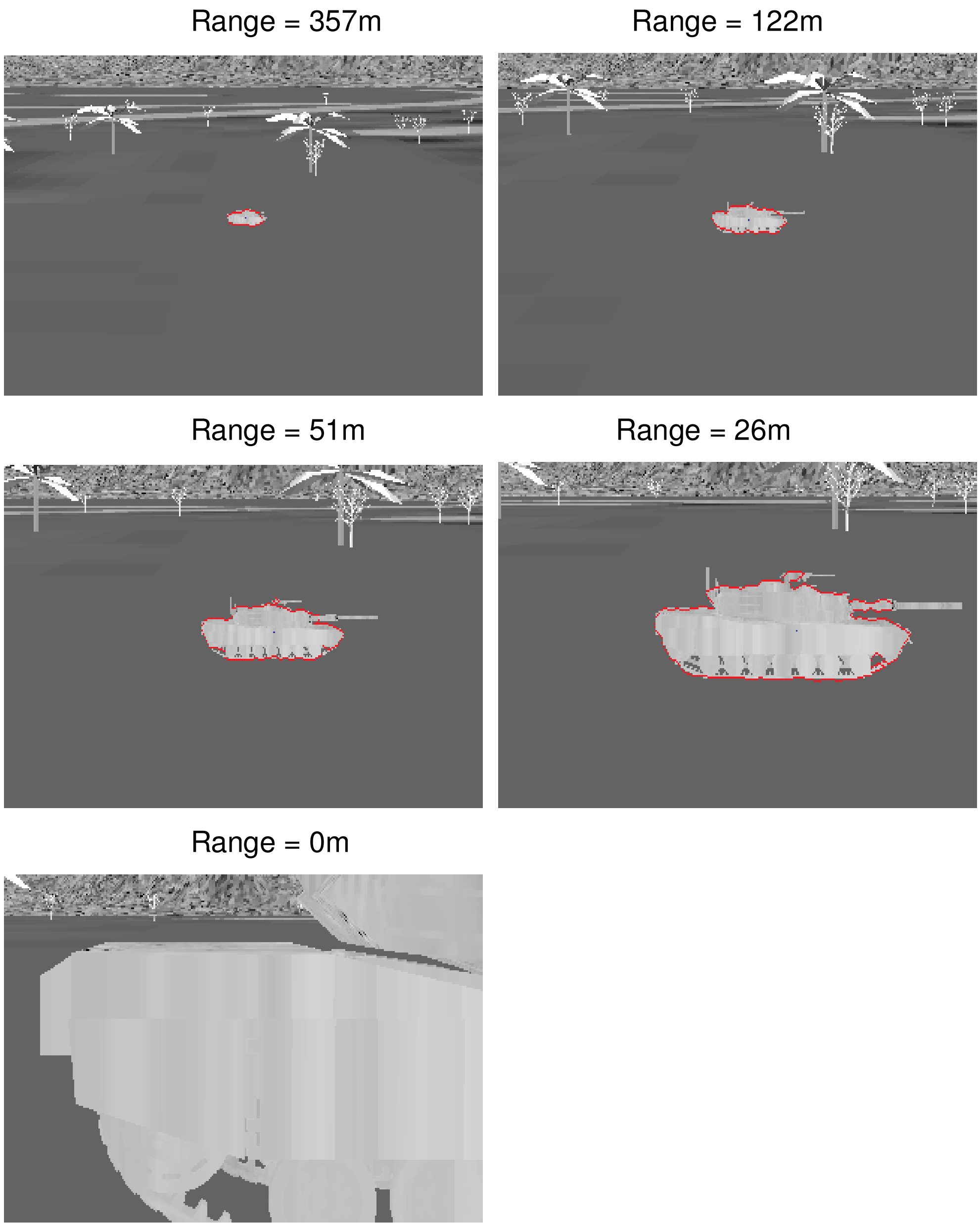

Range = 357m

Range = 122m

Range = 51m

Range = 26m

Range = 0m

Figure 47 Target Hit Using Snake Method

4.2 Proposed Tracking Algorithm

Above, tracking algorithms such as centroid, correlation and active contour were presented in detail. In this thesis, it is decided to use a new tracking algorithm, which combines positive sides of these methods.

Centroid trackers are most applicable for expanding targets because of gate size adaptation capability. However, larger targets often have high internal detail, which are more suitably tracked by correlation or active contour algorithm. Therefore, when the target occupies a big portion of the scene, active contour algorithm is switched from centroid method.

Centroid trackers are robust in low-clutter scenarios, with medium-to-high target SNRs. Centroid algorithm is less effective on lower SNR targets, or in high clutter. Therefore, when the target is a blob-like small point in the scene, correlation method is preferred [22].

In the terminal phase, point of impact (POI) is selected as the center of mass of active contour. Using that information, missile is guided to the high vulnerability points.

Using above facts, below flow chart is proposed as a new tracking algorithm for an imaging infrared anti-tank missile application [23]. In the following chapter, comparison of centroid, correlation, snake and proposed algorithm will be presented.

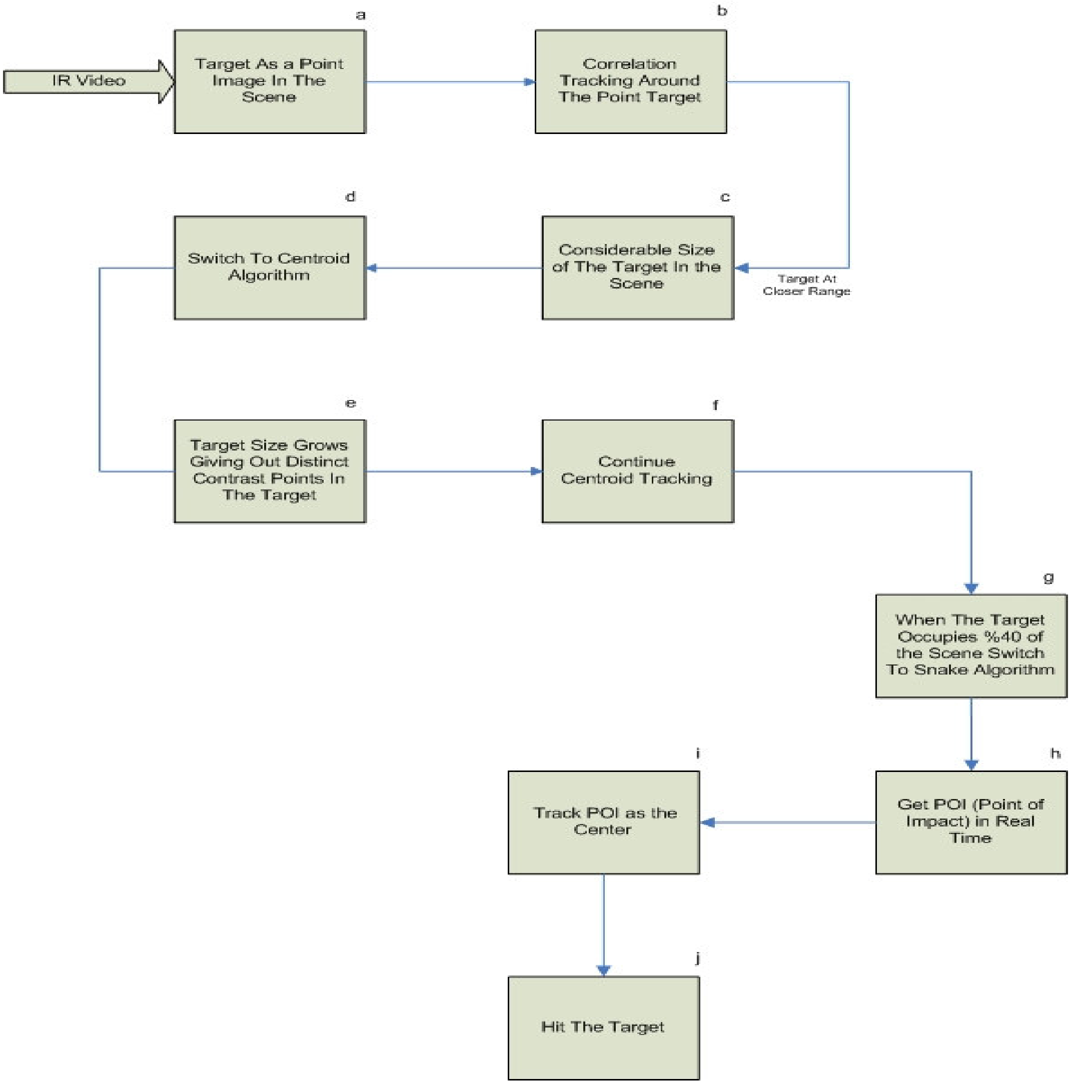
IR Video
a
Target As a Point Image In The Scene
b
Correlation Tracking Around The Point Target
Target At Closer Range
c
Considerable Size of The Target In the Scene
d
Switch To Centroid Algorithm
e
Target Size Grows Giving Out Distinct Contrast Points In The Target
f
Continue Centroid Tracking
g
When The Target Occupies %40 of the Scene Switch To Snake Algorithm
h
Get POI (Point of Impact) in Real Time
i
Track POI as the Center
j
Hit The Target

Figure 48 Proposed Tracking Algorithm Flow Chart

The sample snapshots of proposed tracking method are given in Figure 49.

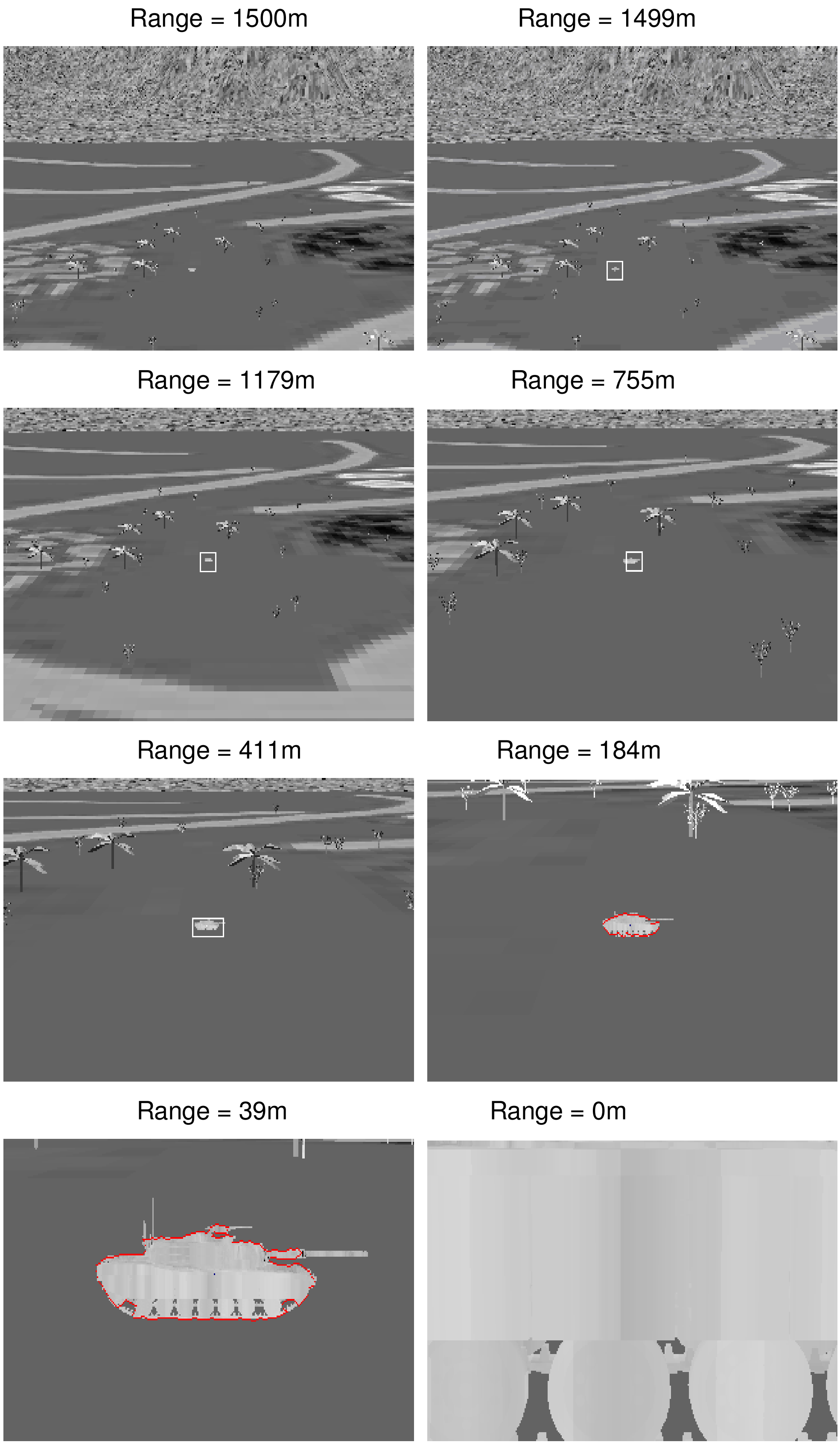

Range = 1500m

Range = 1499m

Range = 1179m

Range = 755m

Range = 411m

Range = 184m

Range = 39m

Range = 0m

Figure 49 Target Hit Using Proposed Method

4.3 Guidance Control

Flight autopilot control part takes desired angle commands in the longitudinal and lateral planes, which are generated by the Guidance Control section. Guidance control loop creates the necessary angle values for the missile in order to provide the desired directions.

After the operator locks on the enemy target, gimbal follows the target by nulling the error angle as described in chapter 4.1.2. But, usually it is not enough to hit the target. Missile body should follow the gimbal in order to direct the missile towards it's enemy. The angle between gimbal and missile body axis is called the gimbal angle. Therefore, guidance control should null the gimbal angle in a proper way. In the pursuit method, the missile is steered so that the velocity vector of the missile always points at the target. Because enemy tank is assumed stationary, Proportional Navigation Guidance (PNG) (instead of Pursuit Guidance) will be used in this thesis.

Gimbal angle y-axis and x-axis components are nulled by PID controllers in both longitudinal and lateral planes as described in Figure 50.

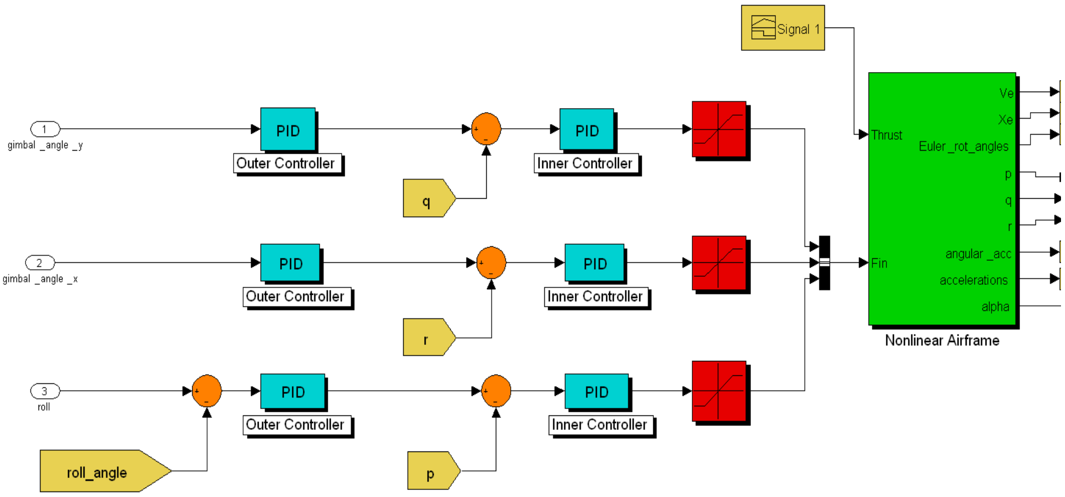

Figure 50 Nulling Gimbal Angle Scheme

Inner PID controllers were described in chapter 3.3.1 in flight autopilot section. Response Optimization of Simulink is used for determining gain values for outer PID controllers. “gimbal_angle_y” and “gimbal_angle_x” angles are produced by the Gimbal.

CHAPTER 5

SIMULATION RESULTS

Simulation studies are carried out in order to present the effectiveness of the proposed tracking algorithm described in the previous chapter. This new algorithm is compared with centroid, correlation and active contour algorithms for different test scenarios. Target tank is assumed stationary in the simulations, because usually it's velocity (~11m/s) is much more smaller than generic anti-tank missile velocity (~320m/s).

5.1 Simulation Criteria

Comparison is made between the proposed algorithm and traditional algorithms using the criteria: (1) Hit Point (2) Track Loss Rate as described below.

5.1.1 Hit Point

A tank's protection is not only the ability to avoid detection, but also to avoid getting high damage from enemy fire. Therefore, increasing tank kill rate attributes higher hit points.

A heavy armor is applied to tanks for protection of its crew and tank itself. Tank armor aims to protect against antitank missiles, mines, bombs, etc. Even if there exists many protection techniques such as steel armor plates, composite armors, active protection systems, etc., tank is not invulnerable. In Figure 51, critical vulnerable points of a German Tiger tank are presented [25].

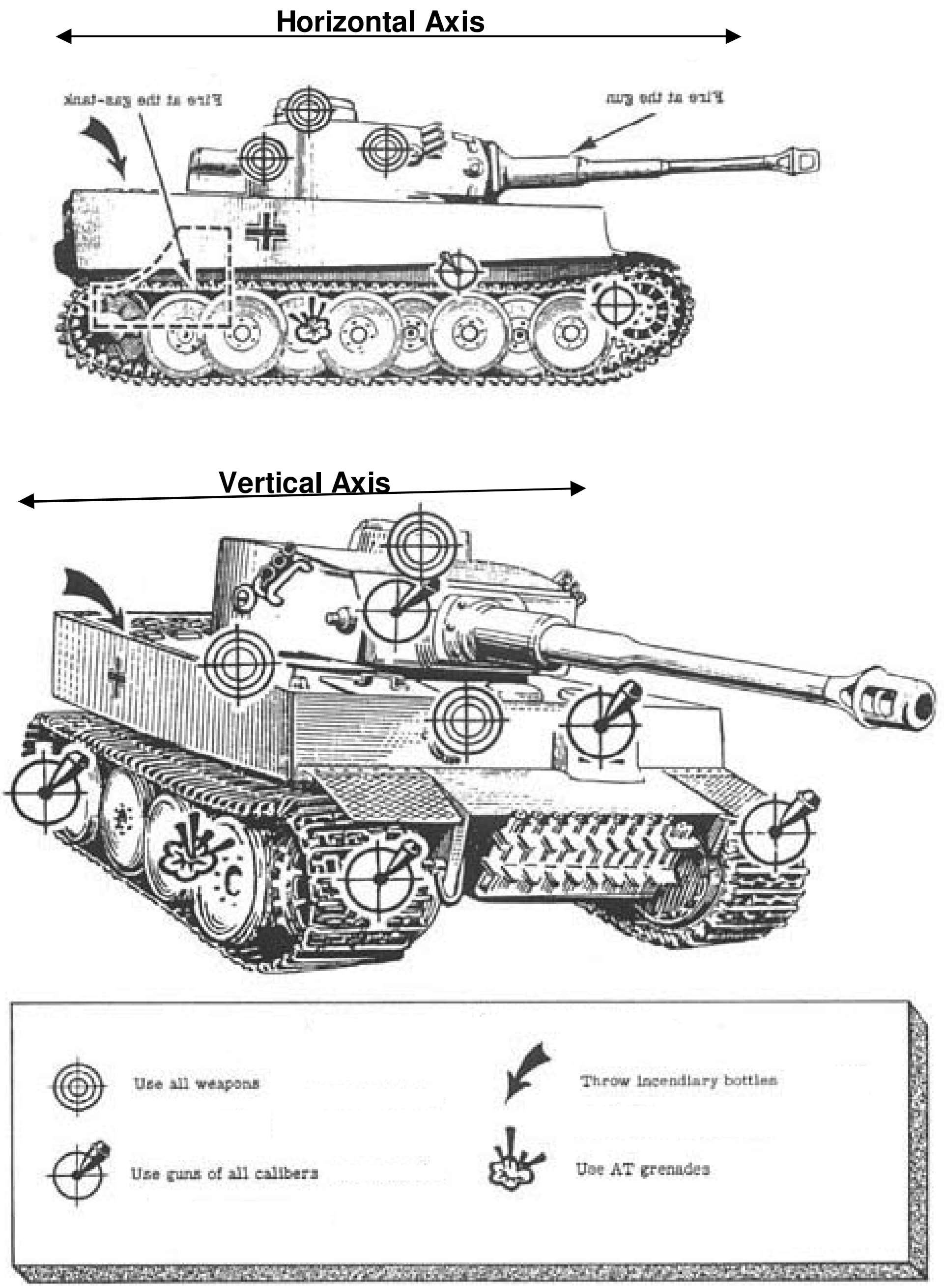

Figure 51 Tiger Tank Vulnerability

The mobility of tanks depends upon the proper functioning of the suspension parts (sprocket, idler, wheels and tracks). A particularly vulnerable part is the sprocket. Therefore, all of these parts are vulnerable to antitank missiles and gets high points for damage assessment.

The rear part contains engine and gasoline tanks and penetrating this part will disable and explode tank easily. Thus, these parts get high points for damage assessment too.

The turret is a particularly important and a vulnerable target and is associated with high hit points. The rest of the tank is associated with lower hit points.

Considering above facts, below vulnerability hit point graphs are assumed in tank’s horizontal and vertical axes in meters. In order to find the total hit point, horizontal and vertical hit points’ average is found.

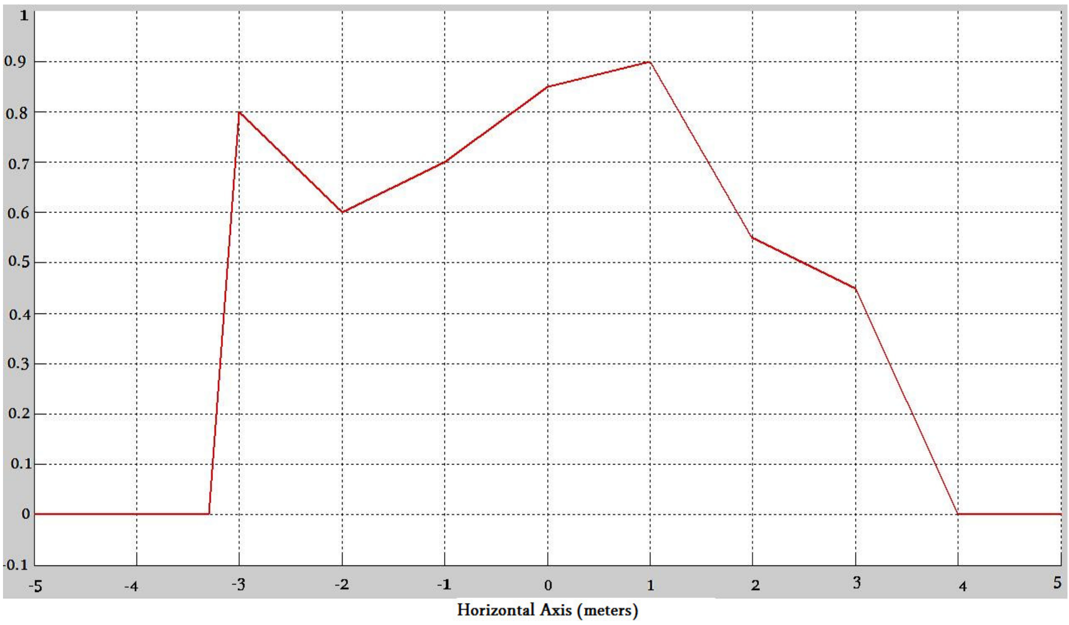

Figure 52 Horizontal Hit Point versus Horizontal Tank Axis

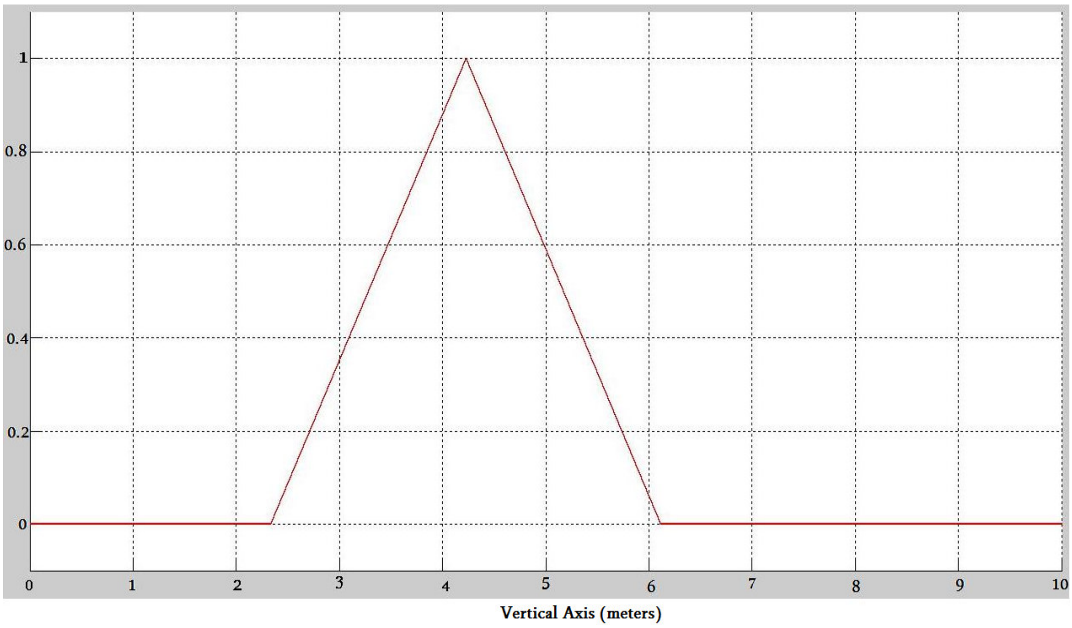

Figure 53 Vertical Hit Point versus Vertical Tank Axis

5.1.2 Track Loss Rate (TLR)

Once tracks are formed and confirmed from the operator, the missile should destroy its target with minimum human interaction. Therefore, system is generally designed to perform closed-loop fire-and-forget tracking on a target. However, sometimes it is not possible to hit the target easily without any track loss. Minimizing track loss rate is very essential for developing tracking algorithms. TLR is defined as follows:

$$TLR = 1 - \frac{NOTF}{TNOF} \tag{5.1}$$

where NOTF is number of tracked frames and TNOF is total number of frames in missile flight.

5.2 Simulation Scenarios

The tracker's performance will be evaluated with respect to the variance of five parameters, which are target contrast, clutter, field-of-view, noise and countermeasure analysis.

5.2.1 Target Contrast

Contrast is the difference in intensity that makes target distinguishable from its background. Tracker performance is generally increasing while contrast is raising and vice versa. Various definitions of contrast are used for different requirements and Weber contrast is used in this thesis as described below

$$Contrast\_Ratio = 100 \times \frac{I_t - I_b}{I_b} \qquad (5.2)$$

where I_t and I_b are representing the target and background average intensity. In Figure 54, sample snapshots of different contrast values are presented.

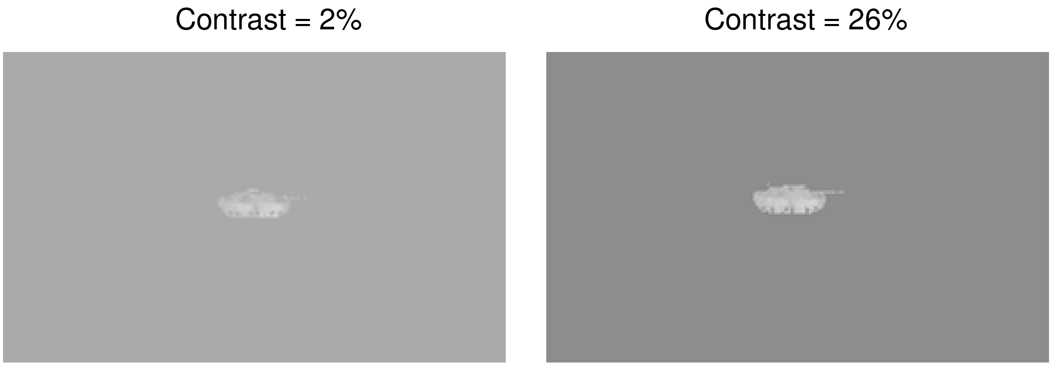

Contrast = 2%

Contrast = 26%

Figure 54 Target Contrast

In order to vary the contrast, background intensity value is gradually decreased and performance metrics are presented in Table 2.

Contrast Ratio (%)	Proposed Algorithm		Centroid Algorithm		Correlation Algorithm		Snake Algorithm	
	Hit Point	TLR	Hit Point	TLR	Hit Point	TLR	Hit Point	TLR
70	0.77	0.03	0.73	0.13	0.64	0.04	0.75	0.68
51	0.81	0.06	0.73	0.09	0.15	0.05	0.74	0.75
39	0.71	0.03	0.70	0.18	0	0.05	0.78	0.70
22	0.79	0.03	0.73	0.43	0.5	0.04	0.80	0.61
8	0.70	0.03	0.77	0.53	0.45	0.03	0.74	0.61

Table 2 Performance Metrics for Varying Contrast Ratios

For easy understanding, four point of impacts related with proposed, centroid, correlation and snake algorithms for 70% contrast are showed in Figure 55.

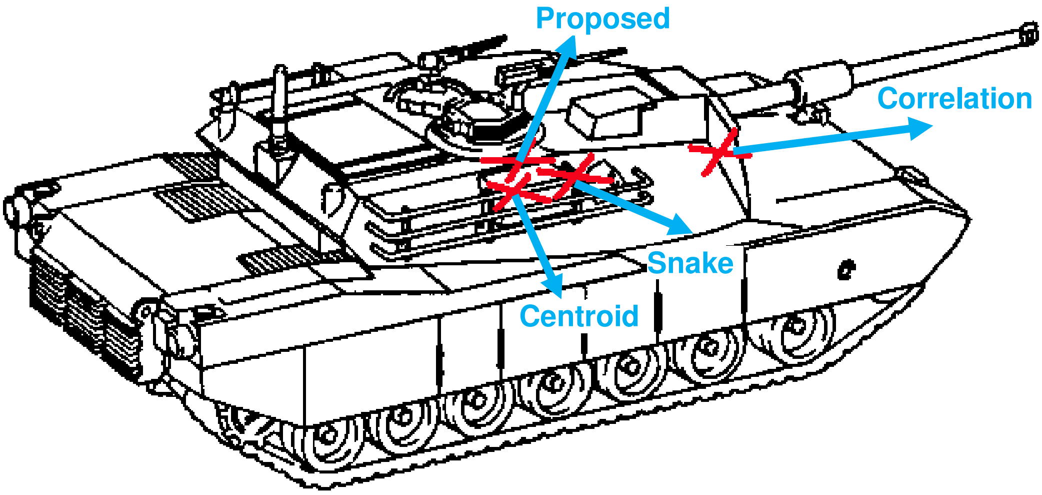

Figure 55 Point of Impacts for 70% Contrast Scenario

Centroid and snake algorithms have high track loss rate compared to the proposed algorithm and the correlation method. Because the centroid algorithm is sensitive to lock-on loss and snake algorithm requires relatively big target size. On the contrary, the centroid and snake methods get higher hit points than the correlation algorithm. Because proposed algorithm’s terminal phase is based on snake algorithm, it generally gets higher hit points. While contrast ratio is decreasing, track loss rate increases a little bit in the centroid and snake methods and there is no change in others. While contrast ratio is decreasing, centroid algorithm's hit point stays stabile, because histogram information does not affected for a smooth background.

Correlation method can get lower hit points, because in the terminal phase, algorithm can select wrong impact points. Figure 56 is an example of wrong target tracking in the correlation method.

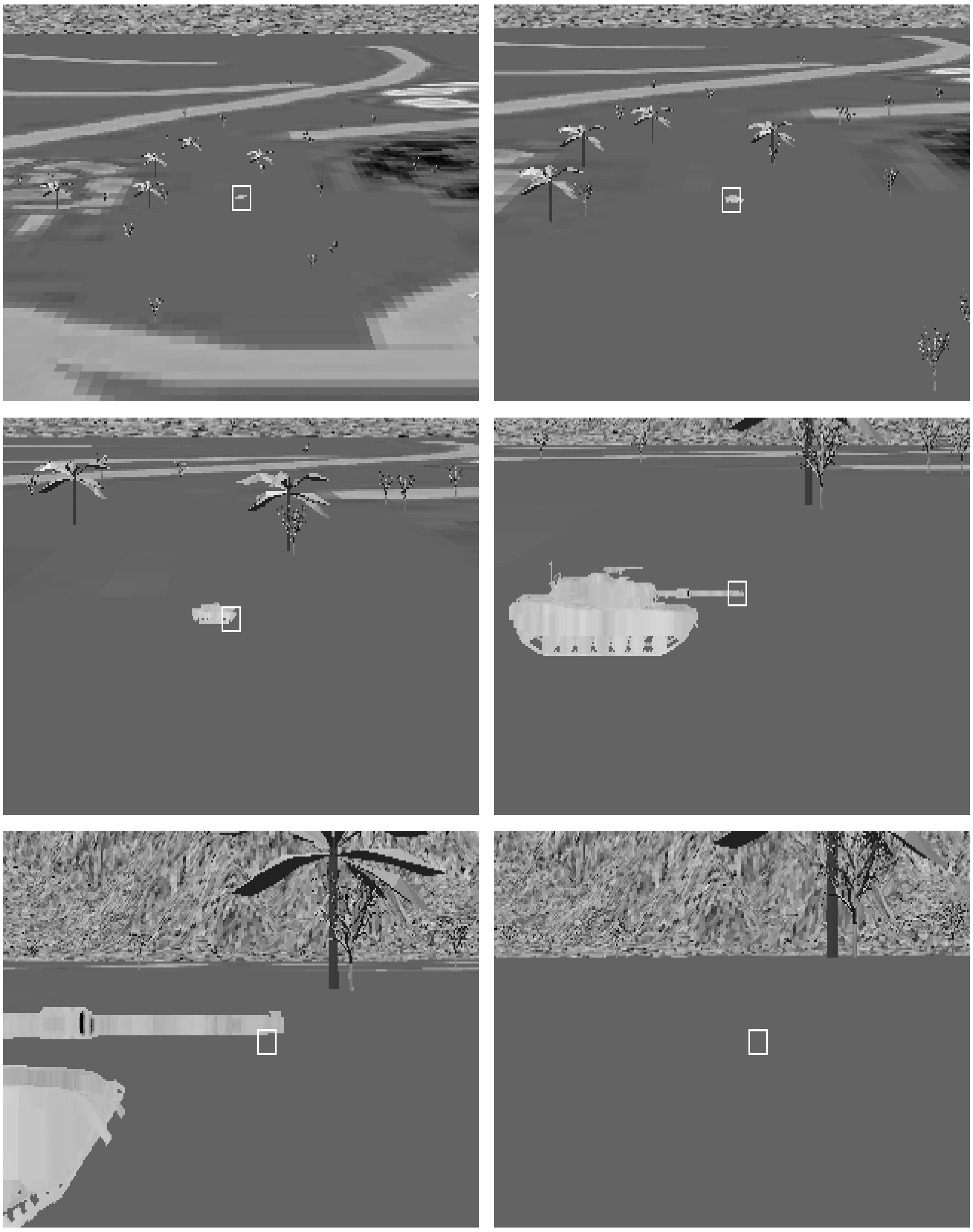

Figure 56 Wrong Target Tracking With Correlation Algorithm

5.2.2 Clutter

For imaging trackers, any object or scene phenomenon, which has significant ability to perturb measurements, is called as clutter. A way to estimate the influence of the clutter is to calculate statistics of the pixel distributions of the scene.

Schemider and Weathersby suggested a measure that they called signal-to-clutter ratio (SCR), which was defined as follows [26],

$$SCR = \frac{\left|\max I_t - meanI_b\right|}{clutter}$$
$$clutter = \left(\frac{1}{N}\sum_{i=1}^{N}\sigma_i^2\right)^{1/2} \tag{5.3}$$

where $\max I_t$ is the maximum target intensity, $meanI_b$ is the mean background intensity, σ_i is the standard deviation of the pixels over an area i and N is the total divided area.

The statistics of the target and background are computed over regions defined in Figure 57. The dimensions of the target region are one-third of the dimensions of the background region and centered within it [27].

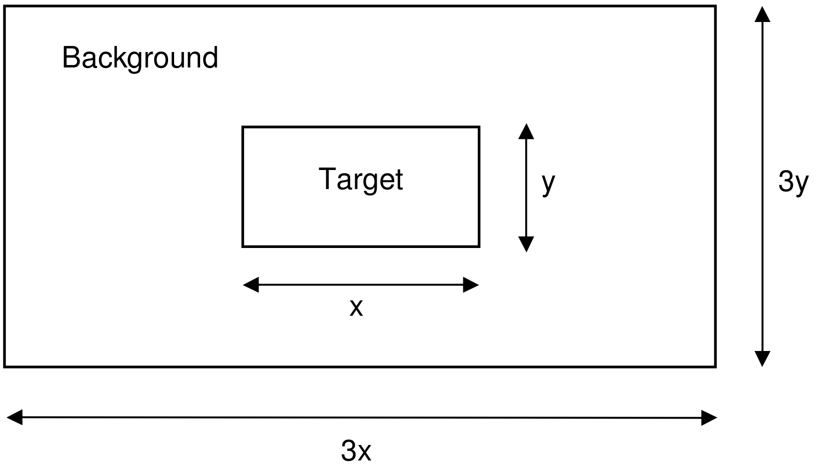

Figure 57 SCR Calculation Dimensions

In Figure 58, sample snapshots of different SCR values are presented [30].

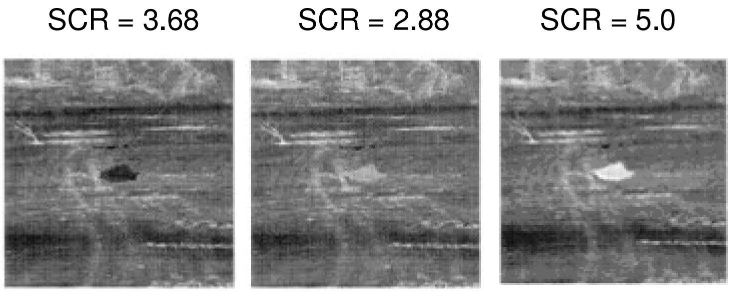

Figure 58 Clutter

For different SCR values, performance of the algorithms with respect to different criteria is presented in Table 3.

SCR	**Proposed Algorithm**		**Centroid Algorithm**		**Correlation Algorithm**		**Snake Algorithm**	
	Hit Point	**TLR**	**Hit Point**	**TLR**	**Hit Point**	**TLR**	**Hit Point**	**TLR**
8.18	0.83	0.04	0.75	0.12	0.64	0.03	0.78	0.71
5.32	0.79	0.03	0.74	0.23	0.64	0.04	0.75	0.75
3.46	0.81	0.03	0.70	0.47	0	0.03	0.75	0.75
2.70	0.72	0.03	0.69	0.53	0.56	0.04	0.73	0.84

Table 3 Performance Metrics for Varying SCR

Centroid and snake trackers are robust in low-clutter scenarios and performance is affected a lot in cluttered scenes. Furthermore, loss rate rises rapidly in high-clutter cases. Therefore, centroid and snake methods are not much applicable for high-clutter situations. On the contrary, correlation and proposed methods are not much affected by the existing clutter.

5.2.3 Field-of-View (FOV)

Field-of-view is an angular extent of missile seeker that is seen at any given moment. It is directly related with the optical magnification. Decreasing FOV increases magnification and it is clear that as the target is magnified more, the number of target pixels is increases.

For a lens projecting an image onto the detector surface, field-of-view is calculated from the detector size (X) and effective focal length (EFL) as follows,

$$FOV = \alpha = 2 \cdot \tan^{-1}\left(\frac{X}{2 \cdot EFL}\right) \tag{5.4}$$

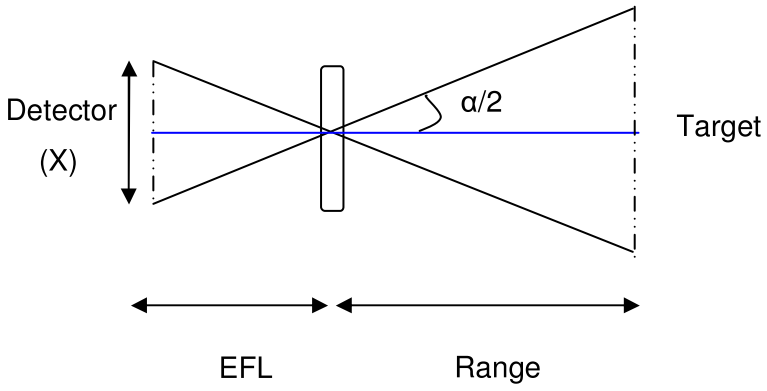

Figure 59 Finding FOV Using Geometry

In Figure 60, sample snapshots of different FOV values are presented.

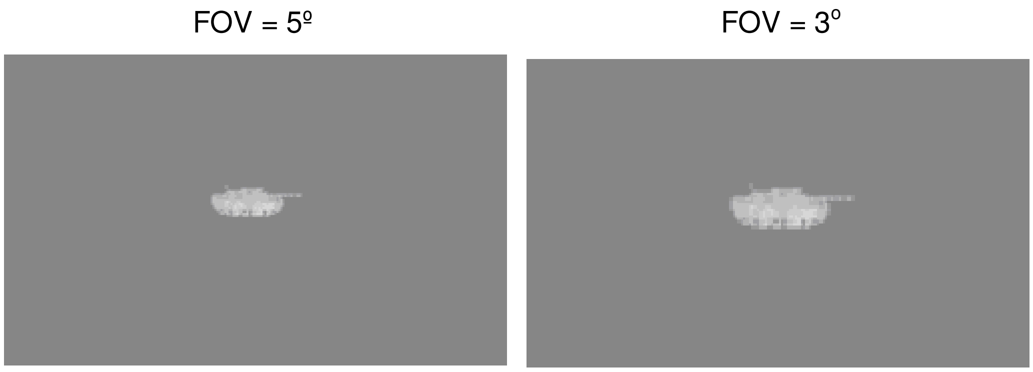
FOV = 5º

FOV = 3°

Figure 60 Sample FOV Snapshots

For different FOV values, performance of the algorithms with respect to different criteria is presented in Table 4.

FOV (degree)	Proposed Algorithm		Centroid Algorithm		Correlation Algorithm		Snake Algorithm	
	Hit Point	TLR	Hit Point	TLR	Hit Point	TLR	Hit Point	TLR
11.5	0.73	0.05	0.75	0.41	0	0.04	0.71	0.69
9.0	0.74	0.05	0.69	0.28	0.49	0.04	0.76	0.67
7.0	0.77	0.05	0.69	0.14	0.51	0.08	0.75	0.25
5.0	0.81	0.03	0.69	0.06	0.48	0.04	0.75	0.11

Table 4 Performance Metrics for Varying FOV

While field-of-view is decreasing, hit point of the proposed algorithm increases a bit, because the distance between missile and target rises when the target occupies 40% of the scene and higher distance give much more time to missile guidance section in order to steer the missile and hit the correct point.

Second of all, centroid and snake algorithms' track loss rates decrease while FOV is decreasing, because enemy target is enlarging. Bigger target increases signal-to-noise ratio and decreases the loss probability a lot.

There is no effect of FOV on the correlation algorithm.

5.2.4 Noise

An imaging system's optic and detector characteristics combined with seeker's environmental effects mainly determine the signal and noise ratios of the system. Noise is a basic measure of image quality. It can originate from many different sources such as sensor fabrication, operating temperature, electronic circuitry, dome heating, etc. for missiles.

Sensor fabrication, operating temperature and electronic circuitry generally produces fixed-pattern noise and Gaussian white noise to the system. Fixed-pattern noise is appeared as white dead pixels in the image and is modeled with Salt and Pepper (S&P) type noise in the simulations.

For a typical launch scenario, dome window heating effects, resulting from missile flight aerodynamic, is an essential phenomena, especially for high velocity missiles. Because typical anti-tank missile’s velocity is less than 1 Mach, dome heating effects are generally low. However, flux variations due to dome heating generate Gaussian white noise in the system, where the power spectrum density is flat over sufficient broadband relative to the signal band of interest.

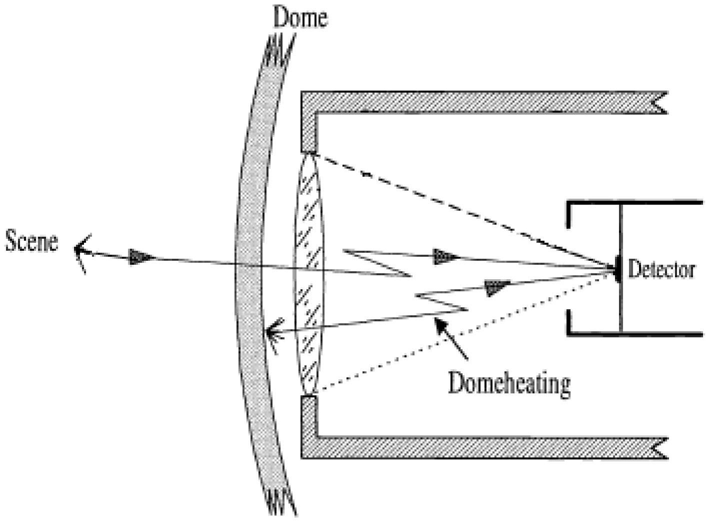

Figure 61 Dome Heating [28]

In Figure 62, sample snapshots of different noise values are presented.

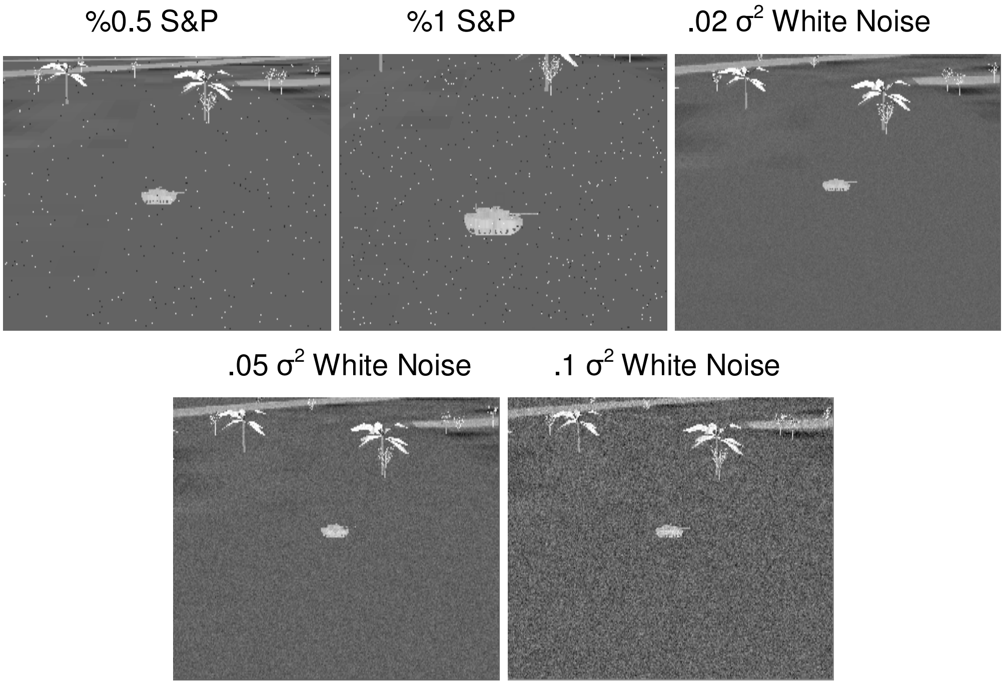

Figure 62 Sample Noise Snapshots

For different noise levels values, performance of the algorithms with respect to different criteria is presented in Table 5.

Noise Level	Proposed Algorithm		Centroid Algorithm		Correlation Algorithm		Snake Algorithm	
	Hit Point	TLR	Hit Point	TLR	Hit Point	TLR	Hit Point	TLR
%0.5 S&P noise	0.71	0.04	0.65	0.34	0.58	0.07	0.73	0.75
%1 S&P noise	0.69	0.03	0.41	0.57	0.56	0.04	0.67	0.77
.02 σ^2 white noise	0.72	0.08	0.65	0.39	0.61	0.04	0.71	0.74
.05 σ^2 white noise	0.67	0.04	0.63	0.45	0.58	0.03	0.65	0.78
.1 σ^2 white noise	0.62	0.03	0.55	0.53	0.61	0.05	0.64	0.81

Table 5 Performance Metrics for Varying Noise

Noise level generally affects system performance in a similar manner for centroid, correlation, snake and the proposed algorithms. Performance decreases while noise level is rising. Track loss rate of the centroid method increases a lot for increasing noise level.

5.2.5 Countermeasure

Modern tanks are provided some infrared countermeasure devices to protect them from infrared anti-tank missiles. They try to confuse missile's infrared guidance so that missiles will miss their target. There are several ways for IR countermeasuring such as active countermeasures, confusing guidance components by adding coded infrared signals to the missile's own infrared signal and passive countermeasures, known as flares, confusing guidance section by making missile seek out the heat signature of flare rather than target.

In this thesis, it is assumed that enemy tank includes one, two or three passive countermeasure flares to protect itself from infrared anti-tank missiles as described in Figure 63.

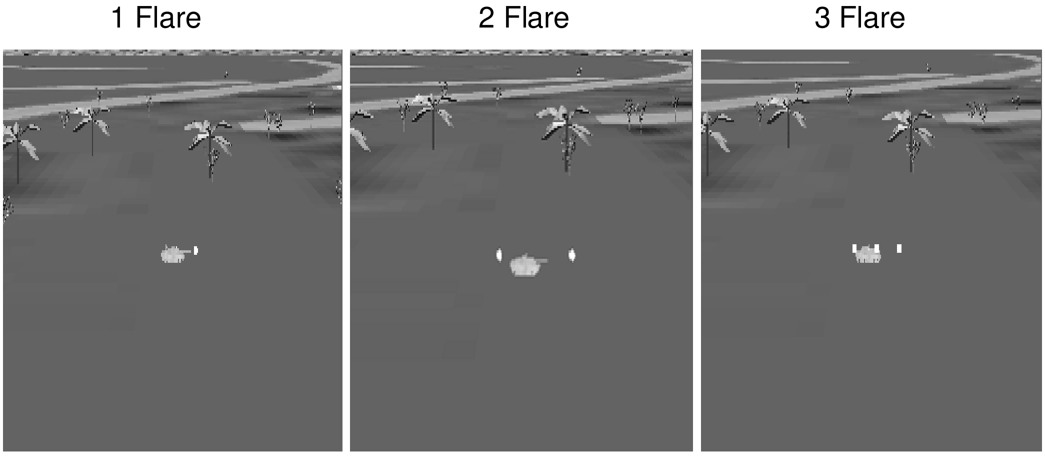

1 Flare

2 Flare

3 Flare

Figure 63 Flares

For different flare numbers, performance of the algorithms with respect to different criteria is presented in Table 6.

Flare States	Proposed Algorithm		Centroid Algorithm		Correlation Algorithm		Snake Algorithm	
	Hit Point	TLR	Hit Point	TLR	Hit Point	TLR	Hit Point	TLR
1 flare	0.76	0.04	0.72	0.28	0	0.03	0.69	0.74
2 flare	0.74	0.03	0.69	0.33	0	0.05	0.69	0.73
3 flare	0.65	0.04	0.69	0.29	0	0.03	0.71	0.76

Table 6 Performance Metrics for Varying Flare Number

Proposed, centroid and snake algorithms are not affected much by flare countermeasures as seen from Table 6. In Figure 64, proposed algorithm with one flare is presented.

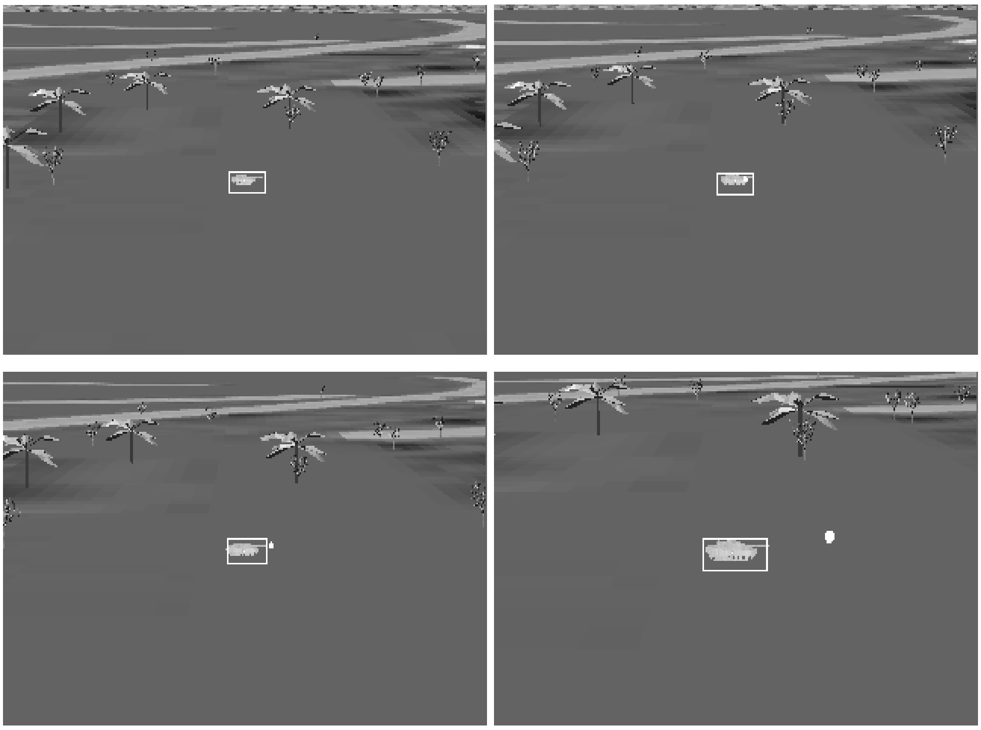

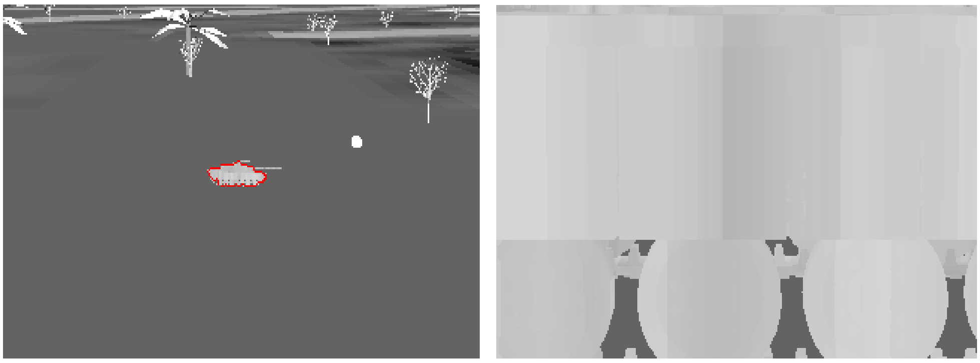

Figure 64 Proposed Algorithm with 1 Flare

In Figure 65, centroid algorithm with one flare is presented.

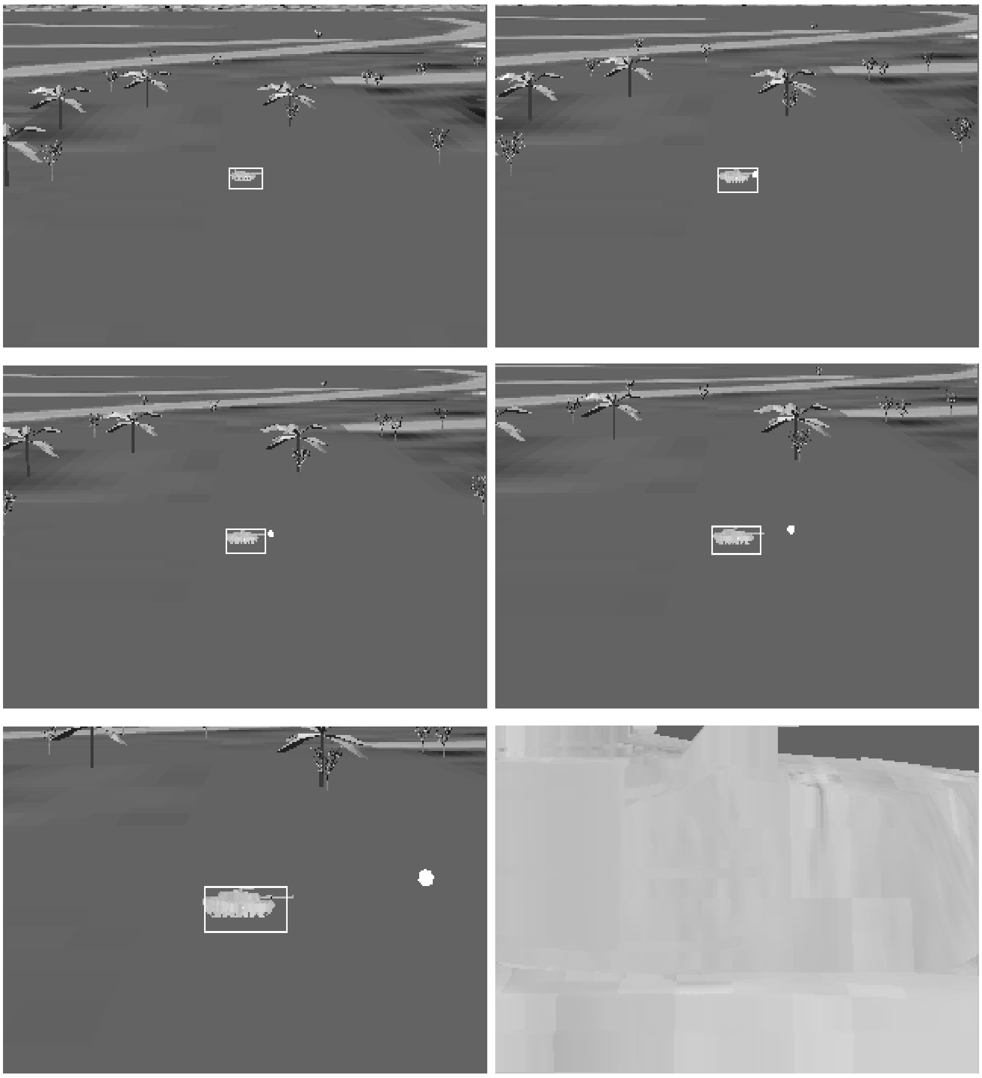

Figure 65 Centroid Algorithm With 1 Flare

In Figure 66, snake algorithm with one flare is presented.

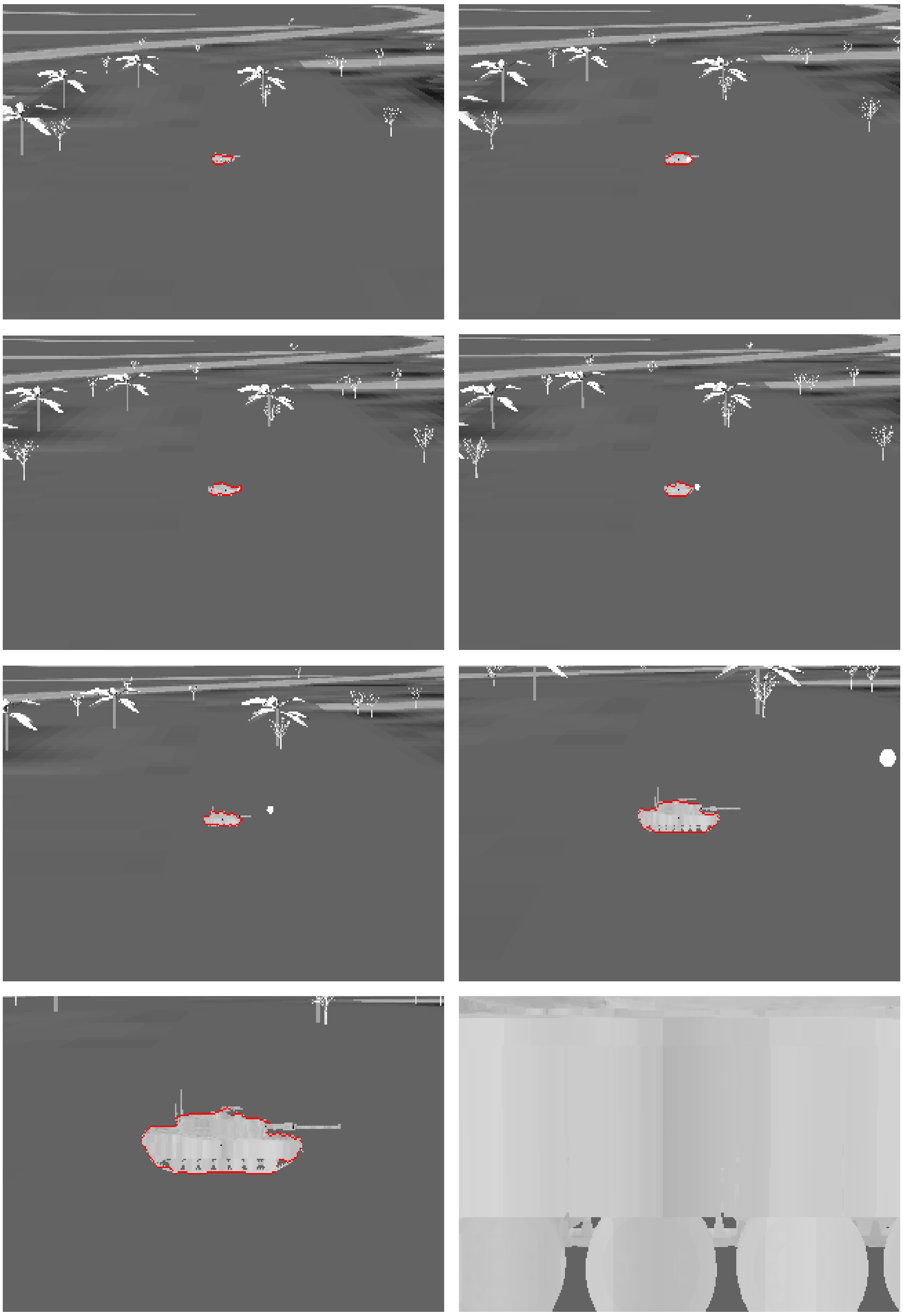

Figure 66 Snake Algorithm with 1 Flare

Passive countermeasures affect the correlation algorithm mostly. Even for 1 flare, algorithm follows flare instead of enemy target as presented in Figure 67.

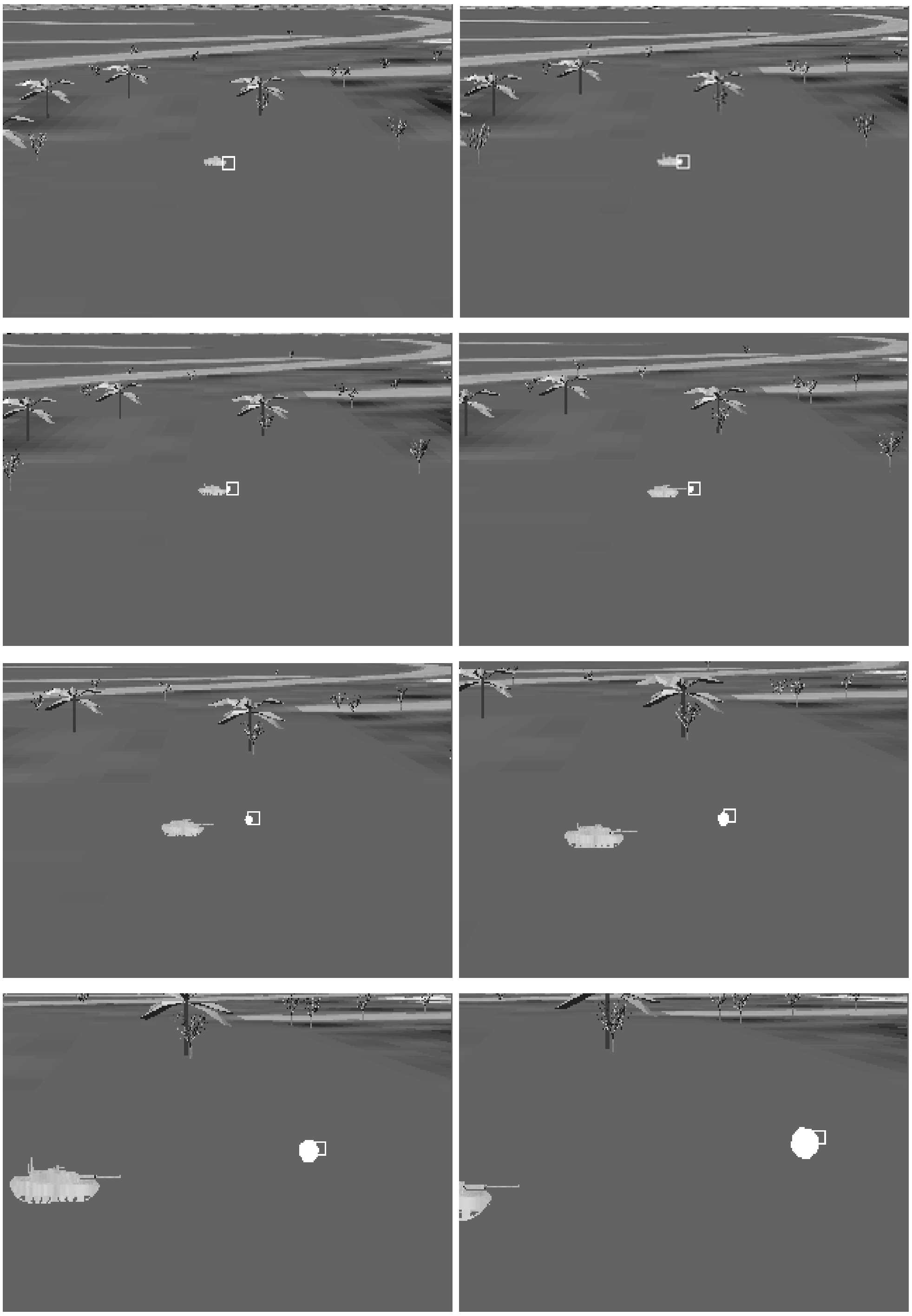

Figure 67 Correlation Algorithm with 1 Flare

CHAPTER 6

CONCLUSION

In this study, two autopilot control schemes (PID and LQR) are developed for an anti-tank missile after constructing their mathematical models. PID control technique is selected for the rest of the work, because it satisfies all of the requirements. Inputs for the autopilot section are considered as target and missile error angle.

A typical imaging infrared seeker model is constructed with its subcomponents imager, gimbal and processor. Generating infrared imaging scene concept is presented. Two-axis and stabilized gimbal structure is developed. Three tracking algorithms such as centroid, correlation and active contour (snake) are considered for the processor section. Then, a new proposed tracking algorithm combining these methods in order to improve kill rate is developed.

Virtual simulation studies are carried out in order to present the effectiveness of proposed tracking algorithm comparing with centroid, correlation and snake algorithms for different test scenarios. This study shows that proposed tracking algorithm increases the hit and kill rate in different scenarios. There are many advantageous of the proposed algorithm, especially in high-clutter and noisy real-world environments. Even when the target tank has one, two or three passive countermeasure flares to protect itself from infrared anti-tank missiles, proposed algorithm can hit and destroy its enemy with higher probability.

As a future work, tracking algorithm could be improved by combining effective filtering blocks such as Kalman Filter. It provides an efficient recursive computational estimate of the state of the process, which improves tracking capability by predicting future states. Second of all, proportional guidance instead of pursuit guidance could be developed in order to destroy moving enemy targets effectively. Target's mathematical model could be implemented as well. Commercial infrared scene generators could be integrated to the work. It increases the ability to simulate infrared scenes more effectively and comparing different wavelengths such as MWIR and LWIR could be possible.

REFERENCES

[1] Terry, A. F., “Short-Range Surface-To-Surface Missile Guidance for Nonlinear Time-Varying Target State Estimation and Missile Dynamics”, Ph.D. Thesis, Texas University, 1995.

[2] Nasburg, R.E., “Tracking and Control Systems”, Hughes Aircraft Company, 1994.

[3] Hilkert, J. M., “Stabilization, Pointing and Tracking System Technology Handbook”, Texas Instruments, 1991.

[4] Zarchan, P., “Tactical and Strategic Missile Guidance”, American Institute of Aeronautics and Astronautics Inc., USA, 1994.

[5] McLean D., “Automatic Flight Control Systems”, Prentice Hall International, 1990.

[6] Boiffier J., “The Dynamics of Flight the Equations”, John Wiley&Sons, 1997.

[7] Fossen T., “Guidance and Control of Ocean Vehicles” John Wiley&Sons, 1994.

[8] Ateşoğlu, Ö., “Different Autopilot Designs and Their Performance Comparison for Guided Missiles”, Master’s Thesis, METU, 1996.

[9] Evcimen, Ç., “Development and Comparison of Autopilots and Guidance Algorithms for Missiles”, Master’s Thesis, METU, 2007.

[10] Paz A. Robert, “The Design of the PID Controller”, Klipsch School of Electrical and Computer Engineering, 2001.

[11] Dorf C. Richard, Bishop H. Robert,“Modern Control Systems“, Prentice Hall, 2001.

[12] Karasu, Ç., “Small Size Unmanned Model Helicopter Guidance and Control”, Master’s Thesis, METU, 2004.

[13] Burns Keith A. and Blake William B. Blake, “Missile DATCOM User’s Manual”, 1993.

[14] Holst, G. C., “Electro-optical Imaging Systems Performance”, JCD Publishing, 2000.

[15] Fischer R. E., Tadic-Galeb B., Yoder P. R., “Optical System Design”, McGraw-Hill Books, 2008.

[16] Vollmerhausen R., “Predicting Field Target Acquisition Performance”, US Army Night Vision and Electronic Sensors Directorate, 2002.

[17] Brackney B. A., Hammon R. K., Hall R. L., Phillips M. A., “Development of Simulation Tools for the Analysis of Captive Flight Test Data for Imaging Infrared Missile Seekers”, Proceedings of SPIE, pp.26-33, 2001.

[18] Çolakoğlu, Ç. “Performance Evaluation of Video Trackers Using Synthetic Scenarios”, Master’s Thesis, METU, 1999.

[19] MATLAB Virtual Reality Toolbox User’s Guide, Mathworks, 2004.

[20] "HSL and HSV" Wikipedia, The Free Encyclopedia. 26 Jul 2008, 18:09 UTC. Wikimedia Foundation, Inc., 27 Jul 2008 <http://en.wikipedia.org/w/index.php?title=HSL_and_HSV&oldid=228043437>.

[21] Blakelock J. H., “Automatic Control of Aircraft and Missiles”, John Wiley & Sons Inc., 1991.

[22] Blackman S., Popoli R., “Design and Analysis of Modern Tracking Systems”, Artech House, 1999.

[23] Venkateswarlu R., Sujata K. V., Rao B. V., “Centroid Tracker and Aim Point Selection”, SPIE Vol. 1697 Acquisition, Tracking and Pointing VI, pp.520-529, 1992.

[24] “VRealm Builder User’s Guide and Reference”, Ligos Corporation, 1997.

[25] “Tactical and Technical Trends: Vulnerability of Tiger Tanks”, US Military Intelligence Service, Section 1, 1943.

[26] Schmieder D. A., Weathersby M. R., “Detection Performance In Clutter With Variable Resolution”, IEEE Trans. Aerop. Electron. Syst., Vol. AES-19, No.3, pp.622-630, 1983.

[27] Scott A. N., Naylor R. B., “Reliable Motion Detection of Small Targets in Video With Low Signal-to-Clutter Ratios”, IEEE Trans., pp.447-456, 1995.

[28] Naveh O., “Sensitivity of Scanning and Staring IR Seekers for Air-to-Air Missiles”, Proceedings of SPIE, pp.692-711, 1997.

[29] "MCLOS" *Wikipedia, The Free Encyclopedia*. 8 Aug 2008, 17:48 UTC. Wikimedia Foundation, Inc. 12 Aug 2008 <http://en.wikipedia.org/w/index.php?title=MCLOS&oldid=230653996>.

[30] Phillips M. A., Sims S. R. F., “A Signal to Clutter Measure for ATR Performance Comparison”, Proceedings of SPIE, pp.74-81, 1997.

[31] Hamarneh G., “Towards Intelligent Deformable Models for Medical Image Analysis”, Ph.D. Thesis, Chalmers University of Technology, 2001.

[32] Kass M., Witkin A., Terzopoulos D., “Snakes: Active contour models” International Journal of Computer Vision, 1988.

[33] F. L. Kok, “Deformable Contours: Modeling, Extraction, Detection, and Classification” Ph.D. Thesis, University of Wisconsin-Madison, 1994.

APPENDIX A

MISSILE DATCOM USER MANUAL

The fundamental purpose of the Missile DATCOM software is to provide an aerodynamic design and the capability for the user to easily substitute methods to fit specific applications [13].

A.1. Input Definitions

The user can enter the flight conditions and geometry of the desired missile using variety of namelist inputs and control cards. These data should be written in "for005.dat" file.

A.2. Namelist Inputs

Flight conditions, reference quantities, axisymmetric body definitions, etc. briefly all properties of desired missile are provided by ten namelists. These namelists are summarized as follows:

Namelist	**Definition**
FLTCON	Flight conditions (angle of attack, Mach numbers, etc.)
REFQ	Reference quantities (reference area, length, etc.)
AXIBOD	Axisymmetric body definitions
ELLBOD	Elliptical body definitions
PROTUB	Protuberance information and geometry
FINSETn	Fin descriptions by fin set (n is the fin set number 1,2,3 or 4)
DEFLCT	Panel deflection values
TRIM	Trimming information

INLET	Inlet geometry
EXPR	Experimental data

Table 7 Namelist Inputs

The following rules are common for all namelists:

- Namelist parts start with symbol “$” and ends with the same symbol.
- The namelist can be input any order.
- Namelist inputs are column independent and can begin in any column including the 1st. If a namelist is continued to a second card, the continued card must leave column 1 blank. Also, the card before the continued card must end with a comma. The last usable column is number 79 if column 1 is used and column 80 if column 1 is blank.
- The same namelist can be input multiple times for the same input case. The total number of namelists read, including repeat occurrences of the same namelist name, must not exceed 300.
- The last occurrence of a namelist variable in a case is the value for the calculations.

In our configuration, FLTCON, REFQ, AXIBOD, FINSETn, DEFLCT and TRIM namelists are provided to the software as follows:

A.3. Flight Conditions

In order to define the flight conditions FLTCON namelist should be run. The program is limited to no more than 20 angle of attack and 20 Mach numbers. Therefore, a case is defined as a 10 Mach numbers and 20 angles of attacks as follows:

```
$FLTCON
 NMACH= 10.0,NALPHA= 20.0,ALT= 0.0,
 MACH(1)=.1,.2,.3,.4,.5,.6,.7,.8,.9,1.0,
 ALPHA(1)=-9.,-8.,-7.,-6.,-5.,-4.,-3.,-2.,-1.,0.0,
 ALPHA(11)=1.,2.,3.,4.,5.,6.,7.,8.,9.,10.,
 BETA=0.0,
$END
```

where NMACH defines the number of mach numbers, NALPHA defines the number of angle of attacks, ALT defines the corresponding altitude, MACH(1) defines mach numbers (or speed schedule) matching NMACH, ALPHA(1) and ALPHA(11) defines angle of attacks matching NALPHA, and BETA defines sideslip angle.

BETA and ALT is taken as zero, so it is assumed that the displacement of the aircraft centerline from the relative wind and sea-level altitude as zero.

Supplied data will take place over program calculations.

A.4. Reference Quantities

Inputs for this namelist are optional. A missile scale factor SCALE permits the user to input a geometry that is scaled to the size desired. A case is defined as follows:

```
$REFQ
 SREF= 0.016513,LREF= 0.145,LATREF= 0.145,
 BLAYER=NATURAL,RHR=280.00,XCG= 0.82,ZCG= 0.0,
 SCALE=1.0,
$END
```

where SREF defines reference area, LREF defines reference longitudinal length, LATREF defines reference lateral length, BLAYER defines boundary layer type, RHR defines roughness height rating, XCG defines longitudinal position of center of mass, ZCG defines vertical position of center of mass and SCALE defines missile scaling factor.

SCALE is taken as 1, so there is no scaling on the missile geometry.

A.5. Axisymmetric Body Definitions

An axisymmetric body is defined using this namelist. The body can be specified in one of two ways: OPTION1 and OPTION2. In OPTION1, the geometry is divided into nose, centerbody, and aft body sections. This shape, overall length and base diameter for each section are specified. Contrary to, in OPTION2, the longitudinal stations and corresponding body radii are defined, from nose to tail. It is highly recommended that OPTION1 be used when possible and also OPTION1 is only valid if the Mach number is greater than 1.2, so I selected to use OPTION1. A case is defined as follows:

```
$AXIBOD TNOSE=POWER,POWER=0.145,LNOSE=0.185,DNOSE=0.150,BNOSE=0.0,
 LCENTR=1.377,DCENTR=0.145,
 TAFT=CONICAL,LAFT=0.038,DAFT=0.135,DEXIT=0.120,
$END
```

where TNOSE defines the type of nose shape, POWER defines exponent for power law shapes of nose, LNOSE defines the length of the body segment to where the radius first reaches a maximum, DNOSE defines nose diameter at base, BNOSE defines nose bluntness radius (or radius of truncation), LCENTR defines centerbody length, DCENTR defines centerbody diameter at base, TAFT defines afterbody shape, LAFT defines afterbody length, DAFT defines afterbody diameter at base, DEXIT defines nozzle diameter at base.

A.6. Fin Configurations

Special user specified fin cross-sections and configurations can be input using the namelist FINSETn. The user can specify up to 4 non-overlapping fin sets. The variable “n” specifies the number of fin set. Four type of airfoil sections are permitted for fins: hexagonal, circular arc, NACA (developed by the National Advisory Committee for Aeronautics) and user-defined. Only one type of airfoil section can be specified per fin set, and this type is used for all chord wise cross sections from root to tie. I used two fin sets as follows:

```
$FINSET1
 SECTYP=NACA,
 NPANEL=4.,PHIF=45.,135.,225.,315.,
 XLE=0.89,SWEEP=0.0,STA=0.0,
 SSPAN=0.0,0.21,
 CHORD=0.07,0.07,
$END
$FINSET2
 SECTYP=NACA,
 NPANEL=4.,PHIF=0.,90.,180.,270.,
 XLE=1.365,SWEEP=0.0,STA=0.0,
 SSPAN=0.0,0.125,
 CHORD=0.045,0.045,
$END
```

where SECTYP defines the airfoil type, NPANEL defines number of panels in set, PHIF defines roll angles of each fin, XLE defines the distance from nose to tip to chord, SWEEP defines panel sweep angle, STA defines chord station used in measuring, SSPAN defines semi-span locations and CHORD defines panel chord length at each semi-span location.

A.7. Panel Deflections

This namelist permits the user to fix the incidence angle for each panel in each fin set. A positive panel deflection is one which will produce a negative (counterclockwise when viewed from the rear) roll moment increment at zero angle of attack and sideslip. A case is defined as follows:

```
$DEFLCT
 DELTA2=0.0,10.0,0.0,-10.0,
$END
```

where DELTA2 specifies deflection angles for each panel in fin set 2.

A.8. Trimming Conditions

This namelist instructs the program to statically trim the missile longitudinally. Only one fin set can be used for trimming operation. A case is defined as follows:

```
$TRIM
 SET=2.,
 DELMIN=-25.,
 DELMAX=20.,
 PANL2=.TRUE.,PANL4=.TRUE.,
$END
```

where SET defines fin set to be used for trimming, DELMIN defines minimum negative deflection, DELMAX defines maximum positive deflection and PANLn is TRUE if panel to be used.

A.9. Control Card Inputs

Control cards are one line commands which select program options. Although they are not required inputs, they permit user control over program execution and the types of output desired. Control cards enable the following:

- Printing internal data array results for diagnostic purposes (DUMP)
- Outputting intermediate calculations (PART, BUILD, PRESSURES, PRINT, AERO, PRINT EXTRAP, PRINT GEOM, PLOT, NAMELIST, WRITE, FORMAT)
- Selecting the system of units to be used (DIM, DERIV)
- Defining multiple cases, permitting the reuse of previously input namelist data or deleting namelists of a prior case (SAVE, DELETE, NEXT CASE)
- Adding case titles or comments to the input files and output pages (*, CASEID)
- Limiting the calculations to longitudinal aerodynamics (NO LAT)

Followings are control cards used in the software:

```
CASEID THESIS
DIM M
DERIV RAD
NACA-1-4-0015
NACA-2-4-0012
SPIN
DAMP
PRINT GEOM BODY
SAVE
NEXT CASE
PRINT AERO TRIM
```

where NACE defines the NACA airfoil section designation, SPIN computes spin and magnus derivatives for body alone, DAMP computes longitudinal dynamic derivatives, PRINT GEOM BODY prints the geometric characteristics of the configuration, SAVE saves namelist inputs from one case to the following case but not for the entire run, NEXT CASE indicates termination of the case input data and instructs the program to begin case execution, PRINT AERO TRIM instructs the program to print the body and fin alone pressure coefficient distributions.

A.10. Output Definitions

Missile DATCOM software provides aerodynamic coefficient outputs according to user specified inputs. Output aerodynamic coefficients are summarized as follows:

CN	Normal force coefficient
CM	Pitching moment coefficient
CA	Axial force coefficient
CY	Side force coefficient
CLN	Yawing moment coefficient
CLL	Rolling moment coefficient
CNA	Normal force coefficient derivative with ALPHA
CMA	Pitching moment coefficient derivative with ALPHA)
CYB	Side force coefficient derivative with BETA
CLNB	Yawing moment coefficient derivative with BETA
CLLB	Rolling moment coefficient derivative with BETA
CL	Lift coefficient
CD	Drag coefficient
CL/CD	Lift to drag ratio
XCP	Center of pressure position from the moment reference center divided by reference length
CNQ	Normal force coefficient derivative with pitch rate
CMQ	Pitching moment coefficient derivative with pitch rate
CNAD	Normal force coefficient derivative with angle of attack
CMAD	Pitching moment coefficient derivative with angle of attack

All coefficients are based upon the reference areas and lengths specified at the input phase. The derivatives are computed by numeric differentiation. For body alone and body fin set data CMQ and CMAD are presented as the sum CMQ+CMAD.

A.11. Importing Data

For importing aerodynamics coefficients below code was implemented in MATLAB environment. Output files of Missile DATCOM software were first converted to excel files, and then below MATLAB script can be run. There need some modifications of Missile DATCOM output files before implementing below MATLAB script.

```
%MATLAB code for importing excel files(out1.xls,out2.xls,for006.xls) to workspace
%Writer: Ali Erdem Özcan
%Date: 30.09.2007

clear all
clc
k=1;                          %internal counter
m=0;                           %internal counter
angle_of_attack_number=20;      %The number of angle of attack
mach_number=10;                %Mach number
delta_number=10;               %Number of trim points

[data1]=xlsread('out1.xls');    %Reading excel file 'out1.xls' into data1
angle_of_attack=data1(:,1);     %First column of data1 is angle of attack column
CL=data1(:,2);                 %Second column of data1 is CL(lift coefficient) column
CD=data1(:,3);                 %Third column of data1 is CD(drag coefficient) column
CL_over_CD=data1(:,4);          %Forth column of data1 is CL/CD column
XCP=data1(:,5);                 %Fifth column of data1 is XCP(center of pressure) column

[data22]=xlsread('out2.xls');   %Reading excel file 'out2.xls' into data22
data2=data22(4:212,:);          %Move the matrix 3 steps upper
CN=data2(:,2);                 %2nd column of data2 is CN(normal force coefficient) column
CM=data2(:,3);                  %3rd column of data2 is CM(pitching moment coefficient) column
CA=data2(:,4);                 %4th column of data2 is CA(axial force coefficient) column
CY=data2(:,5);                 %5th column of data2 is CY(side force coefficient) column
CLN=data2(:,6);                 %6th column of data2 is CLN(yawing moment coefficient) column
CLL=data2(:,7);                 %7th column of data2 is CLL(rolling moment coefficient) column
CNA=data2(:,8);                %8th column of data2 is CNA(normal force coefficient derivative with angle
                               %of attack) column
CMA=data2(:,9);       %9th column of data2 is CMA(pitching moment coefficient derivative with angle
                      %of attack) column
CYB=data2(:,10);      %10th column of data2 is CYB(side force coefficient derivative with side-slip
                       %angle) column
CLNB=data2(:,11); %11th column of data2 is CLNB(yawing moment coefficient derivative with
                    %sideslip angle) column
CLLB=data2(:,11);   %12th column of data2 is CLLB(rolling moment coefficient derivative with side-
                    %slip angle) column

[data3]=xlsread('for006.xls');    %Reading excel file 'for006.xls' into data3
[row_data3,column_data3]=size(data3);
for m=0:(mach_number-1)

CNQ((angle_of_attack_number*m+1):(angle_of_attack_number*m+angle_of_attack_number))=data
3(((103*m+234):(103*m+253)),6);

CNAD((angle_of_attack_number*m+1):(angle_of_attack_number*m+angle_of_attack_number))=dat
a3(((103*m+234):(103*m+253)),8);

CMQ_CMAD((angle_of_attack_number*m+1):(angle_of_attack_number*m+angle_of_attack_numbe
r))=data3(((103*m+234):(103*m+253)),9)*100;
end

CNQ=CNQ';                    %Takes its transpose in order to make CNQ as 200x1
CNAD=CNAD';                  %Takes its transpose in order to make CNAD as 200x1
CMQ_CMAD=CMQ_CMAD';          %Takes its transpose in order to make CMQ+CMAD as 200x1
CMQ_CMAD(141,1)=CMQ_CMAD(141,1)/10;  %Modification should be necessary
CMQ_CMAD(159,1)=CMQ_CMAD(159,1)/10;  %Modification should be necessary
CMQ_CMAD(160,1)=CMQ_CMAD(160,1)/10;  %Modification should be necessary
CMQ_CMAD(161,1)=CMQ_CMAD(161,1)/10;  %Modification should be necessary
CMQ_CMAD(179,1)=CMQ_CMAD(179,1)/10;  %Modification should be necessary
CMQ_CMAD(180,1)=CMQ_CMAD(180,1)/10;  %Modification should be necessary


for m=0:9
  for j=1:6
      Delta_neg_25(((120*m)+((j-1)*20)+1):((120*m)+((j-1)*20)+20))        =        data3(((43*(j-
1)+1218+(m*317)):(43*(j-1)+1237+(m*317))),3); %-25 degree panel deflection
      Delta_neg_20(((120*m)+((j-1)*20)+1):((120*m)+((j-1)*20)+20))        =        data3(((43*(j-
1)+1218+(m*317)):(43*(j-1)+1237+(m*317))),4); %-20 degree panel deflection
      Delta_neg_15(((120*m)+((j-1)*20)+1):((120*m)+((j-1)*20)+20))        =        data3(((43*(j-
1)+1218+(m*317)):(43*(j-1)+1237+(m*317))),5); %-15 degree panel deflection
      Delta_neg_10(((120*m)+((j-1)*20)+1):((120*m)+((j-1)*20)+20))        =        data3(((43*(j-
1)+1218+(m*317)):(43*(j-1)+1237+(m*317))),6); %-10 degree panel deflection
      Delta_neg_05(((120*m)+((j-1)*20)+1):((120*m)+((j-1)*20)+20))        =        data3(((43*(j-
1)+1218+(m*317)):(43*(j-1)+1237+(m*317))),7); %-5 degree panel deflection
```

```
        Delta_0(((120*m)+((j-1)*20)+1):((120*m)+((j-1)*20)+20)) = data3(((43*(j-
1)+1218+(m*317)):(43*(j-1)+1237+(m*317))),8);  %0 degree panel deflection
        Delta_pos_05(((120*m)+((j-1)*20)+1):((120*m)+((j-1)*20)+20)) = data3(((43*(j-
1)+1218+(m*317)):(43*(j-1)+1237+(m*317))),9); %5 degree panel deflection
        Delta_pos_10(((120*m)+((j-1)*20)+1):((120*m)+((j-1)*20)+20)) = data3(((43*(j-
1)+1218+(m*317)):(43*(j-1)+1237+(m*317))),10);%10 degree panel deflection
        Delta_pos_15(((120*m)+((j-1)*20)+1):((120*m)+((j-1)*20)+20)) = data3(((43*(j-
1)+1218+(m*317)):(43*(j-1)+1237+(m*317))),11);%15 degree panel deflection
        Delta_pos_20(((120*m)+((j-1)*20)+1):((120*m)+((j-1)*20)+20)) = data3(((43*(j-
1)+1218+(m*317)):(43*(j-1)+1237+(m*317))),12);%20 degree panel deflection
    end
end
Delta_neg_25=Delta_neg_25'; %Make them column vector
Delta_neg_20=Delta_neg_20';
Delta_neg_15=Delta_neg_15';
Delta_neg_10=Delta_neg_10';
Delta_neg_05=Delta_neg_05';
Delta_0=Delta_0';
Delta_pos_05=Delta_pos_05';
Delta_pos_10=Delta_pos_10';
Delta_pos_15=Delta_pos_15';
Delta_pos_20=Delta_pos_20';

% not to care NaN elements of parameters
[row,column]=size(angle_of_attack);
for i=1:row
    if mod(i,(angle_of_attack_number+1))~=0
        if ~isnan(angle_of_attack(i,1))
            angle_of_attack_modified(k,1)=angle_of_attack(i,1);
        else
            angle_of_attack_modified(k,1)=0;
        end

        if ~isnan(CL(i,1))
            CL_modified(k,1)=CL(i,1);
        else
            CL_modified(k,1)=0;
        end

        if ~isnan(CD(i,1))
            CD_modified(k,1)=CD(i,1);
        else
            CD_modified(k,1)=0;
        end

        if ~isnan(CL_over_CD(i,1))
            CL_over_CD_modified(k,1)=CL_over_CD(i,1);
        else
            CL_over_CD_modified(k,1)=0;
        end

        if ~isnan(XCP(i,1))
            XCP_modified(k,1)=XCP(i,1);
        else
            XCP_modified(k,1)=0;
        end

        if ~isnan(CN(i,1))
            CN_modified(k,1)=CN(i,1);
        else
            CN_modified(k,1)=0;
        end

        if ~isnan(CM(i,1))
            CM_modified(k,1)=CM(i,1);
        else
            CM_modified(k,1)=0;
        end

        if ~isnan(CA(i,1))
            CA_modified(k,1)=CA(i,1);
        else
            CA_modified(k,1)=0;
        end

        if ~isnan(CY(i,1))
            CY_modified(k,1)=CY(i,1);
        else
            CY_modified(k,1)=0;
        end

        if ~isnan(CLN(i,1))
            CLN_modified(k,1)=CLN(i,1);
        else
```

```
      CLN_modified(k,1)=0;
    end

    if ~isnan(CLL(i,1))
      CLL_modified(k,1)=CLL(i,1);
    else
      CLL_modified(k,1)=0;
    end

    if ~isnan(CNA(i,1))
      CNA_modified(k,1)=CNA(i,1);
    else
      CNA_modified(k,1)=0;
    end

    if ~isnan(CMA(i,1))
      CMA_modified(k,1)=CMA(i,1);
    else
      CMA_modified(k,1)=0;
    end

    if ~isnan(CYB(i,1))
      CYB_modified(k,1)=CYB(i,1);
    else
      CYB_modified(k,1)=0;
    end

    if ~isnan(CLNB(i,1))
      CLNB_modified(k,1)=CLNB(i,1);
    else
      CLNB_modified(k,1)=0;
    end

    if ~isnan(CLLB(i,1))
      CLLB_modified(k,1)=CLLB(i,1);
    else
      CLLB_modified(k,1)=0;
    end

    k=k+1;
  end
end
```

APPENDIX B

VIRTUAL REALITY TOOLBOX USER MANUAL

The fundamental purpose of the Virtual Reality Toolbox software is to provide a connection between a virtual world to Simulink and MATLAB® [19]. It provides a solution for viewing and interacting with dynamic systems in a 3D virtual reality environment. To provide a complete working environment, the Virtual Reality Toolbox includes the following components:

- VRML editor: A classical VRML authoring tool, VRealm Builder, is included.
- VRML viewer: It visualizes and explores virtual world created by VRML editor.

B.1. VRML Overview

The Virtual Reality Modeling Language (VRML) is the language to display 3D objects with a VRML viewer. Since people started to publish their documents on the World Wide Web, there has been an effort to enhance the content of web pages with a 3D graphics. In 1994, a Virtual Reality Markup Language was first introduced as a 3D web standard. Soon afterward, the name for standards became Virtual Reality Modeling Language (VRML). The result of the effort was to produce the VRML1 specification. The VRML1 standard was implemented in several VRML browsers, but it only allowed static virtual worlds. Quickly a new robust extension of VRML1 was published as VRML2, which includes 3D animation capabilities. In 1997, it was adopted as International Standard ISO/IEC 14772-1:1997 [19]. Since then it is referred as VRML97. The VRML97 standard continues to be improved.

The Virtual Reality Toolbox uses VRML97 technology to deliver a unique, open 3D visualization solution for MATLAB® users.

B.2. VRML Coordinate System

The VRML uses right-handed Cartesian coordinate system; however, it is different from the MATLAB® coordinate system as described in Figure 68.

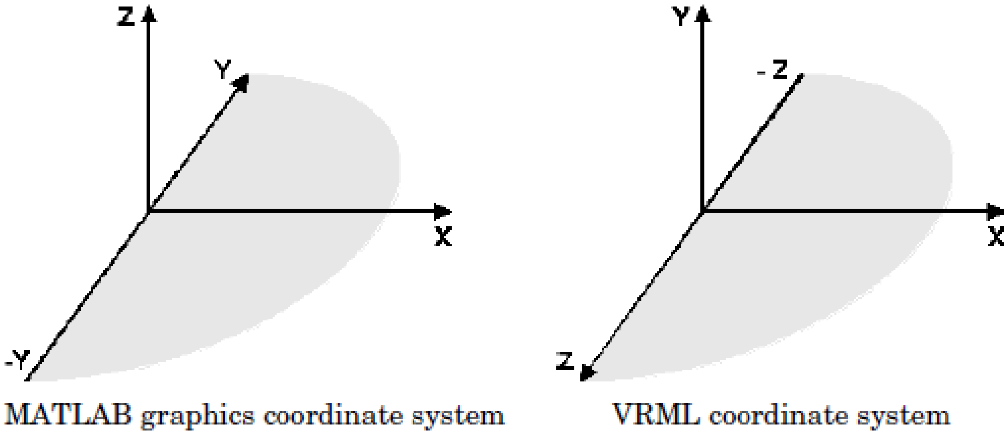

Figure 68 MATLAB and VRML Coordinate Systems

The VRML uses world coordinate system in which the y-axis points upward, the z-axis places objects nearer or farther from the front screen and, the x-axis is the complementing axis. In VRML, rotation angles are also defined using right-hand rule.

B.3. VRML Editor

There is more than one way to create a virtual world described with the VRML code. A text editor to directly write VRML code can be used as well as a VRML editor to create a virtual world without having any knowledge about VRML language. The V-Realm Builder is a flexible, graphically oriented tool for 3-D editing. Its primary file format is VRML. Its graphical interface offers not only graphical representation of 3D scene, but also a hierarchical tree-style view of all the elements present in the virtual world. Editor terminology and design procedures are described below [19,24]:

Viewpoint: It defines a specific location in the local coordinate system from which the user views the scene. There can be any number of viewpoints in the scene, but only one can be active at any given time. One viewpoint is created in front of the missile nose to simulate imaging seeker.

Lights: In general, objects and earth surfaces are illuminated by the sum of all lights in the scene that affect them. Directional light, point light and spot light are the types of light sources that are available. All sources contain intensity and color inputs. The intensity specifies brightness of the light and color defines spectral color property. Three directional light sources are added to the scene in order to simulate sunlight by illuminating everything in the scene from the same angle.

Elevation Grid: It specifies a uniform rectangular grid of varying height in the XZ plane of the local coordinate system. The geometry is described by a scalar array of height values that specify the height of a rectangular surface above each point of the grid. Figure 69 presents earth surface created by elevation grid tool.

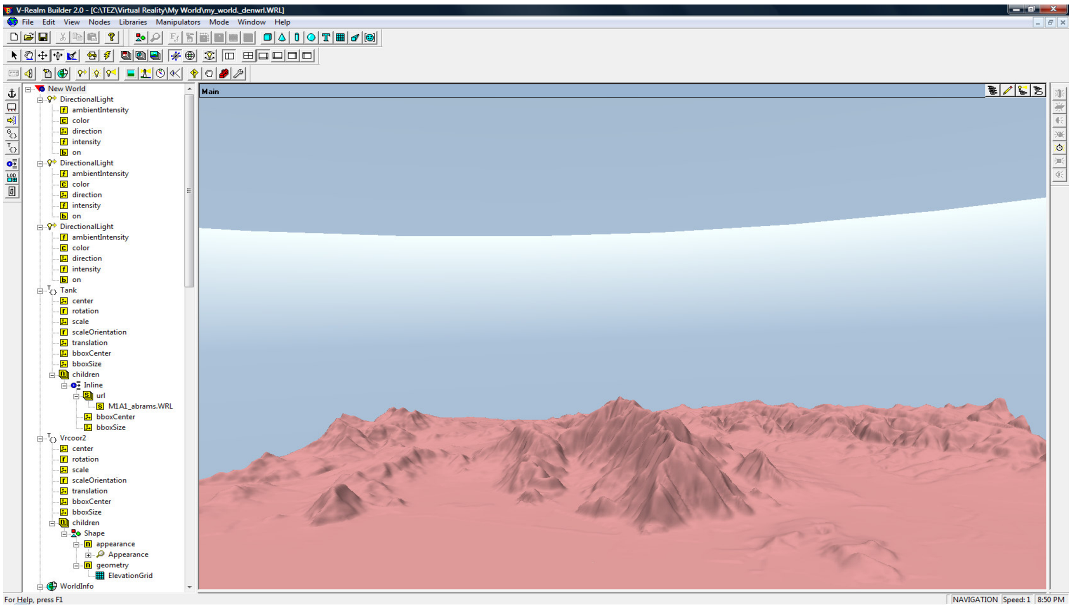

Figure 69 Created Earth Surface

Node Tree: A node refers to any VRML object existing in the environment. For example a building or a window can be a node in the scene. A group node is a VRML node type that groups elements called children together. A building is a group node with windows, doors, and walls as children since they are a subset of larger structure. The Group and Transform nodes are two most basic grouping nodes. The Group node groups its children together but does not impose any special constraints upon them; however Transform node defines a coordinate system for them that is relative to parent's coordinate system. Missile and tank objects are specified using Transform nodes. Figure 70 presents their appearance in the scene.

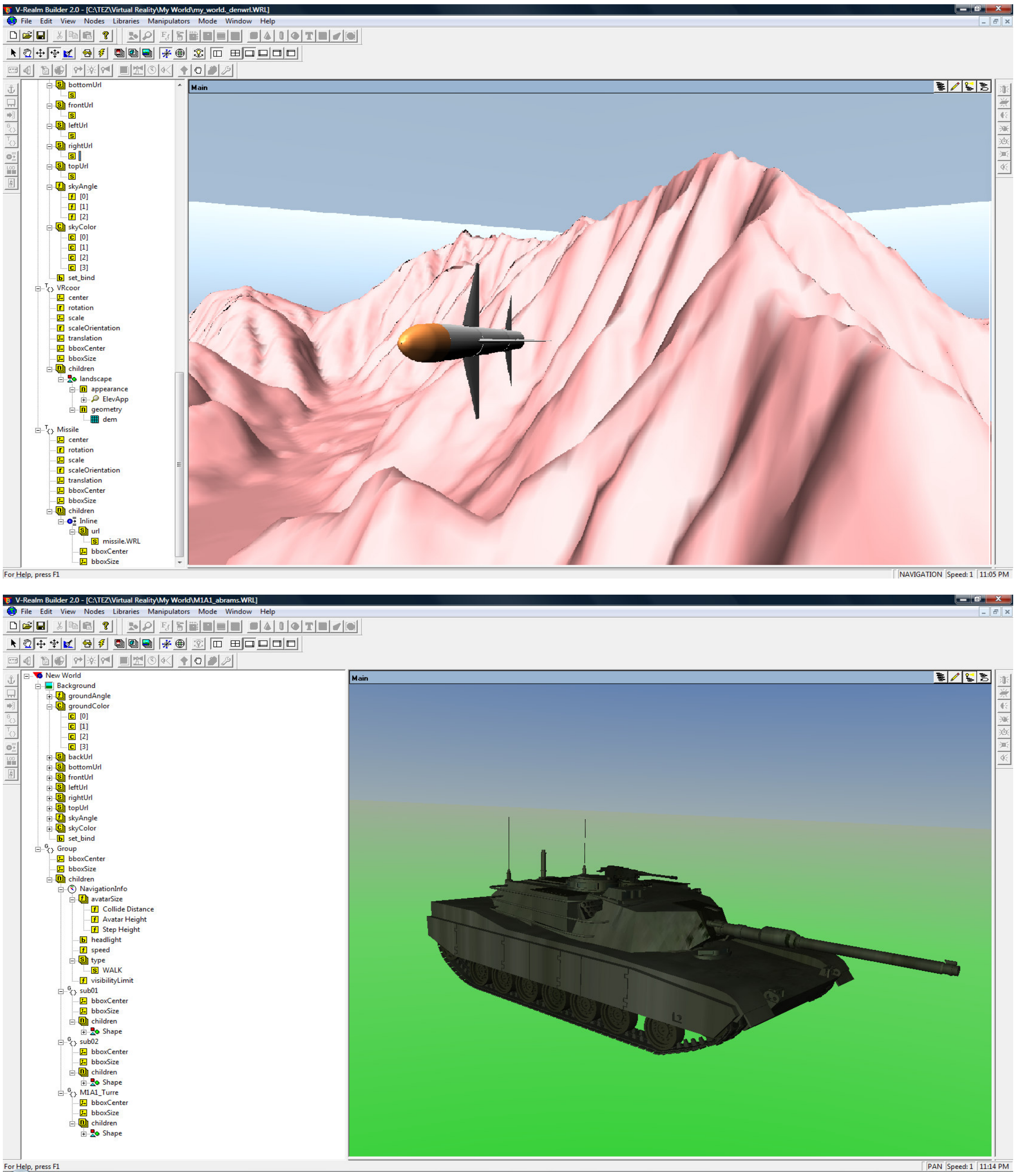

Figure 70 3D Missile and Tank Objects